Project No. 12-3445

Thermodynamic and Microstructural Mechanisms in the Corrosion of Advanced Ceramic Tc-bearing Waste Forms and Thermophysical Properties

Fuel Cycle Research and Development

Thomas Hartmann
University of Nevada, Las Vegas

Kimberly Gray, Federal POC
John Vienna, Technical POC

NEUP Nuclear Energy University Programs
U.S. Department of Energy

Final Report for NEUP 12-3445

Project Title: Thermodynamic and Microstructural Mechanisms in the Corrosion of Advanced Ceramic Technetium-bearing Waste Forms and Thermophysical Properties

Milestone Number: M1NU-12NV-UNLV-0202-068
Work Package Number: NU-12-NV-UNLV-0202-06

Submitted by:

Thomas Hartmann
University Nevada, Las Vegas
Department of Mechanical Engineering
UNLV Radiochemistry Program
Harry Reid Center for Environmental Studies
4505 Maryland Parkway BOX 454009
Las Vegas, Nevada 89154-4009
Phone: (702) 895-1934, E-mail: thomas.hartmann@unlv.edu

Contents

LIST OF FIGURES

LIST OF TABLES

1. Executive Summary

Technetium-99 (Tc, $t_{1/2}$ = 2.13x10^5 years) is a challenge from a nuclear waste perspective and is one of the most abundant, long-lived radioisotopes found in used nuclear fuel (UNF). Within the Hanford Tank Waste Treatment and Immobilization Plant, technetium volatilizes at typical glass melting temperature, is captured in the off-gas treatment system and recycled back into the feed to eventually increase Tc-loadings of the glass. The aim of this NEUP project was to provide an alternative strategy to immobilize fission technetium as durable ceramic waste form and also to avoid the accumulation of volatile technetium within the off gas melter system in the course of vitrifying radioactive effluents in a ceramic melter. During this project our major attention was turned to the fabrication of chemical durable mineral phases where technetium is structurally bond entirely as tetravalent cation. These mineral phases will act as the primary waste form with optimal waste loading and superior resistance against leaching and corrosion. We have been very successful in fabricating phase-pure micro-gram amounts of lanthanide-technetium pyrochlores by dry-chemical synthesis. However, upscaling to a gram-size synthesis route using either dry- or wet-chemical processing was not always successful, but progress can be reported on a variety of aspects. During the course of this 5-year NEUP project (including a 2-year no-cost extension) we have significantly enhanced the existing knowledge on the fabrication and properties of ceramic technetium waste forms.

In our narrative we proposed to address the following five tasks as listed below.

1. Fabrication of dense, single phase, Tc-bearing ceramic monoliths
2. Thermodynamics and kinetics of Tc-leaching
3. Thermodynamics and kinetics of Tc waste-form matrix corrosion
4. Microstructural waste form corrosion mechanism
5. Thermophysical properties of advanced Tc waste forms

Among these five tasks our experimental efforts predominantly focused on task 1 and task 2. This was driven by personal interest and abilities of students and staff, but also by their importance to justify the selection of a waste form as technetium host for permanent storage in a generic repository. We have addressed a far wider work scope for task 1 than proposed in the narrative, while the work scopes on the tasks 2 to 5 were altered due to practical considerations and radiological concerns and are not word-by-word to what was proposed. Naturally our main interest was to fabricate a superior product to potentially induce long-term changes to the current process flowsheet for vitrifying radioactive effluents from used fuel reprocessing. After all, this NEUP project enabled us to become the lead research group on the synthesis and properties of ceramic technetium waste forms in the nation, it gave us the opportunity to full or partly fund more than 13 undergraduate students in engineering or sciences, 8 graduate students, 4 support staff, 2 postdoctoral fellows, two international exchange student, and ¼ of a professor (Table 1). We were able to present our work in domestic conferences as well as in 2 international conferences. For now 8 journal articles and conference papers have been published as results of this NEUP support (Table 1).

Table 1: *Student- and staff contribution and publications to NEUP project 12-3445*

Student / Staff	**Department**	**Degree**
Ariana J. Alaniz	Mechanical Engineering	Undergraduate, graduated
Luc Delgado	Electrical Engineering	Undergraduate, graduated
Brett Werbick	Computer Engineering	Undergraduate, graduated
Nicole Ramos	Mechanical Engineering	Undergraduate, graduated
Izua J. Alaniz	Chemistry	Graduate
Katalin Bene	None-degree seeking	Graduate
Stephanie Molina	Biochemistry	Graduate
Ryan Odiorne	Biochemistry	Graduate
George Unc	None-degree seeking	Graduate
Samantha Suffle	Mechanical Engineering	Undergraduate
Amit Sharma	Mechanical Engineering	Undergraduate
Tristan Dimitrijev	Mechanical Engineering	Undergraduate
Christopher Mead	Mechanical Engineering	Undergraduate, graduated
Matthew Pedraza	Mechanical Engineering	Undergraduate, graduated
Ibrahim Abdullah	Mechanical Engineering	Undergraduate, graduated
Alexander Smith	Mechanical Engineering	Undergraduate, graduated
Daniel Henry	Mechanical Engineering	Undergraduate, graduated
James Maslow	Chemistry	Undergraduate
Florian Wolke	International Student	Graduate
Raja Palaparty	Mechanical Engineering	Graduate
Zachary Crouch	Mechanical Engineering	Graduate
Daniel Koury	Chemistry	Post-Doctoral Fellow
Gerald (Jerry) Egeland	Mechanical Engineering	Post-Doctoral Fellow
Julie Bertoia	Chemistry	Support Staff
Trevor Low	Chemistry	Support Staff
Wendee Johns	Chemistry	Support Staff
Thomas Hartmann	Mechanical Engineering	Associate Professor
Publications		

T. Hartmann, R. Palaparty, F. Wolke: Fabrication and Properties of Advanced Ceramic Waste Forms, Waste Management Symposia 2017, Proceedings, 17311, March 5-9, Phoenix, AZ (2017).

T. Hartmann, I.J. Alaniz-Ortez: Fabrication and Chemical Durability of Ceramic Technetium-Based Pyrochlores and Perovskites as Potential Waste Forms. Advances in Science and Technology, Vol. 94, pp. 85-92, (2014).

T. Hartmann, I.J. Alaniz-Ortez: Fabrication and Chemical Durability of Ceramic Technetium-Based Pyrochlores and Perovskites as Potential Waste Forms. Proceedings CIMTEC 2014, 6th Forum on New Materials, June 15-19, Montecatini Terme, Italy, (2014).

T. Hartmann, A.J. Alaniz, D.J. Antonio: Fabrication and Properties of Technetium-Bearing Pyrochlores and Perovskites as Potential Waste Forms, Waste Management Symposia 2013, Proceedings, 13222, (2013).

A.J. Alaniz, L. Delgado, B. Werbick, T. Hartmann: Prototype *Development of a Remote Operated Hot Uniaxial Press (ROHUP) to Fabricate Advanced Tc-99 Bearing Ceramic Waste Forms,* Waste Management Symposia 2013, Proceedings, 13381, (2013).

A. J. Alaniz, L. Delgado, B. Werbick, T. Hartmann: *Remote Operated Hot Uniaxial Press to Fabricate Tc-99-Bearing Waste Forms.* Atalante 2012: Nuclear Fuel Cycle for a Sustainable Fuel Cycles, Montpellier, France, 2-7 September, Proceedings, A168 (2012).

T. Hartmann, A.J. Alaniz, D.J. Antonio: Fabrication and Properties of Technetium-Bearing Pyrochlores and Perovskites as Potential Waste Forms. Procedia Chemistry, pp. 622-628 (2012).

T. Hartmann, A.J. Alaniz, D.J. Antonio: Fabrication and Properties of Technetium-Bearing Pyrochlores and Perovskites as Potential Waste Form. Atalante 2012: Nuclear Fuel Cycle for a Sustainable Fuel Cycles, Montpellier, France, 2-7 September, Proceedings, A210 (2012).

For task 1, in FY 2012 and FY 2013 we designed and build a hot uniaxial press as an engineering senior design project in an interdisciplinary effort with participating students from mechanical engineering, electrical engineering, and computer science. The hot press was implemented into a standard radiological glove box and designed for pressure-assisted sintering of gram-size Tc-bearing ceramics at temperatures of up to 1200 °C and loads of 100 to 400 MPa. Our mark II design featured a 20,000 psi hydraulic pressure system which was commercial-grade but very much over-engineered. Pressure control for lowering the load to 200 MPa or lower was barely possible and therefore replaced by a simple lever system. The mark III design was appropriate for high-temperature sintering of ceramic powder at a load of about 100 MPa. The applied load is limited by the mechanical strength of the graphite dies we machined from high-dense graphite rods (SGL, Germany). Our current mark IV hot uniaxial press is equipped with an electromechanical load system which exhibits improved load control in the range from 50 to 500 MPa. The uniaxial hot press allowed us to fabricate ceramic pellets of $SrTcO_3$ perovskite, Sr_2TcO_4 layered perovskite, and a variety of pyrochlores in the systems $Ln_2Tc_2O_7$, $Ln_2Ru_2O_7$, $Ln_2(Tc_xRu_{1-x})_2O_7$, $Ln_2(Tc_xTi_{1-x})_2O_7$, and $Ln_2((Tc,Ru)_xTi_{1-x})_2O_7$ with theoretical densities between 50 and 75 %. The sample masses were typically between 0.2 and 0.3 g and were limited by the total amount of ammonium pertechnetate we had available for the duration of this project, but our processes are upscalable by a factor 10 without major modifications. Prior to high-temperature sintering, precursors were prepared through dry-chemical and wet chemical processing. High-temperature sintering was either performed pressure-less in evacuated fused silica ampoules or using the hot-uniaxial pressing. We have noticed, that technetium in contact with graphite might undergo reduction to form small metallic precipitates within the pellet matrices. To mitigate technetium reduction the revised sintering procedure included hot press-based sintering at 700 °C for 2-3 days, followed by pressure-less sintering in platinum foil and fused silica at 1150 °C for 3 days. As a result virtually phase-pure monolithic ceramic lanthanide technetium pyrochlores could be obtained with theoretical densities of up to 70 %.

In FY 2016 we further developed a promising technical approach for continuously depleting the Tc-content of the glass melter feed by precipitating Tc from the effluents of the off-gas capture and recycling systems and subsequently for effectively immobilizing Tc as durable ceramic waste form. This process is based on a wet-chemical coprecipitation synthesis route to fabricate gram-size, phase-pure Tc-based pyrochlores with the model composition $Sm_2(Tc_{0.5-x}Ru_xTi_{0.5})_2O_7$. Titanium dioxide was added to the process in order to enhance sinterability and therefore to increase theoretical densities and mechanical strength such as compressive strength and fracture toughness of the pellets. The coprecipitations process is up-scalable to technical scale. Pertechnetate ($Tc^{[VII]}O^{4-}$), the dominant Tc-species in the off-gas washer solution, was successfully reduced to technetate ($Tc^{[IV]}O_2$) within hours using tin(II) chloride in excess at pH 4.5 to 7 to subsequently allow for its immobilization and the fabrication of Tc-pyrochlore. Microstructure and mechanical properties of surrogate waste form $Sm_2(Ru_{0.5}Ti_{0.5})_2O_7$ could be significantly improved compared with earlier studies and theoretical densities of 72 % were observed.

To task 2 in FY 2012 and FY 2013 ASTM C1285-02 (PCT-B) and ASTM C1220-10 (MMC-1) standard corrosion tests were performed to collect based-line leaching and corrosion data on vitreous reference materials such as the borosilicate glasses SRM-623, PNNL ARM-1, PNNL 76-68, and LAW4, a Tc-99

containing glass we fabricated at UNLV. We have realized that the product consistency test (PCT-B) for highly radioactive technetium based ceramics might be not practical and its application would raise major radiological concerns since the size fraction 75-106 µm (200-140 mesh) has to be extracted for testing. To mitigate the risks of contamination our research work related to task 2 and 3 focused on the evaluation of technetium leaching and waste form matrix corrosion of monolithic samples after applying ASTM C1220-10. For the ARM-1 glass the corrosion rates were determined to average 6.11 10^{-7} g/mm^{2}xday for the 7 days test and 2.75 10^{-7} g/mm^2•day for the 28 days corrosion testing. For the 76-68 reference glass the average corrosion rate was 5.08 10^{-7} g/mm^2•day and 5.6 10^{-7} g/mm^2•day for the 7 days and the 28 days corrosion testing, respectively. Technetium containing borosilicate glass was successfully synthesized within the UNLV radiochemistry laboratories. The target Tc-content was 1 wt.-% technetium-99 and a 5 gram batch was fabricated. ASTM C1220-10 (MCC-1) corrosion tests of Tc-LAWE4 glass for 7 and 28 days revealed Tc-99 release of 0.64 %, and 1.01 % of the total inventory and a specific mass loss of 1.34 10^{-6} and 6.43 10^{-7} g/mm^2•day, was measured, respectively. In comparison to this, corrosion experiments on monolithic $Nd_2Tc_2O_7$ pellets fabricated by dry-chemical processing and pressure-less sintering showed a specific mass loss of 1.48 10^{-7} g/mm^2•days, which is by a factor 4 lower than the specific mass loss observed for corroding Tc-99 containing LAWE4-type borosilicate glass. The Tc-99 release was measured to 0.67 % of the total Tc inventory of the pellets. We have further performed 28 days C1220-10 leaching experiments of monolithic $SrTcO_3$ pyrochlore specimens. The ceramic $SrTcO_3$ specimens corrode severely under the applied test conditions and smaller specimens disintegrated completely. The corrosion data do confirm exceptionally high leaching rates and high specific mass losses for $SrTcO_3$ after 28 days C1220-10 testing. The specific mass-loss of $SrTcO_3$ was determined to be 2.14 10^{-5} g/mm^2•days which is about a factor 33 larger than the specific mass loss for the Tc-loaded borosilicate reference glass LAWE4. About half of the strontium inventory and more than half of the technetium content of the pellets were leached out or subject to homogeneous and pitting corrosion. Because the strontium-technetium perovskite showed this high susceptibility to chemical corrosion, we shifted our focus to the lanthanide technetium pyrochlores as promising waste forms for immobilizing fission technetium.

In FY 2015 monolithic $Nd_2Tc_2O_7$ pyrochlore specimens were produced by hot-uniaxial pressing at 900 ° and 1100 °C. These samples were containing small inclusions of metallic technetium due to Tc reduction by the graphite die material. This further translates to increased technetium leaching and higher corrosion rates. The average specific mass loss was 6.465 10^{-6} g/mm^2•days for 7-days C1220-10 experiments and 7.94 10^{-6} g/mm^2•days for 28-days testing. The presence of metallic technetium inclusion induced increased technetium leaching by about one order of magnitude. By combining hot pressing with high-temperature sintering we have produced phase pure monolithic ceramic pyrochlores with stoichiometry $Pr_2Tc_2O_7$ and $Nd_2Tc_2O_7$ exhibiting specific mass losses of 6.76 10^{-7} and 2.58 10^{-6} g/mm^2•days, respectively. For most of the tested pyrochlores congruent leaching was observed and lanthanide and technetium are found in the leachates in equal proportions. However, some samples of $Pr_2Tc_2O_7$ and $Nd_2Tc_2O_7$ investigated do not show congruent leaching and the release of Tc was about a factor 7 higher than the release of the lanthanides. This high selective leaching of Tc is a result of microscopic inclusions of metallic technetium in the pellets. We further successfully fabricated $Nd_2Tc_2O_7$

specimens entirely by hot uniaxial pressing after 24 hours at 1000 °C and 80 MPa. These specimens show an average specific mass loss of 7.37 10^{-6} g/mm^2•days.

Alternative to radioactive specimens, we fabricated surrogate pyrochlore waste forms with the stoichiometry $Sm_2Ru_2O_7$. The ceramic ruthenates are characterized by low theoretical densities (≈50 %) similar to the technetates and their susceptibility to leaching/corrosion is comparable as well. In 7-days corrosion testing an average specific mass loss of 2.998 10^{-6} g/mm^2•days was determined. At this we have noticed that the retention of Ru^{+4} bond in the crystal structure is better than the retention of Sm^{+3} under the given corrosion scenario and the corrosion is not strictly congruent and the leachates contain higher concentrations of Sm than of Ru.

To address the research tasks 3 and 4 and to gain knowledge on the mechanism of the waste from matrix corrosion we prepared specimens for SEM-based energy-dispersive X-ray spectroscopy (EDS). To determine whether the corrosion is congruent or heterogeneous, specimens were prepared in an orientation perpendicular to the surface which was exposed to corrosion and the leaching media and small (3 mm) segments were polished off from the pellet-rims. This allowed us to eventually determine alterations in the elemental lanthanide to technetium ratios as a result of selective leaching. Based on elemental analysis of the leachates, the pyrochlore pellets $Pr_2Tc_2O_7$ and $Nd_2Tc_2O_7$ showed some degree of incongruent (heterogeneous) leaching, but in such a minor degree, that it could not be confirmed by SEM-based microanalysis and the elemental ratio lanthanide to technetium was very much 1:1. SEM-based EDS analysis on porous microstructures with µm-grain sizes could not provide the sensitivity needed to quantify chemical alterations with sufficient accuracy and reproducibility. We therefore considered the use of laser ablation mass spectrometry (LA-ICP-MS) for quantitative microanalysis but the spatial resolution is with 0.5-1 mm insufficient. Electron probe micro-analysis (EPMA) is the method of choice for microanalysis, but did not provide satisfactory results because of high porosity and the small crystallite sizes which define the pyrochlore microstructures. The microstructure of $Pr_2Tc_2O_7$ after hot-pressing and high-temperature sintering showed open porosity of about 50 % and loosely arranged crystallites in the size range between 2 and 50 µm. $Nd_2Tc_2O_7$ showed lower crystallinity and noticeably smaller crystallites. However the corrosion experiments to not induce any measurable alteration in the microstructures of any waste form pyrochlore tested.

Specimens of $Sm_2Ru_2O_7$ pyrochlore surrogate waste forms were prepared for SEM-based EDS to investigate selective leachability and matrix corrosion. The microstructure of $Sm_2Ru_2O_7$ was imaged using electron microscopy and quantitative SEM-based EDS analysis. Even though the data show significant scattering, the overall trend shows higher relative Ru concentrations (lower Sm concentrations) at the rim-area of the pellet. Therefore we can conclude a deviation of the expected congruent corrosion scenario due to relatively increased leaching of samarium in contact to the leachate under the test conditions. This observation is also confirmed by the results of the corrosion tests and the lanthanides samarium, neodymium showed higher susceptibility to leaching than Ru or Tc. The relative Sm and Nd concentrations within the leachates were elevated by a factor 2 to 3, relative to the concentrations of Ru or Tc.

To determine whether the corrosion is congruent or heterogeneous, a specimen of $Sm_2(Ru_{0.5}Ti_{0.5})_2O_7$ was prepared for SEM-based EDS analysis in an orientation perpendicular to the surface formerly

exposed to the corrosion medium. Successive spectra were collected starting from the edge (former surface) and then moving inwards in 30 µm steps. The specimen contains two crystallographic phases $Sm_2(Ru_{0.5}Ti_{0.5})_2O_7$ and $Sm_2(Ti_{1-x}Ru_x)O_5$, therefore a low Ru-content might indicate the presence of the latter. Even through EDS point analysis shows significant data scattering, probably as a result of small grain sizes and insufficient absorption correction, the corrosion scenario can be described as congruent rather than heterogeneous since overall changes in the ratio trivalent/tetravalent cations ($Sm^{3+}/(Ru^{4+}+Ti^{4+})$) as a function of distance to the corroded surface cannot be concluded.

Thermophysical property measurements under task 5 have not been addressed in a way we intended to do. Our aim was to improve waste form properties in regard to density, microstructure and mechanical properties first, before engaging in expensive liquid helium-heavy measurements using the physical property measurement system (PPMS). In earlier studies we have discovered superconductivity of Tc-bearing ternary oxides ($SrTcO_3$, and Sr_2TcO_4) through a.c. susceptibility measurements at surprisingly high critical temperatures (Tc) of 7.8 K and 7.0 K, respectively. The ruthenium homolog Sr_2RuO_4 has a critical temperature for superconductivity of Tc = 0.9 K. Our aim was to collect heat capacity data of the ceramic Tc-based waste forms but we haven't addressed this task by now.

2. Experimental Results

The NEUP project 3445 produced a vast amount on results which are compiled within this chapter and listed based on the tasks proposed in the narrative:

a) Fabrication of dense, single phase, Tc-bearing ceramic monoliths
b) Thermodynamics and kinetics of Tc-leaching
c) Thermodynamics and kinetics of Tc waste-form matrix corrosion
d) Microstructural waste form corrosion mechanism
e) Thermophysical properties of advanced Tc waste forms

2.1 Fabrication of dense, single phase, Tc-bearing ceramic monoliths

The fabrication of dense, single phase Tc bearing ceramic monolithic waste forms is the cornerstone of the experimental aspects of this NEUP project and we gained a great deal of knowledge by pursuing a variety of strategies including dry chemical processing and wet chemical synthesis with changing protocols for high-temperature annealing and sintering. Our experimental endeavor was only possible because handling gram amounts of technetium oxide powder in the UNLV radiochemistry laboratories was possible and all radiological measures to control and mitigate potential contamination were available and in place.

2.1.1 Design and fabrication of a radiological uniaxial press

In 2006 we initiated our experimental research on the fabrication of lanthanide-technetium pyrochlore. We were successful in fabricating highly crystalline, phase-pure $Ln_2Tc_2O_7$ pyrochlore structures (for Ln = Pr, Nd, Sm, Gd, and Lu) as loose powders (50-150 mg) applying dry-chemical synthesis in platinum

coupons vacuum-sealed in fused silica ampoules[1]. We were confident, that the pyrochlore structure type can serve as an excellent waste form since technetium is structurally bond as tetravalent cation and because of its structural relation to the anti-fluorite structure type of e.g. urania or zirconia. These structures show, in ion-beam irradiation studies, exceptionally high tolerances to radiation damage and therefore it is very unlikely, that also the pyrochlore structures could be altered in any way due to the decay of technetium (λ=213,000 years, β^-, Q = 293.5 KeV). However, to consider pyrochlores as viable waste form candidates for immobilizing fission technetium we must be able to fabricate them as dense monolithic ceramics in at least gram size quantities. One potential approach to achieve this is to apply sintering under uniaxial load at elevated temperature.

We entertained an engineering senior design project with students from mechanical engineering and electrical engineering and computer science in order to design, build, program and test a radiological uniaxial hot press[2][3]. In FY 2013 we could report the development and advancement of the Remote Operated Hot Uniaxial Press (ROHUP) for fabricating, dense, gram-size, single phase, ^{99}Tc-bearing ceramic waste forms. Designing, machining or procuring of all structural components and the final assembly was completed in FY 2013. The flowchart in Figure 1 sketches the overall ROHUP development stages during this senior design project to represent the mark I design stage

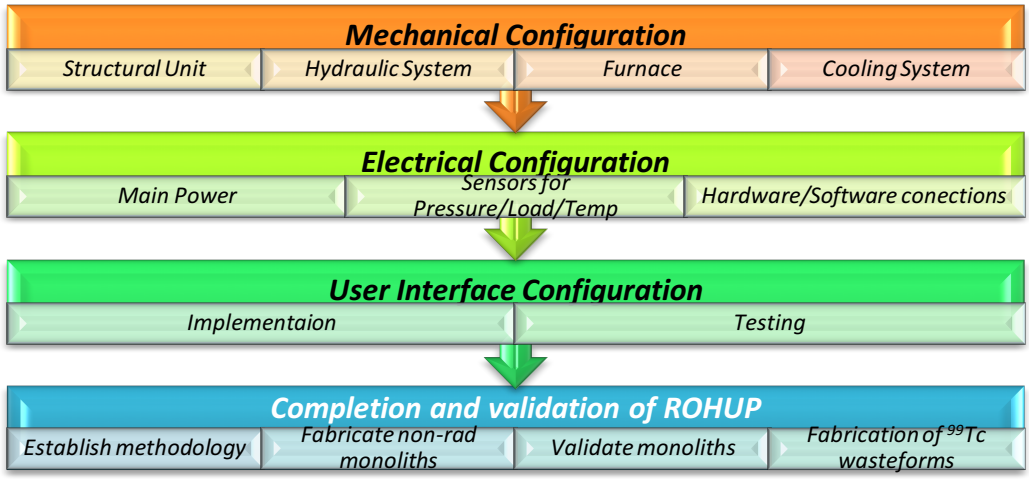

***Figure 1**: Flowchart to display the hot-press (ROHUP) development stages.*

[1] **T. Hartmann**, **A. Alaniz**, **F. Poineau**, **P. F. Weck**, **J. A. Valdez**, **M. Tang**, **G. D. Jarvinen**, **K. R. Czerwinski** and **K. E. Sickafus**: Structure Studies on Lanthanide Technetium Pyrochlores as Prospective Host Phases to Immobilize 99Tc and Fission Lanthanides from Effluents of Reprocessed Used Nuclear Fuels. Journal of Nuclear Materials, 411, 60-71, (2011).

[2] **A.J. Alaniz**, **L. Delgado**, **B. Werbick**, **T. Hartmann**: Prototype Development of a Remote Operated Hot Uniaxial Press (RoHUP) for the Fabrication of Tc-99 Bearing Waste Forms. WM2013 Conference, February 24 – 28, 2013, Phoenix, Arizona USA.

[3] **A.J. Alaniz**, **L. Delgado**, **B. Werbick**, **T. Hartmann**: Remote Operated Hot Uniaxial Press to Fabricate Tc-99-Bearing Waste Forms. Atalante 2012: Nuclear Fuel Cycle for a Sustainable Fuel Cycles, Montpellier, France, 2-7 September, Proceedings, A168 (2012).

The mark I radiological hot press design (ROHUP) is displayed in figure 2 together with the solid works drawing.

Figure 2: *Mark I design of a remote operated radiological uniaxial press (ROHUP) together with the Solid Works drawing.*

In FY 2014 we applied modifications to the hot press design for better pressure control in the low-pressure application regime and loads between 50 to 150 MPa. These design changes were necessary to operate the hot press on small samples and 5-mm graphite dies for high-temperature sintering. Pressure control provided by the large 20,000 PSI hydraulic system was lacking in the lower pressure regime. For experiments in this low-pressure range the hydraulic system was replaced by a mechanical lever, where the compressive load is applied by the addition of per-calibrated lead weights.

Figure 3 shows changes to the top-part of the hot press assembly of the modified system. A new top plate was machined to incorporate a lever that will apply a weighted force to the top of the specimens. For simplicity reasons we replaced the hydraulic components with a robust level design where the pressure can be adjusted by adding previously calibrated lead weights to the lever. For the calibration a Futec pressure sensor was used and the final applied load is a result of the addition of each individual lead weight. This setup allows for more accuracy than the previous method.

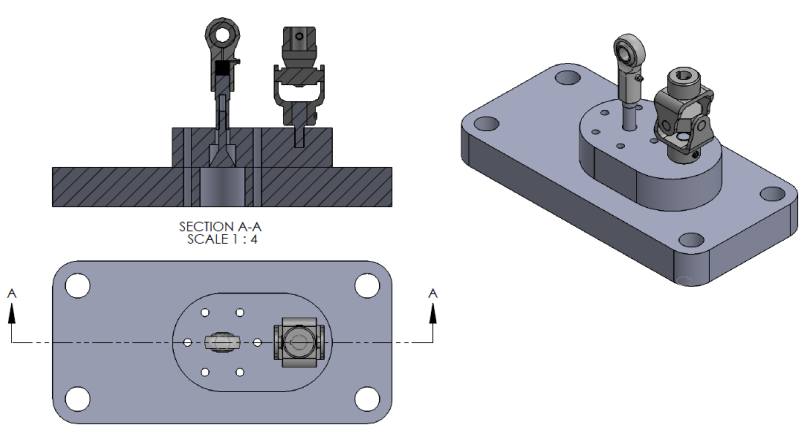

Figure 3: *Solid-Works Drawing of Modified Top Plate Assembly operating the Hot Press in a Low-Pressure Regime*

Subsequently, the Hot Uniaxial Press (HUP) was now successfully implemented in a standard-size glove box and operates in the low-pressure range (50-100 MPa) using 5-mm graphite dies under argon atmosphere and at temperatures up to 1100 °C. Figures 4 and 5 show the Hot Uniaxial Press sintering $SrTCO_3$ at 770 °C and 75 MPa under argon atmosphere in a standard-size radiological glove box.

Figure 4: *Hot Uniaxial Press implemented in a standard size glove box operating at 770 °C and 75 MPa under argon. The lead weights (right) are marked and calibrated for pressure in regard to the current level settings*

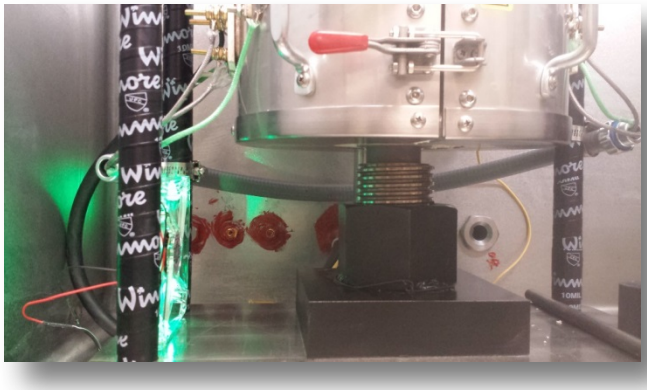

Figure 5: *Adjustable stage of Hot Uniaxial Press together with temperature control for stage and hot press stand. Air cooling was implemented at 770 °C furnace temperature the temperature at the stage close to the corundum support was measured to be 125 °C, and the bottom plate at frame to be 50 °C.*

The mark II design was used during the course of this proposal, manufacturing dense technetium-bearing ceramics. In FY 2014 the hot uniaxial press was used to successfully fabricate three pellets of $SrTcO_3$ perovskite with masses of about 0.20 gram each. The monolithic specimens were fabricated by sintering the stoichiometric powder mixture at 770 °C under a load of 75 MPa for 7 days in an argon atmosphere. The achieved densities were with about 75% theoretical still rather low and the mechanical strength were not great as well, but sufficient to survive the sample preparation procedure prior to corrosion testing. We further produced three pellet of "Sr_2TcO_4" after sintering at 570 °C, 550 °C and 650 °C and 75 and 80 MPa for 8-12 days under argon atmosphere. Under the condition of the hot uniaxial press and the graphite die materials, tetragonal Sr_2TcO_4 could not be obtained with large yields and SrO was still present after sintering despite changing the sintering temperature from 570 °C to 550 °C and 650 °C under a load of 80 MPa. However, sintering at 650 °C induced the formation of a proto-crystalline phase which can be indexed based on the tetragonal K_2NiF_4 lattice of Sr_2TcO_4. The fabrication of technetium-or ruthenium pyrochlore required sintering temperatures of about 1150 °C. Under the reducing conditions of the hot uniaxial press mediated by the graphite die material, reduction of either metal is initiated at temperatures as low as 700 °C. Further increasing temperature to 900 °C or 1100 °C induced the reduction of technetium to the metallic state and sintered pellets exhibited metallic inclusions of Tc or Ru, and significant increased leaching in subsequent corrosion tests. We have tested corundum as die material and Friatec AG (Friedrichsfeld, Germany) was able to fabricate alumina dies with high precision and their use as dies was successful in order to synthesize technetium containing ceramic monoliths. However, the alumina piston tends to jam in the die and a sample recovery was not always possible and the use of a suitable lubricant is beneficial.

In FY 2016, the lever system was replaced by an electro-mechanical mechanism to allow for precise pressure control in the range from 50 to 400 MPa (Figure 6). This new design was implemented and the Arduino code tested. It is also important to note that a newly designed automated hot press will be used in place of the manual press in making the 6-mm diameter pellets. The hot press consists of four basic components: the controller, load cell, pressing apparatus, and a furnace. The user provides the following input: desired pressure, size of die to be used, and length of time to be pressed. The controller will apply an electrical current to the press motor, which will apply a load to the die and is controlled by the load cell which actively monitors the load applied to the die; if the load is ever found to drop, the controller will apply pressure once more until the desired pressure is achieved. The controller was designed using an Arduino Mega 2560, 20x4 LCD display, 4x3 keypad, hx711 load cell amplifier, and a motor driver. In terms of the rest of the hot press: the furnace and load cell were purchased from a third party, while the pressing apparatus consists of a geared press attached to a high torque motor.
The following images are showing the new design features for the hot-uniaxial press (Figures 6).
We further have written a new code for the Arduino controller for optimized pressure control.

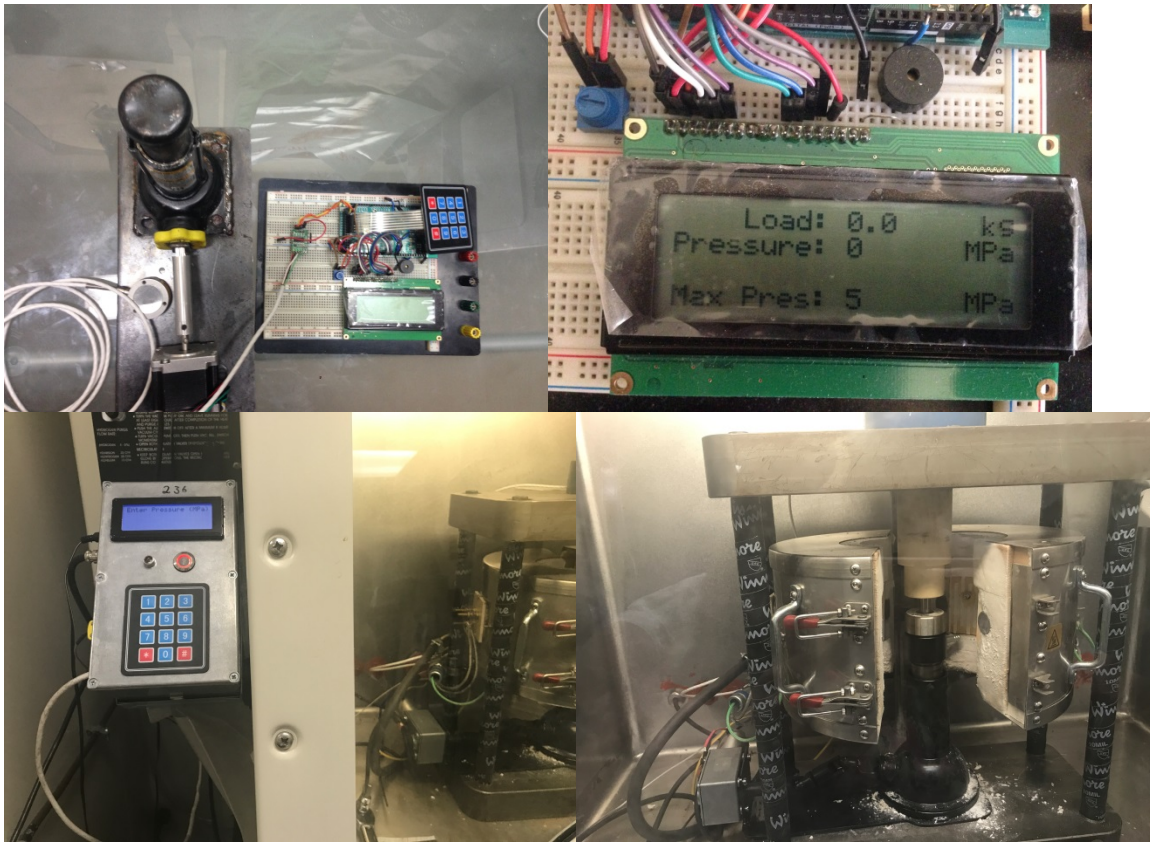

Figure 6: *Mark III uniaxial hot press design applying an electro-mechanical load system and a hard-wired controller. The hot press is located in a radiological atmosphere controlled glove box.*

2.1.2 Fabrication of ceramic $SrTcO_3$ perovskite

To fabricate monolithic $ScTcO_3$ perovskite waste forms using the mark II hot uniaxial press we machined several sets of 5 mm graphite using 45 mm and 5 mm rod material. The (nuclear grade) graphite was purchased from SGL, Germany, had has highest density and superior mechanical properties (Figure 7).

Figure 7*: Machined 5-mm graphite dies from 45 mm SGL high density rod material (left) with piston assembly and Pt diffusion inhibitors (right). The sample will be placed between the Pt discs.*

For the synthesis of $SrTcO_3$ perovskite, a stoichiometric powder mixture of pre-annealed SrO and re-crystallized TcO_2 was ground in an Agate mortar with acetone and separated into 3 samples of about 0.2 g each. For the first sample no binder was added, while 10 wt.-% and 1 wt.-% zinc stearate (binder) were added for the other samples, respectively and mixed by vortexing for 1 minute. The powders were funneled into the dies and sandwiched between 5 mm Pt diffusion inhibitors within the graphite piston assemblies.

The die assemblies were transferred into the HUP glove box and placed between the ceramic support parts (corundum, custom-made by Friatec AG, Friedrichsfeld, Germany) and shielded by a fused silica tube. The fused silica tube is surrounding the graphite die assembly and any volatilization of Tc as Tc_2O_7 would condensate as yellow precipitation at the colder zones of the glass. So far, no condensation was observed. After raising the stage, the clam-shell furnace was closed and the pressure (load) was step-wise increased by adding weight to the lever. The pressure was set to 75 MPa and the temperature to 450 °C to eventually decompose the binder. After 1 hour the temperature was raised to 770 °C. The argon pressure of the glove box was set slightly above atmospheric pressure to avoid potential oxidation of the die material. After 7 days at 770 °C and 75 MPa under argon atmosphere the monolithic pellets were removed from the dies and analyzed. The use of binder has a significant impact on the pellet densities and the monolithic $SrTcO_3$ perovskite samples were sintered to theoretical densities of 71 %, 33 %, and 66% using 0 wt.%, 10 wt.% or 1 wt.% binder, respectively. The use of 1 wt.% binder is recommended for radiological reasons and to mitigate the spread of powders in the glove box.

The crystalline phase content of the uncrushed $SrTcO_3$ monolithic pellets were analyzed by XRD/Rietveld structure refinement techniques and the presence of tetragonal (*Imma*) $SrTcO_3$ perovskite as major phase was confirmed (Figure 8). Using the uncrushed pellet lowered the quality of the collected data but allowed for subsequent corrosion testing.

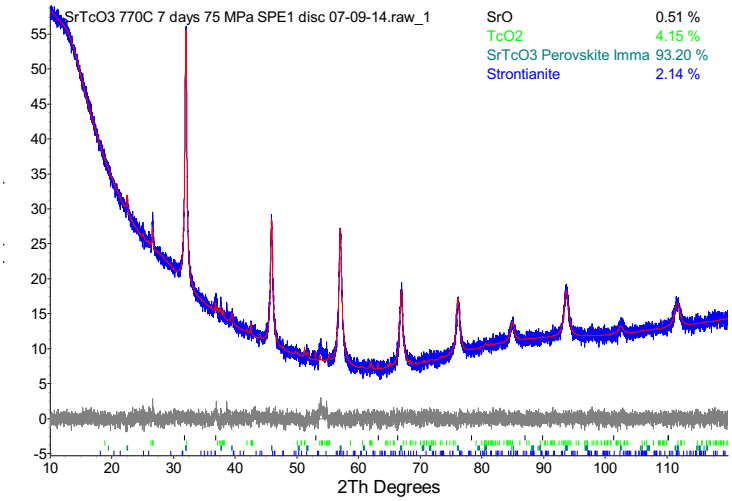

Figure 8: *XRD/Rietveld analysis of $SrTcO_3$ after 7 days at 770°C and 75 MP. The HUP-based synthesis was successful and the presence of tetragonal $ScTcO_3$ as major phase was confirmed. The pattern was taken from the uncrushed pellet.*

The hot-press based synthesis of monolithic $SrTcO_3$ specimens was very much successful and the mechanical properties of the pellets were sufficient to allow for sample preparation by grinding and polishing.

2.1.3 Fabrication of ceramic Sr_2TcO_4 layered perovskite

To synthesize monolithic Sr_2TcO_4 layered perovskite, stoichiometric powder mixture of pre-annealed SrO and re-crystallized TcO_2 was ground in an Agate mortar with acetone and separated into 3 samples of about 0.2 g each. All samples were blended with 1 wt.-% zinc stearate (binder) by vortexing for 1 minute. The powders were funneled into the graphite dies and sandwiched between 5 mm Pt diffusion barriers. The pressure of the hot press was set to 80 MPa and the temperature raised to 450 °C and after 1 hour to 570 °C, 550 °C, or 650 °C. The argon pressure of the glove box was set slightly above atmospheric pressure and after 10 days the monolithic pellet were removed and analyzed.

While the synthesis of monolithic $SrTcO_3$ pellets using the hot press was fully successful, the synthesis of monolithic Sr_2TcO_4 pellets was not. After sintering at 650 °C we observed a grow-in of a proto-crystalline phase which can be indexed based on a Sr_2TcO_4 lattice (Figure 9). The sintered monolithic Sr_2TcO_4 pellets did undergo swelling and disintegration within 2 hours after exposing to atmospheric conditions due to the hydrolysis of unreacted SrO (Figure 10).

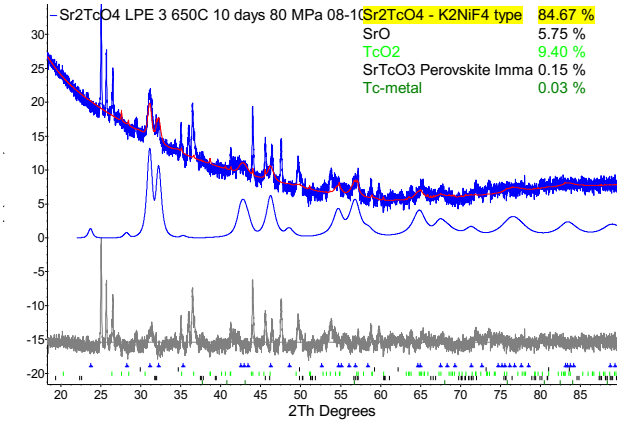

Figure 9: *XRD/Rietveld analysis of monolithic "Sr_4TcO_4"pellet after 10 days at 650 °C and 80 MPa. The calculated content of the "Sr_2TcO_4" phase is highlighted (blue pattern). Sintering at 650 °C induced the grow-in of a proto-crystalline phase which can be indexed based on a Sr_2TcO_4 lattice.*

Figure 10: *HUP produced monolithic "Sr_2TcO_4"pellet (10 days at 570°C and 80 MPa), before (top) and after (bottom) XRD analysis. The pellet lost its physical integrity during the 2 hours of XRD analysis due to swelling and potentially the formation of strontium hydroxide.*

2.1.4 Fabrication of ceramic lanthanide-technetium and ruthenium pyrochlores

In this chapter we would like to provide an overview on the different attempts and synthesis route to eventually fabricate monolithic samples of lanthanide-technetium pyrochlore. Small 50-100 mg amounts of $Ln_2Tc_2O_7$ pyrochlore (Ln = Pr, Nd, Sm, Gd, Lu) could be fabricated as rather loose powder by dry-chemical synthesis and sintering of stoichiometric oxide mixtures at 1150 °C for 2-3 days in vacuum sealed platinum coupons[1]. The fabrication of dense ceramic technetium pyrochlores is the essential research task in this NEUP project and the information are provided in chronological order.

2.1.4.1 Fabrication of ceramic lanthanide-technetium pyrochlore by hot-uniaxial pressing

To fabricate monolithic $Nd_2Tc_2O_7$ pyrochlore, stoichiometric powder mixtures of pre-annealed Nd_2O_3 and re-crystallized TcO_2 were ground in an agate mortar with acetone and separated into triplets of about 0.3 g each. All samples were blended with 1 wt.-% zinc stearate (binder) by vortexing for 1 minute. The powders were funneled into the graphite dies and sandwiched between 5-mm Pt disks which act as diffusion barriers for carbon. The pressure of the hot press was set to 80 MPa by the addition of pre-calibrated lead-weights onto the lever system of the Mark II design. The furnace temperature was raised to 500 °C to eventually decompose the Zn-stearate binder, and after 1 hour to 1100 °C, or to 900 °C. The argon pressure of the glove box was set slightly above atmospheric pressure to avoid potential oxidation of the die material. After 3 days at 1100 °C or 2 and 7 days at 900 °C and 80 MPa, the monolithic pellet were removed from the graphite die and analyzed by XRD (Figure 11). After 3 days at 1100 °C phase analysis showed a complete reduction of TcO_2 to metallic Tc and the Nd_2O_3 did not participate in solid state reaction. As a result, phase formation of $Nd_2Tc_2O_7$ pyrochlore was virtually absent as a result of Tc reduction by the graphite dies at elevated temperature. Following these observations, sintering at temperatures above 700 °C in contact to graphite induces the reduction of technetium and ruthenium. Therefore we may have to use different die material such as corundum and/or limit the hot press temperature to 700 °C and apply a subsequent sintering step at 1150 °C under inert (non-reducing) conditions using fused silica ampoules and a regular tube furnace.

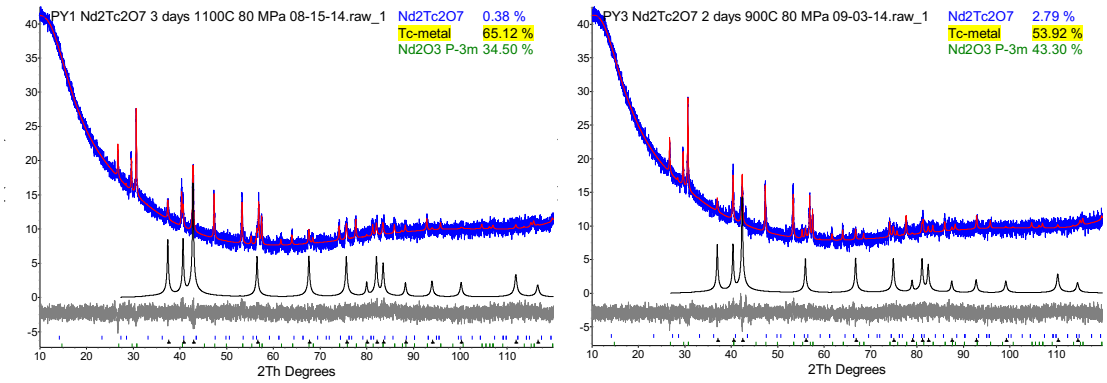

Figure 11: *XRD/Rietveld analysis of HUP produced monolithic "$Nd_2Tc_2O_7$"pellets after 3 days at 1100 °C (left) and 7 days at 900°C (right). In all cases $Tc^{[IV]}$oxide was nearly completely reduced to technetium metal.*

2.1.4.2 Fabrication of ceramic lanthanide-technetium pyrochlore by hot-uniaxial pressing at 700 °C followed by pressure-less sintering at 1150 °C

A stoichiometric powder mixture of pre-annealed Nd_2O_3 and re-crystallized TcO_2 was ground in an agate mortar with acetone and separated into triplets of about 0.3 g each. All samples were blended with 1 wt.-% zinc stearate (binder) and the powders were funneled into the graphite dies and sandwiched between 5-mm Pt disks. The load of the hot press was set to 80 MPa by the addition of pre-calibrated lead-weights onto the lever system (Mark II design). The furnace temperature was raised to 500 °C to eventually decompose the Zn-stearate binder, and after 1 hour to 700 °C. After 2 days at 700 °C, the monolithic pellets were removed from the graphite die and vacuum-sealed in fused silica tubes for subsequent 3 days sintering at 1150 °C (Figures 12).

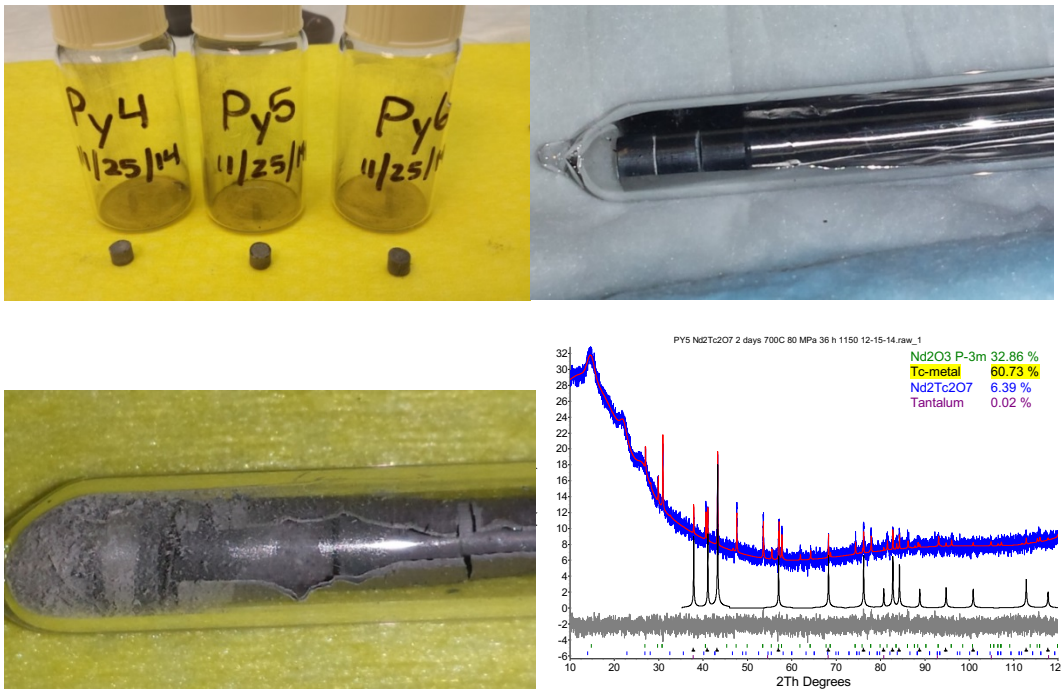

Figure 12: *$Nd_2Tc_2O_7$ pyrochlore pellets after hot pressing at 700 °C (top left), after vacuum sealing in fused silica (top right), after annealing at 1150 °C for 3 days (bottom left). The tantalum foils, which was inserted as diffusion inhibitor suffered oxidation and corrosion and eventually also induced the reduction of technetium. XRD-based phase analysis (bottom right) indicated the reduction of technetium but also increased amounts of pyrochlore phase of about 6 wt.-%.*

The achieved theoretical densities are with 3.56 g/cm^3 and 51 % theoretical (based on $Nd_2Tc_2O_7$) much lower than expected (Table 2) and the density we have observed after pressure-less sintering. The reduction of technetium oxide after at 700 °C under hot press condition followed by pressure-less

sintering at 1150 °C is very much surprising and lowering the hot-press temperature eventually to 600 or 500 °C might not be an option. Tantalum foil was introduced as diffusion barrier the high temperature annealing step. We were surprised noticing severe oxidation of tantalum during high-temperature sintering in contact to the pyrochlores. In this regard, the contact with tantalum might have caused the reduction of technetium oxide to some degree.

Table 2: *Fabrication of "$Nd_2Tc_2O_7$" Pellets by hot-pressing at 700 °C and subsequent pressure-less sintering at 1150 °C.*

$Nd_2Tc_2O_7$ Pellet	PY 4	PY 5	PY 6
Sintering conditions	2 days 700 °C @ 80 MPa, 3 days @ 1150 °C	2 days 700 °C @ 80 MPa, 3 days @ 1150 °C	2 days 700 °C @ 80 MPa, 3 days @ 1150 °C
Mass of Powder before sintering	0.2823 g	0.3381 g	0.3431 g
Mass of Powder after sintering (difference %)	0.2439 g 0.0384 g, -13.6 %	0.2905 g 0.0476 g, -14 %	0.3063 g 0.0368 g, -10.7 %
Density (g/cm^3)	3.36	3.72	3.56
Theoretical pellet density considering $Nd_2Tc_2O_7$ ρ = 7.03 g/cm^3	48 %	53 %	51 %
Observation	Metallic Tc, unreacted Nd_2O_3, little pyrochlore	Metallic Tc, unreacted Nd_2O_3, little pyrochlore	Metallic Tc, unreacted Nd_2O_3, little pyrochlore

2.1.4.3 Fabrication of $Pr_2Tc_2O_7$ and $Nd_2Tc_2O_7$ pyrochlore by hot-pressing and pressure-less sintering of ceramic precursors

Stoichiometric powder mixtures (about 300 mg) of pre-annealed Pr_2O_3 orNd_2O_3 powder (Strem Chemicals) and re-crystallized TcO_2 were ground in an agate mortar with acetone, cold-sealed in platinum envelopes, vacuum-sealed in fused silica tubes, and sintered at 1150 °C under argon for 72 hours. The successful synthesis of phase-pure $Pr_2Tc_2O_7$ and $Nd_2Tc_2O_7$ pyrochlore powders was confirmed by X-ray diffraction and Rietveld structure refinement. These pyrochlore powder precursors were blended with 1 wt.-% zinc stearate (binder) by vortexing for 1 minute and the powders were funneled into the graphite dies and sandwiched between 5-mm Ta disks for hot-press based palletization.

The hot press load was set to 80 MPa by the addition of pre-calibrated lead-weights onto the lever system (Mark II design) and the furnace temperature was raised to 500 °C to eventually decompose the Zn-stearate binder, and after 1 hour to 700 °C. After 3 hours at 700 °C, the monolithic pellets were removed from the graphite die, vacuum-sealed in fused silica tubes which were sleeved with platinum foil, and sintered at 1150 °C under argon for 3 days (Figures 13).

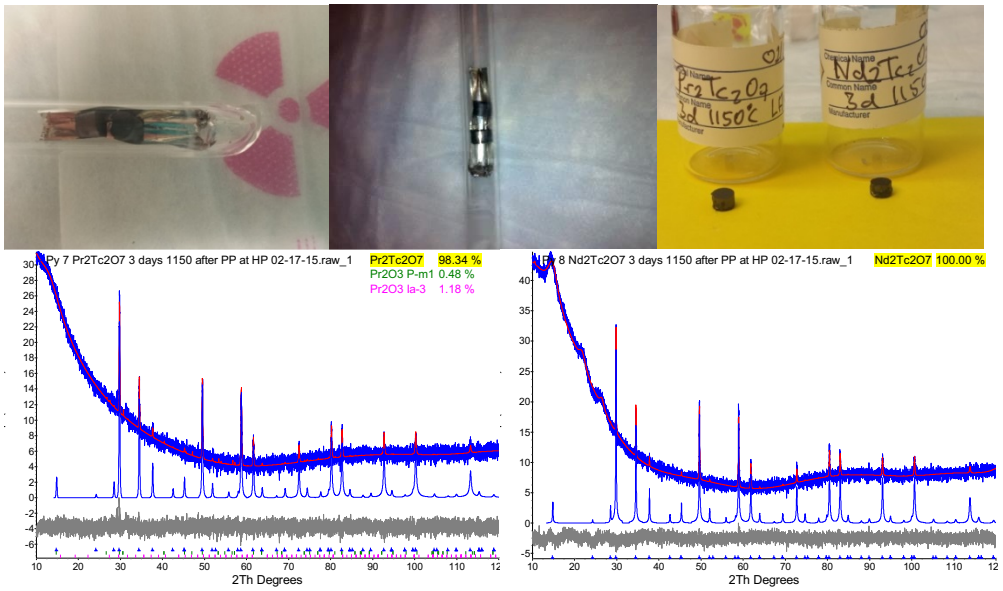

Figure 13: *Pr_2Tc_2O7 & $Nd_2Tc_2O_7$ pyrochlore precursor pellets in sealed fused silica ampoules before (top left) and after sintering (top middle), pellets after final sintering (top right). Phase analysis showed virtually phase pure $Pr_2Tc_2O_7$ and $Nd_2Tc_2O_7$ pyrochlore pellets and hot-uniaxial pressing of ceramic precursor at 700 °C and subsequent high temperature sintering might be a successful route for dry chemical fabrication of ceramic monolithic technetium pyrochlores*

Hot-pressing of precursor powders at 700 °C for 3 hours and subsequent sintering for 3 days at 1150 °C did not induce the reduction of technetium oxide and virtually phase pure technetium pyrochlores were obtained. In addition, the pellets showed sufficient mechanical strength to persist grinding and polishing for subsequent corrosion testing. However, the technetium-based pyrochlores still show porous microstructures eventually due to the lack of inter-diffusion and material transport during the sintering process and the achieved theoretical densities are lower than expected. For $Pr_2Tc_2O_7$ we measured a density of 4.149 g/cm^3 and 68.2 % theoretical, and for $Nd_2Tc_2O_7$ we observed a density of 3.891 g/cm^3 and 55.3 % theoretical (Table 3).

Table 3: *Fabrication of $Pr_2Tc_2O_7$ and $Nd_2Tc_2O_7$ Pellets PY 7 and PY 8*

Pyrochlore Pellet	PY 7	PY 8
Sintering conditions	Fabrication of ceramic precursor, compacting powder at 700°C @ 80 MPa for 3 hours, sintering pellets for 3 days at 1150 °C under argon	
Mass of Pellet after sintering	0.27826 g	0.25510 g
Volume of Pellet	0.06707 cm^3	0.06556 cm^3
Density (g/cm^3)	4.189	3.891
Theoretical pellet density ($Pr_2Tc_2O_7$, $Nd_2Tc_2O_7$ ρ = 6.09 & 7.03 g/cm^3)	68.2 %	55.3 %
Observation	Pellets with sufficient mechanical strength for subsequent corrosion testing Amount of precursor was not sufficient to cut pellets into triplicate discs.	
Future Measure	Grinding and polishing for C1220 corrosion testing to come, SEM-based microstructural analysis	

2.1.4.4 Fabrication of $Sm_2Ru_2O_7$ pyrochlore surrogate waste form using custom made corundum die sets

To allow for hot uniaxial pressing of oxide powder mixtures at elevated temperatures (700 – 1100 °C) we have designed two die sets using DEGUSSIT AL23 corundum as die material of choice (Figure 14). In the past we have noticed significant reduction of RuO_2 and TcO_2 and the formation of metallic Ru and Tc inclusions while using graphite dies at temperatures of 700 °C and higher. The use of corundum (Al_2O_3) might prevent the reduction of RuO_2 and TcO_2 and further allows for significant higher loads during hot-pressing. The FRIATEC AG is one of the leading companies and was willing to manufacture two corundum (DEGUSSIT AL23) 5-mm die sets with surface finishes of 6 μm and overall tolerances of 1/100 mm (10 μm). AL23, our material of choice, shows high compressive strength (3.5 GPa), combined with a low linear expansion coefficient (8.2 10^{-6}/K) and a maximum service temperature (in air) of 1950 °C.

Figure 14: *Ceramic corundum (DEGUSSIT AL23) 5-mm die-set fabricated by FRIATEC AG with tolerances of 1/100 mm and a surface finish of 6 μm*

A triplicate of non-radioactive samples were fabricated in a combination of hot uniaxial pressing and high temperature annealing using custom made alumina (corundum) die material. For these experiments we replaced the graphite dies with corundum to avoid reduction of technetium oxide and ruthenium oxides as earlier observed. Here we have successfully fabricated $Sm_2Ru_2O_7$ using hot uniaxial pressing with AL23 dies at 700 °C and 80 MPa, followed by high temperature synthesis at 1150 °C in vacuum-sealed and Pt-sleeved fused silica tubes. After corrosion testing the phase content of the samples were analyzed and XRD pattern and Rietveld refinement plot is displayed in Figure 15. The presence of the cubic $Sm_2Ru_2O_7$ pyrochlore phase as well as the grow-in of orthorhombic Sm_3RuO_7 with pentavalent ruthenium was observed.

To fabricate surrogate $Sm_2Ru_2O_7$ pyrochlore samples, a stoichiometric powder mixture of pre-annealed Nd_2O_3 and RuO_2 (Strem Chemicals) was ground in an agate mortar with acetone and separated into 3 samples of about 0.3 g each. All samples were blended with 1 wt.-% zinc stearate (binder) by vortexing for 1 minute. The powders were funneled into the custom-made DEGUSSIT AL23 corundum die. The load of the hot press was set to 80 MPa. The furnace temperature was raised to 500 °C to decompose the Zn-stearate binder, and after 1 hour to 700 °C. After 1 day at 700 °C, the monolithic pellets were

removed from the corundum die and vacuum-sealed in platinum-sleeved fused silica tubes for subsequent 3 days sintering at 1150 °C (Figure 15).

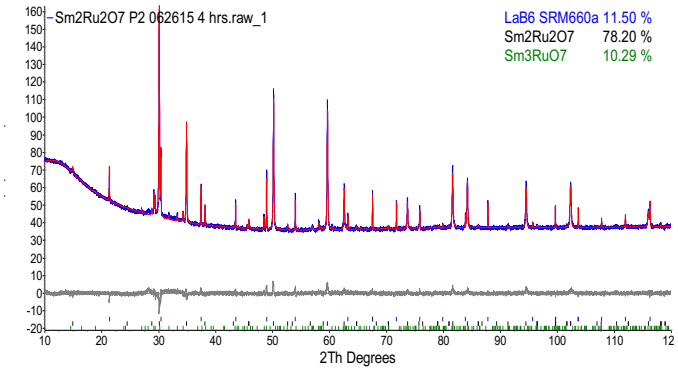

***Figure 15:**.XRD/Rietveld structure refinement of $Sm_2Ru_2O_7$ after C1220-10 corrosion testing for 7 days. The presence of $Sm_2Ru_2O_7$ pyrochlore phase (88.4 (± 0.3) wt.-%) as well as the grow-in of Sm_3RuO_7 (11.6 (± 0.3) wt.-% were observed. The partial oxidation of ruthenium might be a result of sintering the hot pressed pellets in fused silica ampules. Even though the silica tubes were sleeved with platinum foil, partial contact between pellet and silica tube was not completely prevented and the partial oxidation of ruthenium initiated the formation of orthorhombic Sm_3RuO_7 in the contact zone*

The geometric data of the fabricated surrogate $Sm_2Ru_2O_7$ pellets after their preparation for the envisioned subsequent corrosion testing are listed in Table 4. The sintered densities $Sm_2Ru_2O_7$ pellets are with between 43 to 49 % theoretical, low.

***Table 4**: Fabrication of $Sm_2Ru_2O_7$ surrogate fuel pellets using hot-uniaxial pressing in corundum die followed by high temperature sintering in vacuum-sealed fused silica ampoules*

Pyrochlore Pellet	PY 9	PY 10	PY 11
Sintering conditions	Fabrication of ceramic precursor, compacting powder at 700°C @ 80 MPa for 3 hours, sintering pellets for 3 days at 1150 °C under argon		
Mass of Pellet after sintering (gram)	0.20065	0.18708	0.21585
Volume of Pellet (cm^3)	0.05765	0.05766	0.05845
Density (g/cm^3)	3.481	3.245	3.693
Surface Area (cm^2)	0.8761	0.8847	0.8783
Theoretical pellet density ($Sm_2Ru_2O_7$ ρ = 7.53 g/cm^3)	46.2 %	43.1 %	49.0 %
Observation	Pellets with sufficient mechanical strength for subsequent corrosion testing. Formation of green Sm_3RuO_7 in the contact zone to the Pt-sleeved silica ampoule.		

2.1.4.5 Fabrication of $Nd_2Tc_2O_7$ pyrochlore using custom made AL23 corundum die sets

Monolithic samples of $Nd_2Tc_2O_7$ were fabricated using one of the AL23 corundum die set. At this one pellet was sintered for 1 day at 1000 °C and 80 MPa using hot pressing, and two pellets were sintered at 700 °C @ 80 MPa followed by high temperature sintering in vacuum-sealed silica ampules at 1150 or 1160 °C. Sintering under hot press conditions for 24 hours was sufficient to convert most of the educts to $Nd_2Tc_2O_7$ pyrochlore (Figure 16). However, it became apparent that some TcO_2 volatilized and that

the AL23 die material was not inert and secondary phase formation with the oxides was observed. We were unable to remove the complete pellet since the oxides reacted with the die set and the die piston was jammed.

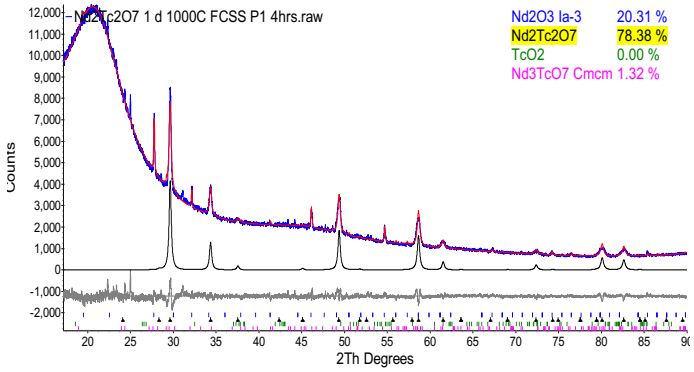

***Figure 16**: XRD/Rietveld Analysis of $Nd_2Tc_2O_7$ after 24 hours sintered in an AL23 corundum die at 1000 °C and 80 MPa. Part of TcO_2 volatilized and the pyrochlore formation yield is therefore low. AL23 is not inert at elevated temperatures and reactions between AL23 and the oxides were observed. The phases pyrochlore, and the new phase, orthorhombic $Nd_3Tc^{[V]}O_7$, were identified*

In agreement with earlier observations in the surrogate Sm_2O_3 – RuO_2 system, technetium can be partly oxidized at high temperature in contact with silica or in this case corundum and the formation of a new phase with penta-valent technetium, $Nd_3Tc^{[V]}O_7$, was characterized and its crystal structure determined Figure 18. $Nd_3Tc^{[V]}O_7$ crystalizes in the orthorhombic space group *Cmcm* and is isomorph with the ruthenate Nd_3RuO_7. Even though the crystallinity of the specimen was not high, we were able to refine the crystal structure of $Nd_3Tc^{[V]}O_7$. The lattice parameters of $Nd_3Tc^{[V]}O_7$ was refined to ***a*** = 10.9695(8) Å, ***b*** = 7.4939(5) Å, and ***c*** = 7.5349(4) Å. The $Nd_2Tc_2O_7$ pyrochlore samples fabricated by hot pressing (24 hrs @ 700 °C/80 MPa) and high-temperature sintering at 1160 °C for 3 days, show pyrochlore formation but also the presence of $Nd_3Tc^{[V]}O_7$ and metallic technetium (Figure 17).

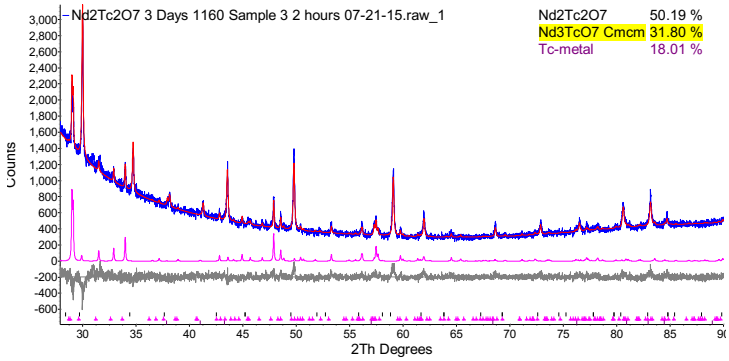

***Figure 17:** XRD-Rietveld analysis of $Nd_2Tc_2O_7$ pyrochlore after hot pressing followed by 3 days at 1160 °C. The phases pyrochlore, metallic technetium and orthorhombic $Nd_3Tc^{[V]}O_7$, were identified.*

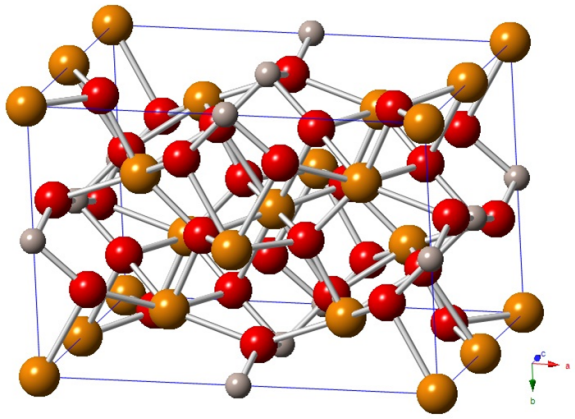

Figure 18: *Refined crystal structure of orthorhombic $Nd_3Tc^{[V]}O_7$ which is isomorph with $Nd_3Ru^{[V]}O_7$ and crystallizes in the space group Cmcm. The lattice parameters of $Nd_3Tc^{[V]}O_7$ could be refined to a = 10.9695(8) Å, b = 7.4939(5) Å, and c = 7.5349(4) Å.*

Annealing under slightly oxidizing conditions at 1160 °C does not only induce the formation of $Nd_3Tc^{[V]}O_7$ with pentavalent technetium, it also enables the disproportionation of technetium dioxide into heptoxide and metallic technetium. The presence of little oxygen above 1100 °C promotes the decomposition of TcO_2 in the reaction scheme: $3TcO_2 + ½O_2 \rightarrow Tc_2O_7\uparrow + Tc$ (metal). In this context, metallic technetium in the samples was formed after the silica ampules lost their integrity and open sintering (under argon) of the pyrochlore samples occurred. In addition condensation of heptoxide at the cooled flange areas of the furnace was confirmed as well.

2.1.4.6 Parametric sintering for improving $Nd_2Ru_2O_7$ pyrochlore densities and mechanical strengths

Parametric sintering studies were engaged on $Nd_2Ru_2O_7$ surrogate pyrochlore waste forms in order to improve materials properties such as density, fracture toughness and compressive strength. Hereby we applied routine ceramic processing by sintering cold-pressed "green" pellets (~5 mm diameter, 250-300 mg) at 1150 °C in argon or in vacuum sealed fused silica ampules.

As a first test we aimed to fabricate $Nd_2Ru_2O_7$ pellets with the intention to increase theoretical pellet densities. As shown in Table 5, our experiments demonstrate that the densities remain virtually unchanged after high temperature sintering process relative to the green pellet densities. This behavior was earlier described for the monolithic $Nd_2Tc_2O_7$ waste form as well. As a result of these first scoping tests, high-temperature sintering did not result increased densities and the oxide particles did not engage in intense inter-diffusion, nucleation, grain growth to closing the pore space, even though the formation of $Nd_2Ru_2O_7$ was achieved. The cold-pressed green pellet densities of 49.5 % in average did not increase after sintering at 1150 °C for 3 days and the pore space contribution remained unchanged. The average density after sintering was with 46.8 %, and nearly identical with the densities of the green pellets. The slight decrease in densities is partly explained by burning off the binder (1 wt.-% zinc stearate) which was added to improve pellet formation during pressing.

***Table 5**: Experimental date on $Nd_2Ru_2O_7$ pellet fabrication before and after sintering.*

Pellet	Process	Binder	Mass (mg)	Diameter (mm)	Height (mm)	Volume (cm^3)	ρ (g/cm^3)	Theoretical Density (%)
RP 1	Hot-pressed @ 700 °C for 1 day	1 %	127.8	5.02	2.58	0.05106	2.508	35
RP 2	Hot-Press @ 700 °C for 1 day	1 %	145.5	5.02	2.77	0.05106	2.85	39
RP 3a	Cold-pressed in steel die @ 400 MPa	1 %	138.1	5.00	1.96	0.0385	3.587	49
RP 3b	Cold-pressed in steel die @ 400 MPa	1 %	80.8	5.00	1.20	0.0236	3.424	47
RP 4	Cold-pressed in steel die @ 400 MPa	1 %	258.7	5.04	2.16	0.0938	3.505	48
RP 5	Cold-pressed in steel die @ 400 MPa	1 %	252.7	5.04	3.25	0.0648	3.897	54
	Sintering in vacuum sealed fused silica ampoules under Argon at 1150 °C for 3 days							

	Mass (mg)	Volume (cm^3)	ρ (g/cm^3)	Theoretical Density (%)	Changes due to Sintering (% absolute)
RP 3a	134.3	0.0453	2.965	41	**-8**
RP 3b	78.1	0.0224	3.487	48	**+1**
RP 4a	153.0	0.0431	3.549	49	**+1**
RP 4b	96.1	0.0310	3.105	43	**-5**
RP 5	245.6	0.0638	3.849	53	**-1**

2.1.4.7 Fabrication of $Sm_2Ru_2O_7$ and $Sm_2(Ru_{0.5}Ti_{0.5})_2O_7$ surrogate waste form using standard ceramic processing

In a first experiment ceramic $Sm_2Ru_2O_7$ pyrochlore was synthesized applying standard dry ceramic processing. At this the oxide powders of Sm_2O_3 and RuO_2 were mixed in stoichiometric proportions and subsequently ground in order to fabricate about 1 g of chemic pyrochlore. Next, the powder was divided into triplicates, each of which was uniaxially pressed using a 6-mm steel die. A pressure of 300 MPa was applied for approximately one minute. Two pellets were successfully made and the density of each green pellet was calculated to 63.6 % and 65.2 % theoretical. The pellets were vacuum sealed in a SiO_2 tube which was lined with platinum foil and sintered under argon-low for a period of 4 days and 12 hours at 1150^{o}C. The densities of sintering slightly decreased to 56.6 % and 57.3 % theoretical. Analysis by powder X-ray diffraction confirmed the presence of $Sm_2Ru_2O_7$ and Sm_3RuO_7 indicating that part of the ruthenium was oxidized from a +4 to a +5 state and also orthorhombic Sm_3RuO_7 was formed. It was concluded that the sample was not crystallized enough to make a definitive evaluation. In order to obtain a higher theoretical density we were considering the use of a sintering agent such as titanium oxide to eventually enhance solid state diffusion.

The aim now was to fabricate ceramic $Sm_2(Ru_{0.5}Ti_{0.5})_2O_7$ pyrochlore. At this, powders of Sm_2O_3, RuO_2, and TiO_2 were mixed in stoichiometric proportions to form 1g of powder and subsequently ground. Zinc Stearate (1 wt.%) was added as a binder and lubricant for pellet pressing. The powder was divided into triplicates, each of which were uniaxially pressed using a 6-mm steel die. A pressure of 400 MPa (1.25 ton-force) was applied for approximately one minute to press each pellet. The densities of the green pellet were between 64.5 % and 65.2 % theoretical. The pellets were wrapped in tantalum foil and vacuum sealed in a fused silica tube and annealed under argon-flow for a period of 4 days and 12 hours at 1150^{o}C. To our surprise, the sintered densities decreased to about 51 % theoretical in average. The phase content was quantified by powder X-ray diffraction and a significant amount of ruthenium metal was revealed and as a result the overall composition (without RuO_2) shifts to a relative higher Sm_2O_3 content and into the stability field of Sm_2TiO_5. The orthorhombic structure of Sm_2TiO_5 was present as the major phase. Additionally, a small amount of the pyrochlore phase, $Sm_2Ti_2O_7$, was identified. The lattice parameter of this pyrochlore of ***a*** = 10.2345 Å indicating no significant solid solution formation with ruthenium (Figure 19)

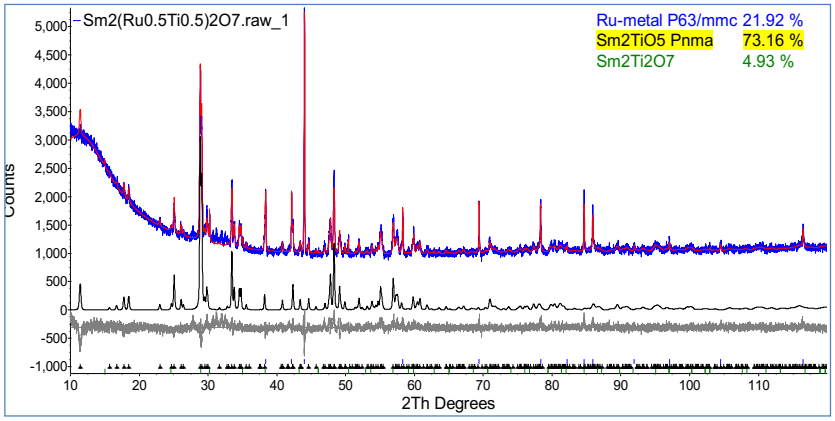

Figure 19: *$Sm_2(Ru_{0.5}Ti_{0.5})_2O_7$ was annealed for 4 days at 1150^{o}C and XRD/ Rietveld Analysis revealed the presence of Sm_2TiO_5 and $Sm_2Ti_2O_7$ pyrochlore together with metallic ruthenium*

2.1.4.8 Dry-chemical ceramic fabrication of $Sm_2(Ru_{0.5}Ti_{0.5})_2O_7$ at 1400 °C

These experiments were performed at elevated sintering temperatures and using platinum foil instead of tantalum foil. To synthesize $Sm_2(Ru_{0.5}Ti_{0.5})_2O_7$ pyrochlores the powders of Sm_2O_3, RuO_2, and TiO_2 were mixed in stoichiometric proportions, zinc stearate (1 wt.%) was used as a binder. Next, the powder was divided into three portions, each of which were uniaxially pressed using a 6-mm steel die. A pressure of 400 MPa (1.25 ton-force) was applied for approximately one minute to press each pellet to densities of about 62 % theoretical The pellets were sintered under argon-flow for a period of 1 day at 1150°C and 3 days and 12 hours at 1400°C (Figure 20). The sintered pellet densities were slightly increased and between 62 and 64 % theoretical.

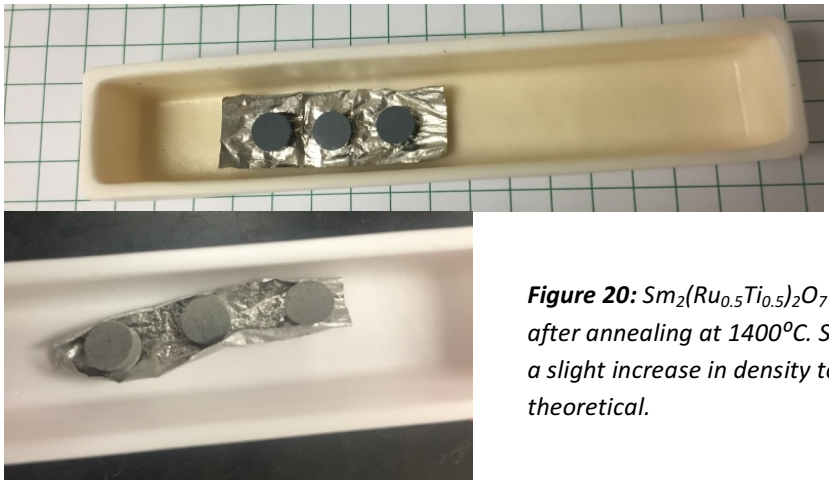

Figure 20: *$Sm_2(Ru_{0.5}Ti_{0.5})_2O_7$ before and after annealing at 1400°C. Sintering induced a slight increase in density to 62-64 % theoretical.*

The results of the powder X-ray diffraction confirms the presence of orthorhombic Sm_2TiO_5 as major phase together with $Sm_2Ti_2O_7$ pyrochlore phase and few wt.-% metallic ruthenium (Figure 21). The lattice parameter of the pyrochlore confirms with ***a*** = 10.2345 Å the absent of ruthenium.

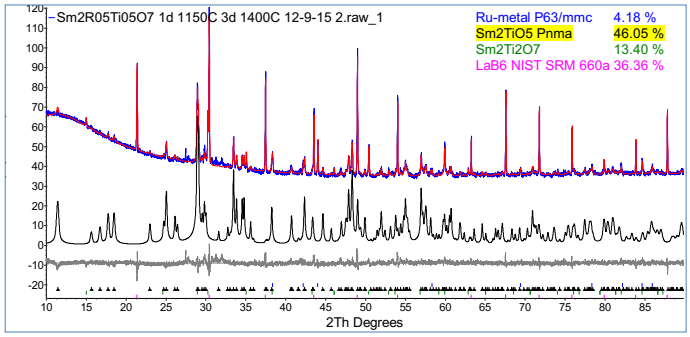

Figure 21: *$Sm_2(Ru_{0.5}Ti_{0.5})_2O_7$ was annealed at 1400°C and XRD/ Rietveld Analysis revealed the presence of Sm_2TiO_5 and $Sm_2Ti_2O_7$ pyrochlore together with metallic ruthenium*

2.1.4.9 Wet-chemical ceramic fabrication of $Sm_2(Ru_{0.5}Ti_{0.5})_2O_7$ at 1400 °C

To remedy the above mentioned problems of low sintered pellet densities, a preparation method for fabricating ceramic $Sm_2(Ru_{0.5}Ti_{0.5})_2O_7$ by wet-chemical coprecipitation was pursued. The starting compounds containing the elements of the final pyrochlore were chosen to be samarium (III) nitrate hexahydrate ($Sm(NO_3)_3 \cdot 6H_2O$), ruthenium (III) chloride ($RuCl_3$), and titanium (III) chloride ($TiCl_3$).

Mass quantities of samarium (III) nitrate hexahydrate, ruthenium (III) chloride, and titanium (III) chloride corresponding to a product of 2 grams (.0036 mol) of $Sm_2(Ru_{0.5}Ti_{0.5})_2O_7$ were calculated (Table 6).

$Sm_2(Ru_{0.5}Ti_{0.5})_2O_7$	
Molecular Weight of Each Element (g/mol)	
Samarium (Sm)	150.36
Ruthenium (Ru)	101.07
Titanium (Ti)	47.867
Oxygen (O)	15.9994
2*(Sm) →	300.72
1*(Ru) →	101.07
1*(Ti) →	47.867
7*(O) →	111.9958
Molecular Weight of $Sm_2(Ru_{0.5}Ti_{0.5})O_7$ (g/mol)	561.6528
53.54	wt-% Samarium
18.00	wt-%Ruthenium
8.52	wt-% Titanium
For preferred result of 2 grams	
1.0708	g Samarium necessary
0.3599	g Ruthenium necessary
0.1705	g Titanium necessary

Table 6: *Calculated Quantities of Samarium, Titanium and Ruthenium to obtain 2 grams $Sm_2(Ru_{0.5}Ti_{0.5})_2O_7$*

The starting compounds were to be reacted with excess ammonium oxalate monohydrate ($(NH_4)_2(C_2O_4) \cdot H_2O$) in concentrated ammonium hydroxide (14 *M* NH_4OH). The precipitates formed from the reaction were predicted to be metal oxalates, which were opted for due to their low solubility and inclination to calcine easily to ultimately form the pyrochlore structure. Theoretical reaction sequences for the each of the three predicted metal oxalates were formulated to determine the quantities of each starting compound necessary. While three separate reactions yielding three different oxalate products were devised, the final goal was to simultaneously co-precipitate all three components.

(i) $2\ Sm(NO_3)_3 \cdot 6H_20 + 3(NH_4)_2C_2O_4 \cdot H_2O \rightarrow Sm_2(C_2O_4)_3 + 6NH_4NO_3 + 15H_2O$

(ii) $2\ RuCl_3 \cdot 3H_2O + 3(NH_4)_2C_2O_4 \cdot H_2O \rightarrow Ru_2(C_2O_4)_3 + 6NH_4Cl + 6H_2O$

(iii) $2\ TiCl_3 + 3(NH_4)_2C_2O_4 \cdot H_2O \rightarrow Ti_2(C_2O_4)_3 + 6NH_4Cl + H_2O$

The amounts of samarium, ruthenium and titanium needed for the final pyrochlore were determined to be equal to the amounts formed in their respective oxalate precursors. For example, to produce the 1.078 g of samarium determined in Table 6, the weight percent of samarium in samarium (III) oxalate [$Sm_2(C_2O_4)_3$] was calculated as 53.25 wt.-%. The mass to wt.-% ratio figured a necessary yield of 2.0109

g (0.00356 mol) $Sm_2(C_2O_4)_3$. Using reaction (i), the molar quantities and subsequently, the mass quantities of the reactants needed for the reaction to proceed were determined. For 0.00356 mol $Sm_2(C_2O_4)_3$, 0.00712 mol (3.164 g), samarium nitrate hexahydrate were determined to be needed. While an amount of 1.577 g ammonium oxalate monohydrate was figured to complete reaction (i), this reactant was to be added in excess to drive the reaction. Corresponding calculations for reactions (ii), and (iii) were performed to determine the required amounts of the remaining two starting compounds. The amounts are shown in Table 7.

Table 7: *Amounts of Reactant Compounds Needed*

Reaction (i)		
Compound	Formula	Mass (g)
Samarium (III) Nitrate Hexahydrate	$Sm(NO_3)_3 \cdot 6H_20$	3.1646
Ammonium Oxalate Monohydrate	$(NH_4)2C_2O_4 \cdot H_2O$	1.5177
Reaction (ii)		
Compound	Formula	Mass (g)
Ruthenium (III) Chloride Trihydrate	$RuCl_3 \cdot 3H_2O$	0.9308
Ammonium Oxalate Monohydrate	$(NH_4)2C_2O_4 \cdot H_2O$	0.7589
Reaction (iii)		
Compound	Formula	Mass (g)
Titanium (III) Chloride	$TiCl_3$	0.549
Ammonium Oxalate Monohydrate	$(NH_4)2C_2O_4 \cdot H_2O$	0.7589

To ensure the effectiveness of the precipitation technique, each of the individual reactions were to be performed separately prior to the envisioned co-precipitation. The calcination stage was intended to transform the oxalate precipitates/co-precipitate into an oxide by removal of carbon dioxide during heating. This is illustrated by: $2\ Sm_2(C_2O_4)_3 + Ru_2(C_2O_4)_3 + Ti_2(C_2O_4)_3 \rightarrow 2Sm_2(Ru_{0.5}Ti_{0.5})_2O_7 + CO/CO_2 \uparrow$

For proper dissociation of the ions of samarium (III) nitrate hexahydrate, ruthenium (III) chloride, and titanium (III) chloride it was planned to dissolve their respective calculated quantities (Table 7) in 1 *M* nitric acid. The necessary quantity and solubility limit of each of the starting compounds in its respective solvent was used to determine the volume of solvent necessary. Since the solubility limits of both ruthenium (III) chloride and titanium (III) were reported as “very soluble”, an arbitrary volume of 20 mL was chosen. The ammonium oxalate monohydrate was to be dissolved in excess in 14 *M* ammonium hydroxide. Its solubility limit was used to make a saturated solution in the ammonium hydroxide. Since the ammonium oxalate monohydrate was to be added in excess, it was ensured that at least twice the needed calculated quantity (Table 7) was put into solution. The volumes of the solvents needed are shown in Table 8.

Table 8: *Volumes of Solvents*

Reactant Compound	Solubility in 1M HNO_3 (g/100mL)	Volume of 1 MHNO_3 Needed (mL)
Samarium (III) Nitrate Hexahydrate	10	32
Ruthenium (III) Chloride Trihydrate	"very soluble"	20
Titanium (III) Chloride	"very soluble"	20
Reactant Compound	Solubility in 14M NH_4OH (g/100mL)	Volume of 14M NH4OH Needed (mL)
Ammonium Oxalate Monohydrate	3	200

To better associate the ruthenium and titanium ions with each other, the ruthenium (III) chloride and the titanium (III) chloride were first dissolved in 1 *M* Nitric Acid and stirred for 1 hour before the samarium (III) nitrate was introduced. Once the ammonium oxalate monohydrate over ammonium hydroxide solution was added, the protocol followed was the same as the one followed for the individual reactions. A schematic flow-sheet of the procedure is shown in Figure 22, while the crucial steps of this flow sheet are illustrated in the Figures 23.

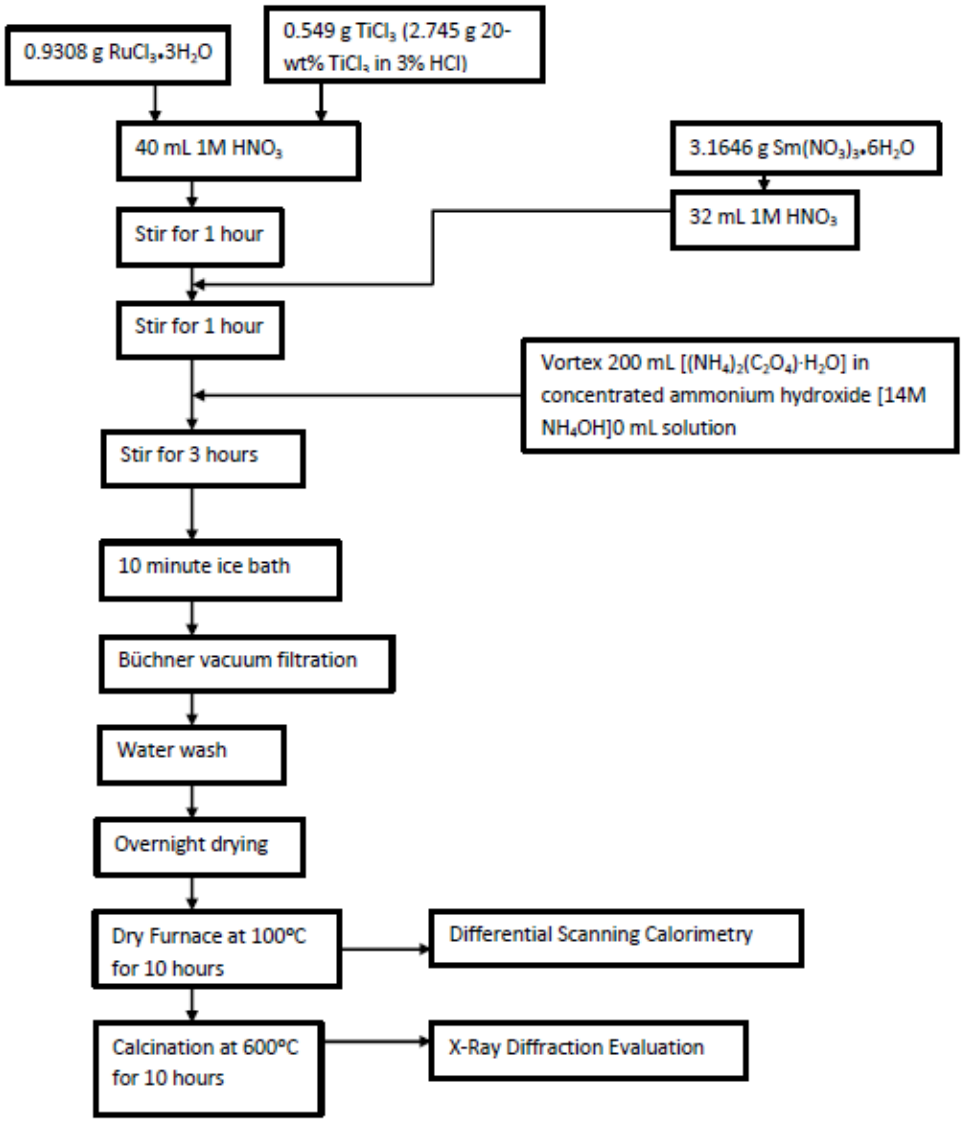

Figure 22: *Schematic of Co-Precipitation of* $Sm_2(Ru_{0.5}Ti_{0.5})_2O_7$

Mixture of Ruthenium (III) Chloride and Titanium (III) Chloride Prior to adding 1M Nitric Acid (left). Precipitation Reaction of Ruthenium (III) Chloride, Titanium (III) Chloride and Samarium (III) Nitrate with Ammonium Oxalate

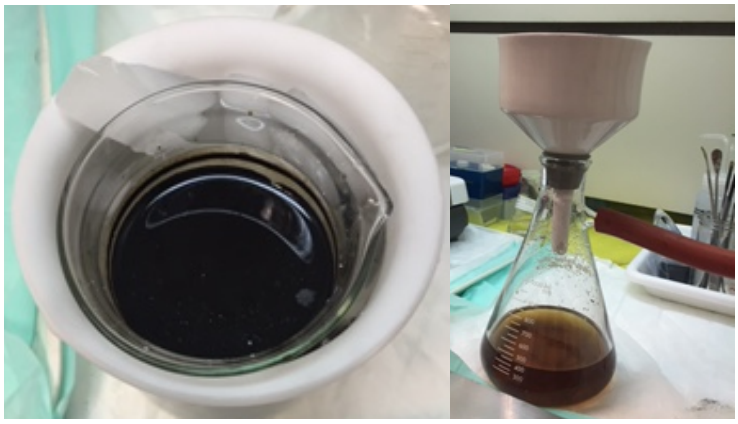

Ice Water Bath to Separate Filtrate and Precipitate (left) and Büchner Filtration Apparatus with Vacuum (right)

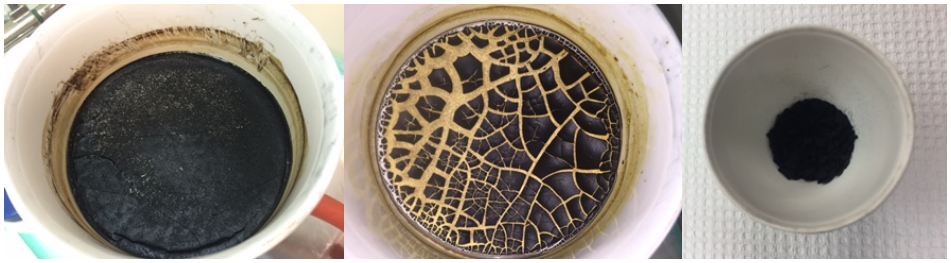

Precipitate formed after Co-Precipitation Before (left) and after Overnight Drying (middle)

Precipitate of $Sm_2(Ru_{0.5}Ti_{0.5})_2O_7$ after 10 hours in Furnace at 600°C (right).

Figure 23: *Illustration of crucial steps of Co-Precipitation of $Sm_2(Ru_{0.5}Ti_{0.5})_2O_7$*

For sintering, 1 gram of the calcined precipitate was ground and portioned three ways, and each of these portions was uniaxially pressed in a 6-mm steel die at 400 MPa for 1 minute. The mass and volume of each of the resulting three green pellets were measured for density calculations. The pellets were placed in a platinum lined ceramic crucible and sintered in a tube furnace under argon for a total of 4.5 days (1 day at 1150°C and 3.5 days at 1400°C). After removal, the mass and volume of each pellet were measured for density calculations. One of the pellets was ground for the analysis by X-ray diffraction (Figure 24).

The masses of the samarium, titanium, and ruthenium precipitates were calculated at specific stages of the experiment and are summarized in Table 9. While the procedure yielded the approximate amounts titanium and samarium predicted, that the yield of ruthenium was less than 25% of the prediction. This

was attributed the formation of a colloidal precipitate (in addition to the solid precipitate recovered) during the reaction. The weight-loss during calcination is shown in Table 10.

Table 9: *Masses of the Precipitates of samarium, ruthenium and titanium tracked during the experiment*

Reaction (i)	Fabrication of Sm_2O_3		
		Phase	Mass (g)
Initial Precipitate		$Sm_2(C_2O_4)_3 + H_20$	2.333
After 10 h @ 100°C	To drive off H_2O	$Sm_2(C_2O_4)_3$	1.9946
After 10 h @ 600°C	Calcination	Sm_2O_3	1.2517
Samarium content		Sm	1.0794
Reaction (ii)	Fabrication of RuO_2		
		Phase	Mass (g)
Initial Precipitate		$Ru_2(C_2O_4)_3 + H_2O$	0.4432
After 10 h @ 100°C	To drive off H_2O	$Ru_2(C_2O_4)_3$	0.3808
After 10 h @ 600°C	Calcination	RuO_2	0.125
Ruthenium content		Ru	0.0949
Reaction (iii)	Fabrication of TiO_2		
		Phase	Mass (g)
Initial Precipitate		$Ti_2(C_2O_4)_3 + H_2O$	0.407
After 10 h @ 100°C	To drive off H_2O	$Ti_2(C_2O_4)_3$	0.3368
After 10 h @ 600°C	Calcination	TiO_2	0.2893
Titanium Content		Ti	0.1733

Table 10: Mass of Precipitate Tracked During Co-Precipitation Method

Co-precipitation	Fabrication of $Sm_2(Ru_{0.5}Ti_{0.5})_2O_7$		
		Phase	Mass (g)
Initial Precipitate		$Sm_2(Ru_{0.5}Ti_{0.5})_2(C_2O_4)O_7 + H_2O$	5.1061
After 10 h @ 100°C	To drive off H_2O	$Sm_2(Ru_{0.5}Ti_{0.5})_2(C_2O_4)O_7$	2.5072
After 10 h @ 600°C	Calcination	$Sm_2(Ru_{0.5}Ti_{0.5})_2O_7$	2.0687

The precipitation yield was with approximately 2 grams about 95% of the expected amount. While the colloidal precipitate from the ruthenium reaction was visibly apparent during the co-precipitation, the filtrate was nearly transparent and much clearer than during the precipitation of the ruthenium oxalate by itself. It was assumed that the formation of colloidal particles might prevent the effective precipitation and filtration of ruthenium (III) oxalate. X-ray diffraction analysis performed after calcination, prior to sintering, only showed a phase of RuO_2 in addition to an amorphous phase. After the sintering however, the X-ray diffraction pattern shows the formation of the pyrochlore phase and the successful incorporation of all three metals in the designated host phase. The density of the pellets pressed from the $Sm_2(Ru_{0.5}Ti_{0.5})_2O_7$ precipitate showed significant increase after sintering as is shown in Table 11. Theoretical densities in the range from 72 to 76 % were measured.

Table 11: *Percent Theoretical Density of $Sm_2(Ru_{0.5}Ti_{0.5})_2O_7$ Pellets before and after sintering at 1400 °C for3.5 days; theoretical density value based on that of $Sm_2(Ru_{0.5}Ti_{0.5})_2O_7$ which is 7.586 g/cm^3*

Sintering of $Sm_2(Ru_{0.5}Ti_{0.5})_2O_7$								
Green Pellet Measurements								
	Mass (g)	Diameter (mm)	Height (mm)	Diameter (cm)	Height (cm)	Volume (cm^3)	Density (g/cm^3)	% Theoretical Density
Pellet 1	0.2613	6.03	2.79	0.603	0.279	0.0797	3.28	43.7
Pellet 2	0.262	6.04	2.85	0.604	0.285	0.0817	3.21	42.8
Pellet 3	0.2081	6.04	2.27	0.604	0.227	0.0650	3.20	42.7
Sintered Pellet Measurements								
Pellet 1	0.2131	4.98	2.02	0.498	0.202	0.0393	5.42	72.2
Pellet 2	0.2137	4.96	1.98	0.496	0.198	0.0383	5.59	74.5
Pellet 3	0.1694	4.95	1.55	0.495	0.155	0.0298	5.68	75.7

It is noted that the height of the pellets was reduced more significantly than the diameter during sintering. Approximately 20 % mass reduction was also observed in all three pellets. The results of phase analysis of co-precipitated $Sm_2(Ru_{0.5}Ti_{0.5})_2O_7$ are displayed in Figure 24.

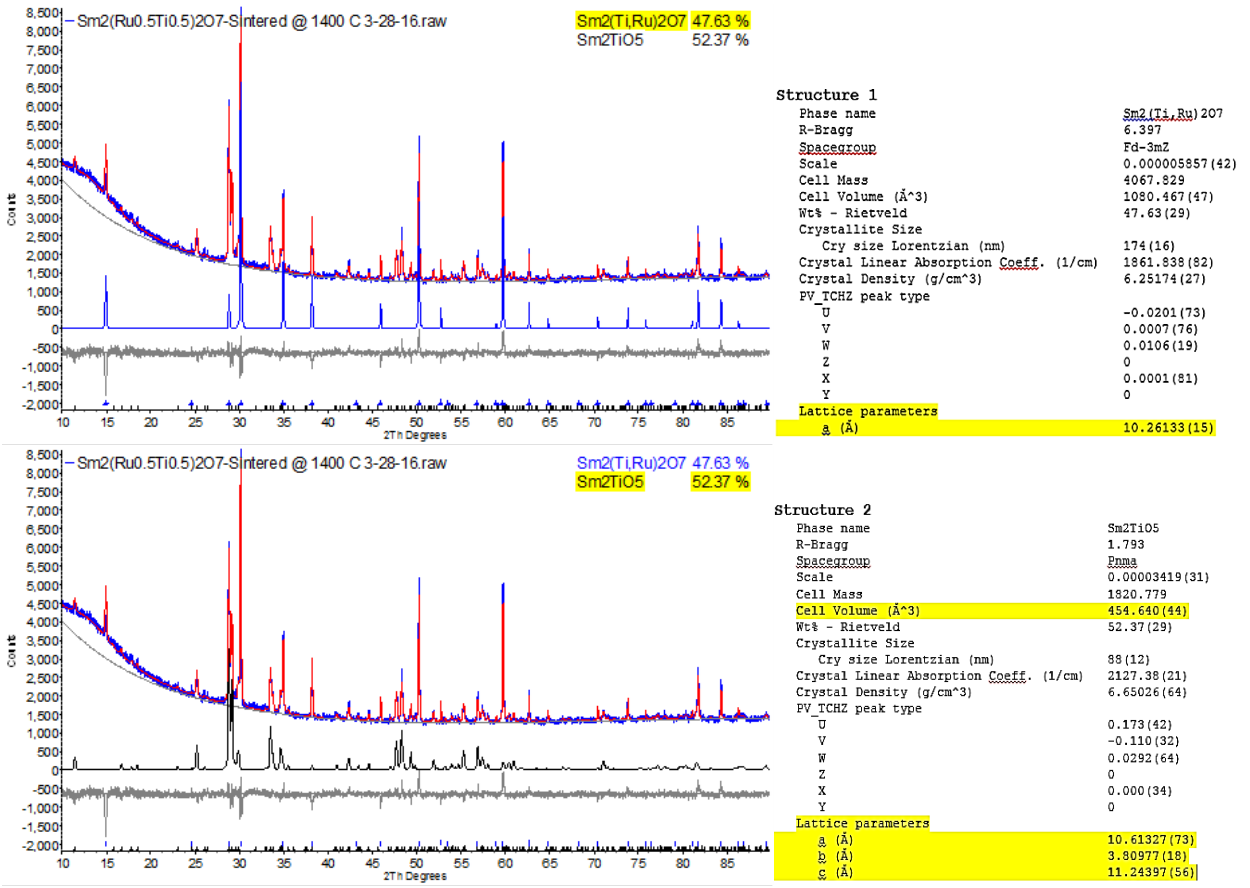

Figure 24: *X-Ray Diffraction Pattern and Data for Sintered Pellet of $Sm_2(Ru_{0.5}Ti_{0.5})_2O_7$ formed from applying the wet-chemical co-precipitation method*

The X-ray diffraction pattern shown in Figure 24 indicates the presence of two phases in the sintered pellet. At this, the host phase is $Sm_2(Ru_XTi_{1-X})_2O_7$ which appears in 10-50 µm crystallites, embedded in Sm_2TiO_5 as matrix phase. Using the published lattice parameters for $Sm_2Ru_2O_7$ and $Sm_2Ti_2O_7$, 10.275 Å and 10.23 Å, the lattice parameter of $Sm_2(Ru_XTi_{1-X})_2O_7$ with 10.2613(2) Å results in an estimated stoichiometry for the host phase of $Sm_2(Ru_{0.7}Ti_{0.3})_2O_7$. This further might represent the solubility limit of Ti within this Sm-Ru based pyrochlore waste form.

2.1.4.10 Wet-chemical ceramic fabrication of $Sm_2(Ru_X,Tc_{0.5-X},Ti_{0.5})_2O_7$

Our overall strategy for the immobilization of technetium from a waste treatment installation and the synthesis of pyrochlore waste form material is summarized in Figure 25.

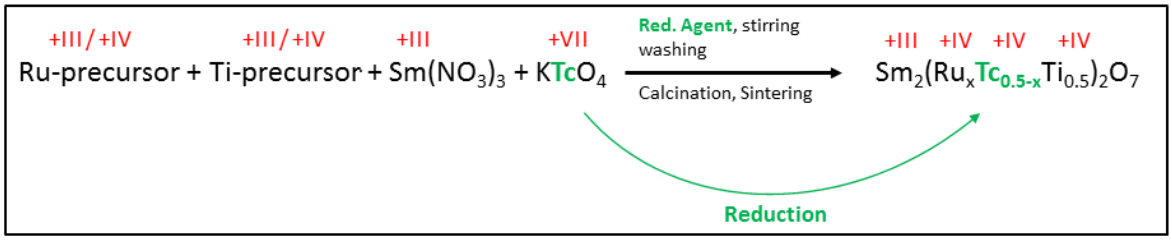

***Figure 25**: General procedure of a pyrochlore formation experiment - Depletion of technetium inventory and the fabrication of pyrochlore waste forms*

We are aiming to develop a process for on-line depleting the technetium inventory of a nuclear waste treatment plant trough the reduction of technetium and to stabilize tetravalent technetium in a ceramic waste form applying a wet-chemical synthesis route. At this, heptavalent technetium will be reduced and tetravalent technetium will be mixed and homogenized with co-precipitated lanthanide and titanium, calcined, cold-pressed, and sintered. One important requirement for the raw-materials is a good solubility in water. $RuCl_3$ was used as the raw-material for ruthenium, the Ru(III) has to be oxidized during the process to reach the tetravalent state. $Sm(NO_3)_3$ was used as a precursor for the Sm(III), the oxidation state of the metal doesn't have to be changed to get incorporated since the oxidation state of samarium in the pyrochlore is +III as well. The introduction of Ti into the mixture was achieved by using two different raw-materials. $TiCl_3$, which has to be oxidized to reach the tetravalent state, and $TiOSO_4$, which already contains Ti^{4+}.

The raw-materials are solubilized in water at pH 7 which produced in a brown solution, caused by the Ru(III). It is not really important in which order the raw-materials are added to the mixture since no reaction or chemical conversion should occur. Afterwards, precipitation is achieved by adding the precipitation agent, an oversaturated solution of $(NH_4)_2(C_2O_4)$ in 14 M NH_4OH to the mixture. The combination of the insoluble metal-oxalates and the very high pH value around 14 initiates quantitative precipitation out of the solution. The precipitate can be separated from this solution by filtration using a Büchner-funnel and filter-papers. The oxalates have to be dried in a furnace at 100 °C for about 10-12 hours. Calcination of the dried filtrates is performed at 500-600 °C within 10 hours and the oxalates were converted to oxides. "Green" pellets were obtained using uniaxial pressing at 400 MPa. The pellets were sintered at 1400 °C for three days under an inert argon atmosphere.

Figure 26 shows the flowsheet of the entire process of pyrochlore fabrication, which takes about 7 days. The experimental details and the adapted flow sheet are displayed in Table 12 and in Figure 22. Figure 23 illustrated the individual precipitation steps. Sintering of the pellets produced theoretical densities of about 70 % theoretical, with good mechanical strength. However, XRD-based phase analysis revealed the presence of metallic ruthenium (Table 13).

***Table 12**: Fabrication details for batches S1, S2, and S3*

Nr.	Compounds	Calcination	Sintering
S1	0.9347g $RuCl_3$ 0.549g $TiCl_3$ 3.1646g $Sm(NO_3)_3$	600°C, 10h	1400°C, 4.5d, Ar
S2	0.9308g $RuCl_3$ 0.569g $TiOSO_4$ 3.1646g $Sm(NO_3)_3$	600°C, 10h	1400°C, 4.5d, Ar
S3	0.9343g $RuCl_3$ 0.549g $TiCl_3$ 3.1615g $Sm(NO_3)_3$	500°C, 10h	1400°C, 4.5d, Ar

***Table 13:** Phase analysis of pellets of the batches S1, S2, and S3 using XRD-based Rietveld Structure Refinement.*

Batch	$Sm_2Ru_2O_7$ (wt.%)	Sm_2O_3 (wt.%)	Ru-metal (wt.%)	Sm_2TiO_5 (wt.%)
S1	**10.38**	-	18.19	71.43
S2	**0.32**	22.81	23.50	53.37
S3	**11.22**	5.39	20.10	63.30

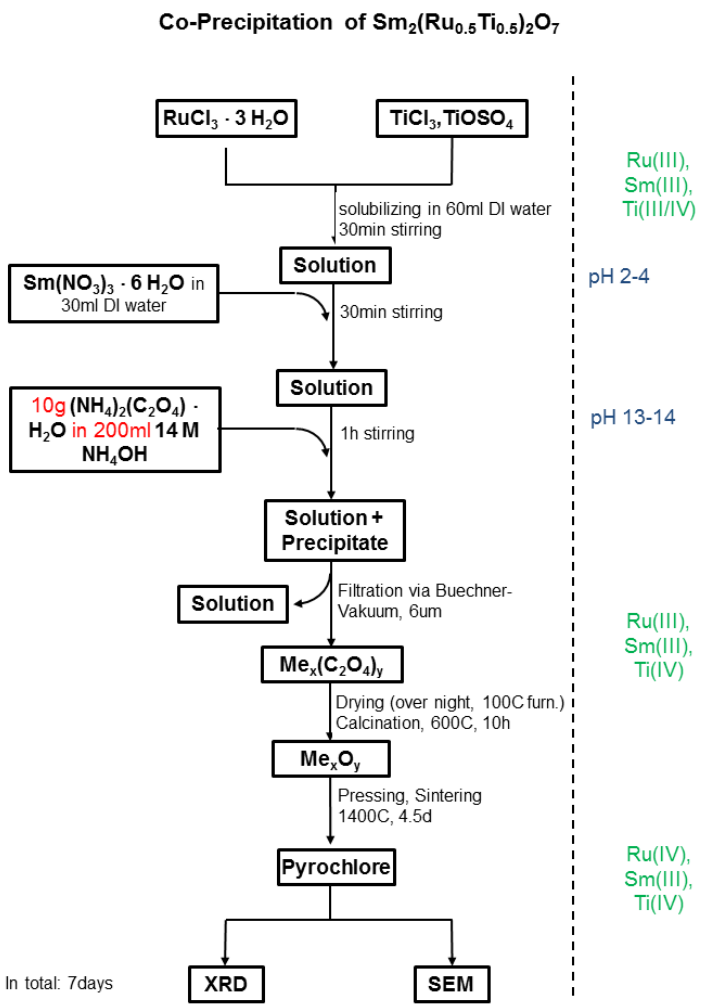

Figure 26: *Flowsheet of the wet-chemical pyrochlore fabrication route*

Incorporation of ^{99}Tc into the Co-Precipitation Flow Sheet and the effectiveness of reducing agents

The successful reduction of Tc(VII) to Tc(IV) from mock-up off gas washer solutions will allow for on-line depletion of technetium under the conditions of a waste treatment facility. Our aim here is to incorporate this reduction set into the precipitation scheme as previously displayed (Figure 27).

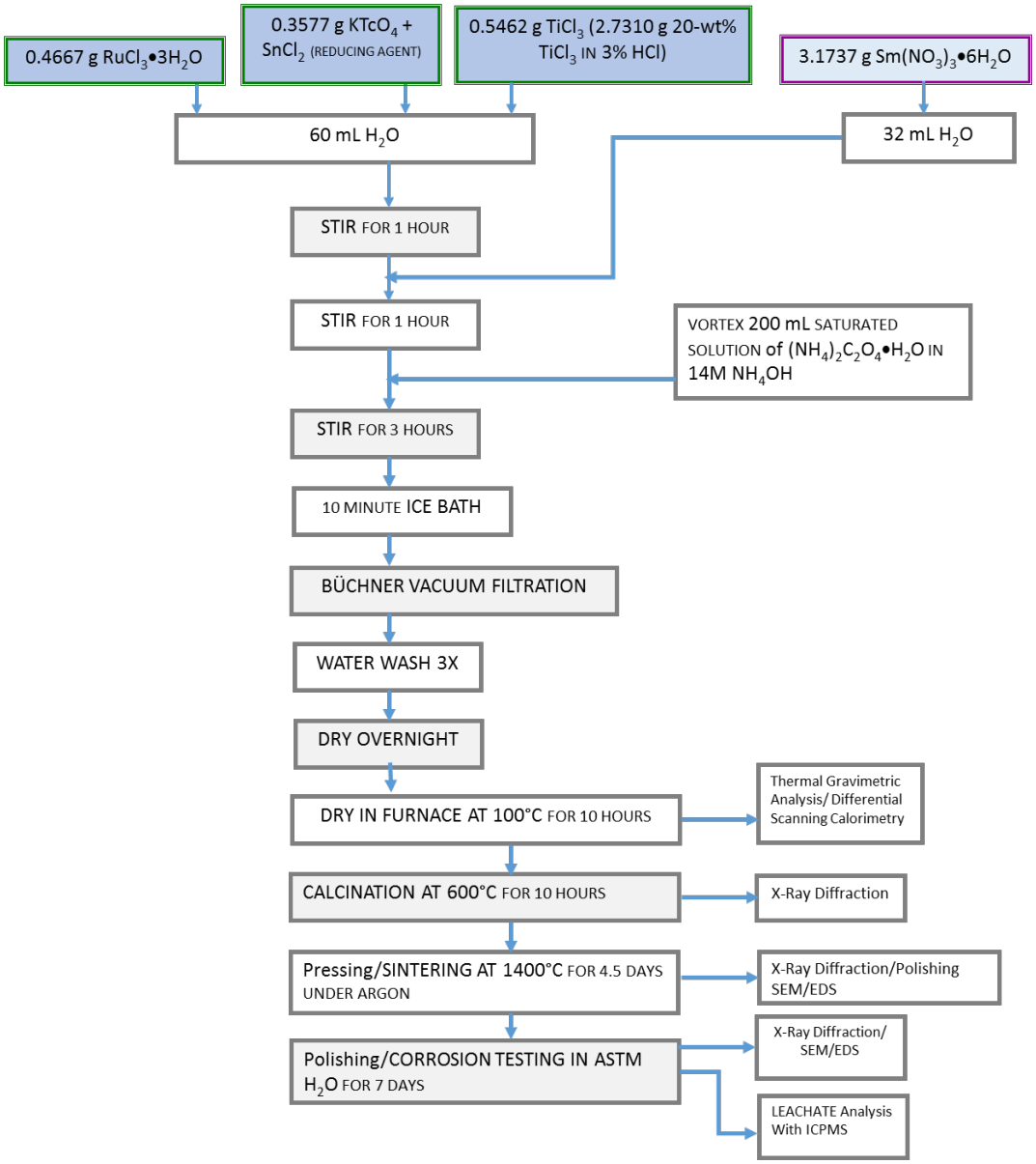

***Figure 27**: Co-Precipitation Scheme for $Sm_2(Ru_{0.25}{}^{99}Tc_{0.25}Ti_{0.5})_2O_7$*[4]

To evaluate the effect of common reducing agents, precipitation studies on the overall performance of non-toxic and non-hazardous reducing agents such as tin(II) chloride ($SnCl_2$), iron(II) sulfate ($FeSO_4$), sodium(II) sulfite (Na_2SO_3) and sodium thiosulfate ($Na_2S_2O_3$) were initiated.

[4] **T. Hartmann**, **R. Palaparty**, **F. Wolke**: Fabrication and Properties of Advanced Ceramic Waste Forms, Waste Management Symposia 2017, Proceedings, 17311, March 5-9, Phoenix, AZ (2017).

The main purpose of this investigation is to understand the conversion of the pertechnetate species (TcO_4^-), into technetium dioxide (TcO_2) containing tetravalent $Tc^{(IV)}$. Since the heptavalent state of technetium is more stable than the tetravalent, most of the Tc-99 quantity in waste and lab compounds is represented by the compounds TcO_4^- and Tc_2O_7. To activate the containing $Tc^{(VII)}$ for the incorporation into the pyrochlore, it has to be reduced by a suitable, if possible non-toxic and non-hazardous, reducing agent, which takes part of the synthesis of the solid-waste-form. In recent studies, mainly published by the Savannah River National Laboratory (SRNL), $FeSO_4$ and $SnCl_2$ were proposed. In addition to that, the two sulfur-containing compounds Na_2SO_3 and $Na_2S_2O_3$ are discussed in the following.

The validation of the performance of a reducing agent can be performed in different ways. One method to quantify the performance is to calculate the ratio of the concentration of the oxidized species of any ion before and after a reduction treatment and a general experimental procedure is sketched in Figure 28.

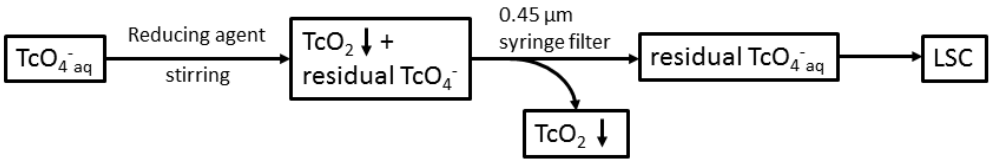

***Figure 28**: Experimental procedure in general*

Liquid-scintillation-counting (LSC) was used to provide quantitative data on the efficiency of technetium reduction. The reducing agent was mixed with an aqueous pertechnetate solution, which can be characterized by its known concentration $[A]_0$. After the reaction is completed, the composition of the system turned from a pure solution of TcO_4^- to a dispersion of a solid TcO_2 precipitate in an aqueous solution containing residual pertechnetate with the concentration $[A]_{res}$. The separation can be performed by a syringe filter. LSC is used to determine the residual concentration of pertechnetate in the solution and the decontamination factor (DF) for each reducing agent can be quantified:

$$DF = \frac{[A]_{res}}{[A]_0} \leq 1$$

Although it is possible to calculate the total amount of the radioactive isotope in the sample, this method is not practicable since some parameters like the counting efficiency of the measurement device has to be known. By using the DF-value, it is possible to calculate the relative amount of pertechnetate which is removed out of the solution, unless an external calibration, which is only valid for this study, is done. Basically, the kinetics and thermodynamics of chemical reactions like redox reactions are affected by a whole series of parameters. Next to the temperature, the impact the concentration on the behavior of the reducing agent is tremendous. In some recent studies, the stoichiometric amount of the reducing agent, concerned to the molar amount of Tc-99, was used. The following calculations illustrate that issue for $SnCl_2$. Commonly, a Tc-99 concentration of 2 mg L^{-1} is used, which corresponds to a molar concentration of 20.22 µM.

According to the reaction

$$Tc^{7+} + 3e^- \rightarrow Tc^{4+}$$

one turnover of this reaction requires 3 electrons for the reduction. $SnCl_2$ provides 2 electrons per turnover

$$Sn^{2+} \rightarrow Sn^{4+} + 2e^- \ (1.5\ eq.)$$

Therefore, a concentration of $SnCl_2$ which is 1.5 times higher than the concentration of pertechnetate is necessary to perform the reaction. The oxidation equations of the other reducing agents look quite similar:

$$Fe^{2+} \rightarrow Fe^{3+} + e^- \ (3\ eq.)$$

$${SO_3}^{2-} \rightarrow {SO_4}^{2-} + 2e^- \ (1.5\ eq.)$$

$${S_2O_3}^{2-} \rightarrow {SO_4}^{2-} + 8e^- \ (0.375\ eq.)$$

Viewing the principle of Le Chatelier, an increase of the concentration of some precursors will always increase the speed of the reaction. Therefore, a better performance is expected, when the equivalent concentration of the reducing agent increases. This issue is also discussed in this report. The next parameter which influences the reaction is the pH-value. To consider this, the performance of the reducing agents at different pH-values is tested. For example, according to the articles published by the SRNL, $SnCl_2$ shows the best performance at pH7, whereas $FeSO_4$ works better at pH 10 or 12.

The parameter of the reaction time, which is equivalent to the stirring time, could show a heavy impact on the kinetics of this reaction. This influence is caused by the tendency of some $Tc^{(IV)}$ species to re-oxidize to the $Tc^{(VII)}$ form. For that reason the influence of this parameter was determined by comparing the remaining pertechnetate concentration in mixtures which were stirred for significant different times, in particular 16 and 96 hours. Another important factor, which could influence the obtained results, is the syringe filter. The separation of the solid precipitate from the solution is strongly influenced by the pore size of the filter. For example, if one precipitation/reducing agent is converting 100 % of the pertechnetate into a precipitate with a very small average grain size, a syringe filter with a wider pore will probably not separate the two phases completely. On the other hand, a system in which a precipitation agent does not reduce the entire $Tc^{(VII)}$ content but generates a precipitate with a bigger grain size instead will be better separated and its performance will be judged better incorrectly. That's why two different syringe filters with 0.20 µm and 0.45 µm were compared.

As reducing agents, tin(II)chloride dihydrate ($SnCl_2 \cdot 2H_2O$, *BDH-VWR analytical*, ACS grade), iron(II) sulfate heptahydrate ($FeSO_4\ 7H_2O$, *Amresco*, ACS grade), sodium sulfite (Na_2SO_3, anhydr., *Amresco*, ACS grade) and sodium thiosulfate ($Na_2S_2O_3$, anhydrous, *Wards Science*, ACS reagent grade) were used. The ionic strength was adjusted with sodium perchlorate ($NaClO_4$, anhydrous, *EMD Chemicals*, ACS grade). Because of the re-oxidation of the tetravalent to the heptavalent state under the influence of any oxidizing agents like oxygen in the breathing air, all experiments were performed in a protector glove box under inert atmosphere, argon. The pH-measurements, which were necessary for the adjustment of the pH-value were made by using a 781 pH/Ion Meter from *Metrohm*, which was calibrated with pH5,

pH7 and pH10 standard buffer solutions at least once a week. The LSC analyses were performed with a Liquid Scintillation Analyzer Tri-Carb 3100TR device from *Perkin Elmer*. The specific $Nd_2Tc_2O_7$ protocol for the β-measurement of the dissolved Tc-99 isotope was operated by the *Quanta Smart*- Software, including a pre-counting delay of 2min, 3 cycles per sample and 5min counting time.

Because of the used Conventional DualLabel (DPM) method, which discriminates the energy of the emitted pulses during the detection, the output provides the total number of counts of 3 different energy ranges, named as areas A-C. Area C covers the entire energy range, so this value was used for the data handling and, since 3 cycles per sample are performed, the average has to be calculated. The scintillation cocktail Ultima-Gold from Perkin Elmer was used. To prepare the samples, 9.9 mL of the cocktail have to be mixed with 0.1mL of the solution which contains the isotope. For the calibration, standard solutions with the Tc-99 concentrations of 0, 0.5, 1, 1.5 and 2 mg/L were prepared. For the blank solutions, 3 pertechnetate solutions with the initial concentration of 2 mg/L and the pH-values 7, 10, and 12 were prepared and analyzed. In a typical precipitation experiment, a pertechnetate and a reducing agent stock solution have to be prepared. Table 14 provides an overview of the prepared stock solutions for the experiments which were made.

***Table 14**: Stock solutions for the experiments to effectively reduce pertechnetate to Tc[IV]*

Compound	Molar mass [g/mol]	Weighed portion [mg]	Volume [ml]
$KTcO_4$	202.001	10.8	250
$SnCl_2\ 2H_2O$	225.64	136.872	100
$FeSO_4\ 7\ H_2O$	278	337.23	100
Na_2SO_3	126.04	76.455	100
$Na_2S_2O_3$	158.11	23.977	100
$NaClO_4$	122.44	6,122	500

All of the reducing compounds and the sodium perchlorate are showing a good solubility and form colorless solutions, why the preparation of the stock solutions is easy. By using the described concentrations, 50 µl of every stock solution have to be added to 10 ml pertechnetate solution, which was used as the standard volume for each sample, if the goal is an equimolar ratio of reducing agent and technetium. According to this, for a 100 % excess of reducing agent, 100 µL have to be added. Afterwards, the pH-value was adjusted by using solutions of nitric acid and sodium hydroxide in different concentrations from 0.01 *M* to 1 *M*, whereby a total volume increase of 1 % was not exceeded.

After the samples were stirred for a defined time at room temperature conditions, the precipitations were separated from the solutions by using a syringe filter. Since there is a risk of possible contamination, a separate filter is required for every sample. To make it easier, the used syringes should have a minimum volume of 10 ml. After that, the LSC-samples were prepared like it is described above and Table 15 provides an overview on the reduction experiments as carried out.

Table 15: *Analyzed samples and the corresponding results*

Sample	*pH*	*Red. Agent*	*Stirring time [h]*	*Conc. [eq.]*	$\overline{\#cpm}$	*Rel. #cpm Residual [%]*	*Rel. [Tc-99] Residual [%]*
FW-1-1	7	$SnCl_2$	16	1	2069	28.3	27.3
FW-1-2	10	$SnCl_2$	16	1	2654	36.9	36.0
FW-1-3	12	$SnCl_2$	16	1	6312	88.8	88.6
FW-1-4	7	$FeSO_4$	16	1	7221	98.7	98.7
FW-1-5	10	$FeSO_4$	16	1	5710	79.3	79.0
FW-1-6	12	$FeSO_4$	16	1	5776	79.8	79.5
FW-1-7	7	Na_2SO_3	16	1	7294	99.7	99.7
FW-1-8	10	Na_2SO_3	16	1	7186	99.8	99.8
FW-1-9	12	Na_2SO_3	16	1	7176	100.0	100.0
FW-1-10	7	$Na_2S_2O_3$	16	1	7396	101.0	101.0
FW-1-11	10	$Na_2S_2O_3$	16	1	7180	99.7	99.7
FW-1-12	12	$Na_2S_2O_3$	16	1	7237	101.7	101.8
FW-1-14	7	$SnCl_2$	96	1	2233	30.5	29.5
FW-1-15	10	$SnCl_2$	96	1	2598	34.7	33.8
FW-1-16	12	$SnCl_2$	96	1	6786	95.4	95.3
FW-1-17	7	$FeSO_4$	96	1	7069	96.6	96.5
FW-1-18	10	$FeSO_4$	96	1	5977	83.0	82.8
FW-1-19	12	$FeSO_4$	96	1	5215	73.3	72.9
FW-1-20	7	Na_2SO_3	96	1	7014	95.8	95.8
FW-1-21	7	$Na_2S_2O_3$	96	1	7026	96.0	96.0
FW-1-22	4.5	$SnCl_2$	16	1	2267	30.1	30.0
FW-1-23	5	$SnCl_2$	16	1	1892	25.9	24.8
FW-1-24	5.5	$SnCl_2$	16	1	2154	29.4	28.4
FW-1-25	6	$SnCl_2$	16	1	2261	30.9	30.0
FW-1-26	6.5	$SnCl_2$	16	1	2036	27.8	26.8
FW-1-27	7	$SnCl_2$	16	2	127	1.7	0.3
FW-1-28	7	$SnCl_2$	16	5	63	0.8	0
FW-1-29	10	$SnCl_2$	16	2	305	4.2	2.9
FW-1-30	10	$SnCl_2$	16	5	629	8.7	7.4
FW-1-31	10	$FeSO_4$	16	2	1579	21.9	20.8
FW-1-32	10	$FeSO_4$	16	5	507	7.0	5.7
FW-1-33	12	$FeSO_4$	16	2	2754	38.7	37.8
FW-1-34	12	$FeSO_4$	16	5	1247	17.5	16.3
FW-1-35	7	$SnCl_2$	2	2	237	3.2	1.9
FW-1-36	7	$SnCl_2$	4	2	259	3.5	2.2
FW-1-37	7	$SnCl_2$	2	5	88	1.2	0
FW-1-38	7	$SnCl_2$	4	5	59	0.8	0
FW-1-39	10	$SnCl_2$	2	2	472	6,6	5.2
FW-1-40	10	$SnCl_2$	4	2	306	4.3	2.9
FW-1-41	10	$SnCl_2$	2	5	393	5.5	4.1
FW-1-42	10	$SnCl_2$	4	5	455	6.3	5.0

The outcome of this study indicated, that the sulfur-containing compounds Na_2SO_3 and $Na_2S_2O_3$ were not efficient reducing agents and not suitable for the reduction of Tc(VII). $SnCl_2$ and $FeSO_4$ on the other hand are promising candidates especially used in excess. Figure 29 illustrates the performance of either candidate as a function of pH and of $SnCl_2$ in excess as a function of stirring time.

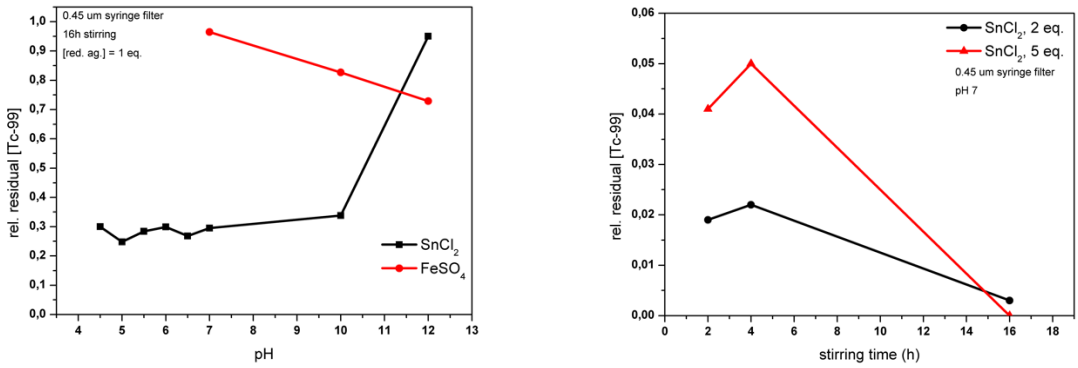

Figure 29: *Performance of the reducing agents $SnCl_2$ and $FeSO_4$ as a function of pH (left) and of $SnCl_2$ in excess as a function of stirring time (right)*

We can conclude that $SnCl_2$ performs well as a reducing agent for pertechnetate when used at pH values below 10. Primarily the $SnCl_2$ shows obviously a better performance in general as the $FeSO_4$, which fits to the results which were obtained at the discussion on the influence of the pH value. In addition, we noticed an increasing reduction power with increasing concentration following the principle of Le Chatelier. Using the $SnCl_2$ with an excess concentration of x2 or x5 the equivalent concentrations resulted in the reduction of virtually all $Tc^{(VII)}$ in the solution within 2 to 4 hours of stirring.

2.2 Thermodynamics and kinetics or technetium leaching and waste-form corrosion

In this chapter we are presenting our experimental results on the leaching behavior and matrix corrosion of ceramic technetium waste forms and ruthenium surrogate waste forms we have successfully synthesized during this NEUP project. Naturally, we are considering Tc leaching and waste form matrix corrosion as the primary criteria for the acceptance of these ceramic structure types as prospective waste forms and alternative to vitreous borosilicates especially when the flowsheet of reprocessing provides us with an obvious opportunity for improvement. The use of ceramics as technetium hosts become especially advantages, if a separate Tc-waste stream is available from an advanced separation process (e.g. UREX+1) which allows treatment and immobilization of Tc separately from the high level waste stream. This chapter summarized our experiments to determine Tc leaching and matrix corrosion of ceramic waste forms is a chronological order.

2.2.1 Corrosion of reference vitreous borosilicates: NIST SRM-623, PNNL ARM-1, and PNNL 76-68

Prior to the experiments on Tc-based ceramics we collected based-line leaching and corrosion data on vitreous reference materials such as the borosilicate glasses SRM-623, PNNL ARM-1, PNNL 76-68, and a LAW4 reference glass for Tc-99 with 1 wt.-% technetium loading. The latter was fabricated at UNLV. We first initiated static leaching experiments on ground standard reference material SRM-623 following the ASTM C1285-02 (PCT-B) test protocol for this product consistency test. We notices that this test is not

practical for radioactive samples and the reference glasses PNNL ARM-1, PNNL 76-68, and the LAW4 Tc-99 glass were tested applying ASTM C1220-10, MMC-1 test protocol on monolithic samples. The tests were performed in triplicates. For applying static leaching/corrosion test ASTM C1285-02 (PCT-B), borosilicate reference glass (SRM-623) was crushed to size fractions from 10 to 200 µm and the size fraction 75-106 µm (200-140 mesh) was extracted for testing (Figure 30).

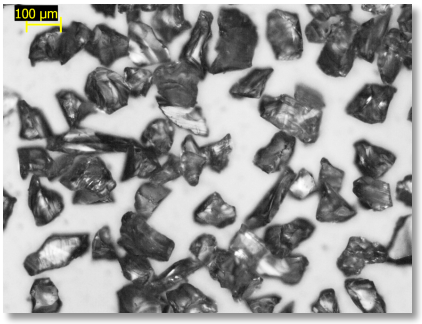

Figure 30: *Glass fraction prior to the PCT testing after sieving. The size fraction was confirmed by optical microscopy*

Static PCT-type corrosion test on SRM-623 borosilicate glass were performed for 7 days and for 14 days and were in compliance with ASTM C1285 in terms of mass differences of the solutions before and after the test (< 5 wt.-%) and the pH measurements showed very consistent results. Elemental analyses of the leachates were performed using an ICP-AES (Thermo Scientific, iCAP 6000) (Figures 31 and 32).

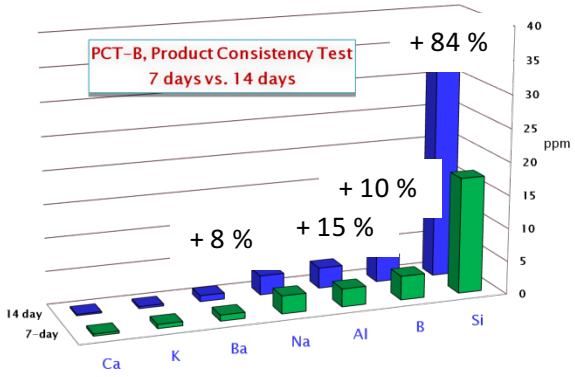

Figure 31: *Comparison of elemental concentration of 7 with 14 days PCT corrosion test on SRM-623 borosilicate glass. Average concentrations are displayed and the relative increase for the 14 day test is shown.*

The mass ratios of dissolved cations relative to the total inventory in the glass matrix are displayed for the 7-day and the 14-day PCT static corrosion tests are shown in Figure 32. The mass ratios for Si, Al, B, Ca, and Na are about $0.7x10^5$ to $1.6x10^5$ for the 7-day PCT, and increase to $1x\ 10^5$ to $1.9x10^5$ for the 14-day test. The potassium concentrations in the 7-day PCT leachates are significantly higher and lead to increased calculated mass ratios of up to $6x10^5$.

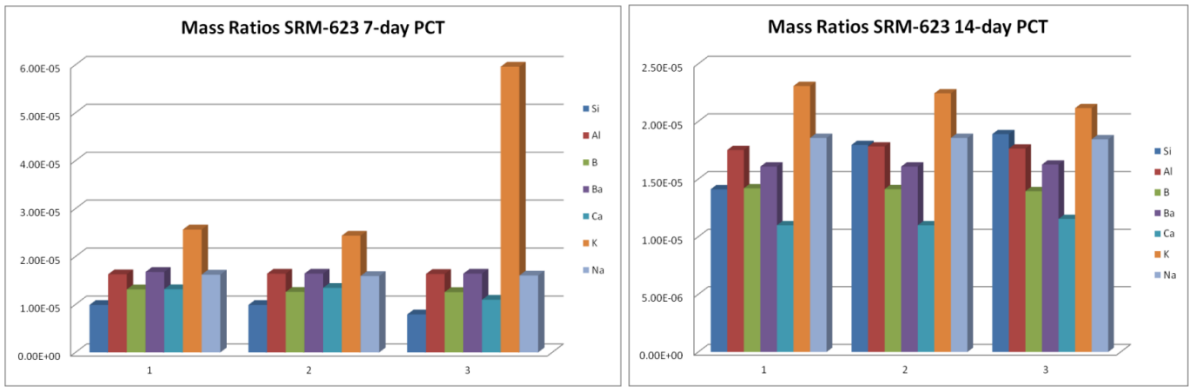

Figure 32: *Mass ratios of dissolved cations relative to total glass inventory for 7 and 14 days PCT corrosion test on NIST SRM-623 borosilicate glass.*

The reference glasses PNNL ARM-1, PNNL 76-68, and LAW4 Tc-99 glass were tested applying static leaching experiments of monolithic test samples (ASTM C1220-10, MMC-1). At this, we received blocks of ARM-1 and 76-68 from PNNL (Figure 33).

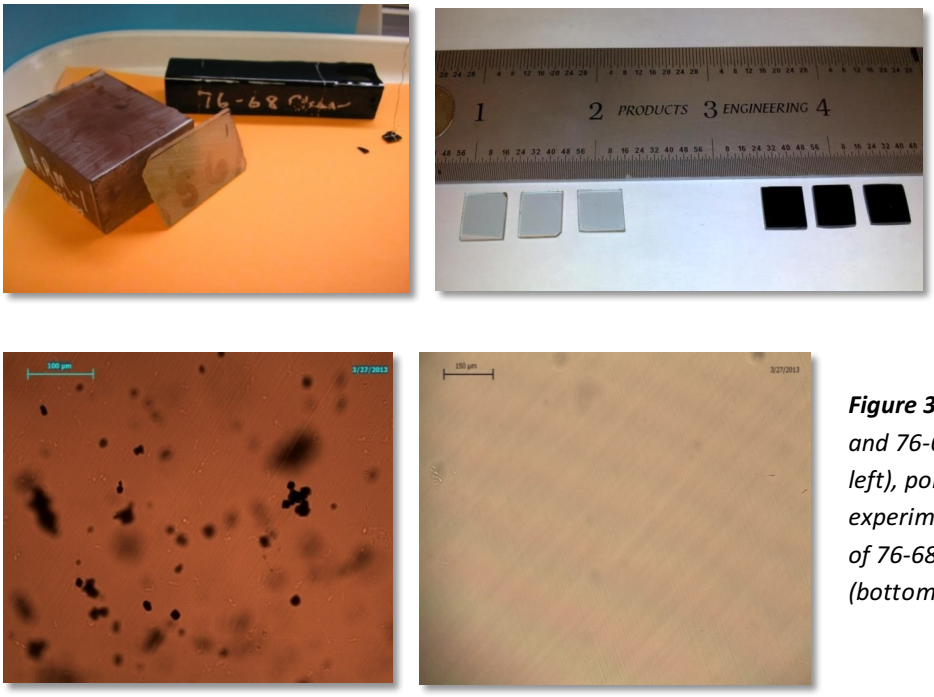

Figure 33: *Reference glasses ARM-1 and 76-68 as received from PNNL (top left), polished for static corrosion experiments (top right). Optical images of 76-68 (bottom left) and ARM-1 (bottom right).*

The reference glass ARM-1 is rather homogeneous, while the 76-68 glass does show a significant amount of dark inclusions (Figure 33). The subsequent corrosion tests were performed in Teflon-lined stainless-steel acid digestion vessels (Parr 23 mL 4749) and the experimental set-up is displayed in Figure 34.

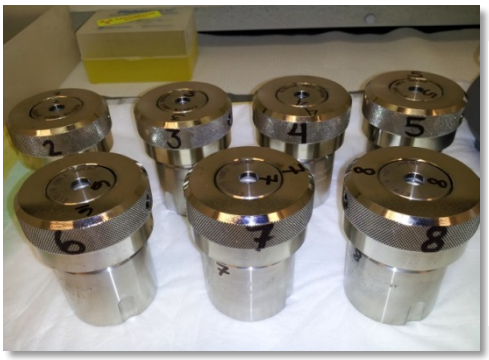

Figure 34: *Stainless steel sample hanger with glass specimen (left), Parr 23 mL 4749 digestion vessels (right).*

Static corrosion tests on ARM-1 and 76-68 borosilicate glass samples were performed in triplicates with durations of 7 days and 28 days, using ASTM C1220-10 (MCC-1) protocols. Our experimental and analytical work tasks were in close compliance with ASTM C1220 and mass differences of the solutions before and after the test were all below the 5-wt.-% maximum limit. Experimental details are listed in Table 16 and the results of elemental analysis can be found in Table 17.

Vessel Number For 7 days testing	Type	Weight of empty vessel + lid (g)	Surface Area (mm^2)	Weight of Sample (g)	Amount of Solution (ml)	Weight of vessel + lid + sample + solution (g)	Solution Mass Diff. (%) after 7 days
	Blank	112.0417	0	0	17.8965	129.9399	<<1%
	Blank	111.6562	0	0	17.8207	129.4804	<<1%
	Blank	110.7142	0	0	17.8827	128.5962	<<1%
	ARM-1	111.5571	194.731	0.2110	19.4599	131.0158	<<1%
	ARM-1	111.6210	184.435	0.2036	18.4633	130.0809	<<1%
	ARM-1	112.6924	183.703	0.2130	18.3869	131.0741	<<1%
	76-68	111.5618	175.309	0.2112	17.5035	129.0618	<<1%
	76-68	111.8604	165.221	0.1883	16.7393	128.5665	<<1%
	76-68	111.5733	166.673	0.1718	16.6786	128.2487	<<1%

Vessel Number for 28 days testing	Type	Weight of empty vessel + lid (g)	Surface Area (mm^2)	Weight of Sample (g)	Amount of Solution (ml)	Weight of vessel + lid + sample + solution (g)	Solution Mass Diff. (%) after 28 days
	Blank	112.0442	0	0	18.5206	130.5648	0.137
	Blank	111.6559	0	0	18.5074	130.1633	0.190
	Blank	110.7138	0	0	18.4946	129.2084	0.216
	ARM-1	111.3464	196.545	0.2868	19.6523	131.2855	0.205
	ARM-1	111.419	194.716	0.2841	19.476	131.1791	0.261
	ARM-1	112.4759	193.590	0.2756	19.3611	132.1126	0.102
	76-68	111.3507	174.864	0.2505	17.4626	129.0638	0.191
	76-68	111.6414	174.957	0.2603	17.5034	129.4051	0.141
	76-68	111.399	174.910	0.2551	17.5063	129.1604	0.195

Table 16: *Experimental data for the 7-days and 28 days C1220-10 (MCC-1) corrosion tests performed on ARM-1 and 76-68 borosilicate glass. (Samples 1-3 are blanks)*

Table 17: *Elemental analysis of leachates by ICP-AES after 7 days (top) and 28 days (bottom) corrosion testing on ARM-1 and 76-68 borosilicate glass samples. Samples 1-3 are blanks.*

	Blank-#1	Blank-#2	Blank-#3	Blank Avg	ARM-1 #4	ARM-1 #5	ARM-1 # 6	ARM Avg	76-68 # 7	76-68 # 8	76-68 # 9	76-68 Avg
	(ppm)	(ppm)	(ppm)	**(ppm)**	(ppm)	(ppm)	(ppm)	**(ppm)**	(ppm)	(ppm)	(ppm)	**(ppm)**
Al	<DL	<DL	<DL	**<DL**	1.163	1.214	1.200	**1.192**	<DL	0.0265	<DL	**<DL**
B	<DL	<DL	<DL	**<DL**	2.221	2.367	2.372	**2.320**	1.435	2.078	1.002	**1.505**
Ba	<DL	<DL	<DL	**<DL**	<DL	<DL	<DL	**<DL**	<DL	<DL	<DL	**<DL**
Ca	0.091	0.068	0.075	**0.078**	0.508	0.498	0.514	**0.507**	0.497	0.709	0.408	**0.538**
K	0.151	0.173	0.189	**0.171**	0.094	0.096	0.093	**0.094**	0.172	0.183	0.162	**0.173**
Na	<DL	<DL	<DL	**<DL**	1.601	1.723	1.741	**1.688**	1.895	2.766	1.334	**1.998**
Si	<DL	<DL	<DL	**<DL**	11.340	11.930	11.900	**11.723**	7.809	11.410	5.460	**8.226**
Sr	<DL	<DL	<DL	**<DL**	<DL	<DL	<DL	**<DL**	<DL	<DL	<DL	**<DL**
NOTE* Averages for Ca and K for ARM & 76-68 sample have been blank corrected												

	Blank-#1	Blank-#2	Blank-#3	Blank Avg	ARM-1 #1	ARM-1 #2	ARM-1 # 3	ARM Avg	76-68 # 1	76-68 # 2	76-68 # 3	76-68 Avg
	(ppm)	**(ppm)**	**(ppm)**	**(ppm)**	**(ppm)**	**(ppm)**	**(ppm)**	**(ppm)**	**(ppm)**	**(ppm)**	**(ppm)**	**(ppm)**
Al	<DL	<DL	<DL	**<DL**	2.105	2.051	2.077	**2.078**	0.182	0.178	0.174	**0.178**
B	<DL	<DL	<DL	**<DL**	3.729	3.742	3.809	**3.760**	6.669	6.324	6.472	**6.488**
Ba	<DL	<DL	<DL	**<DL**	<DL	<DL	<DL	**<DL**	<DL	<DL	<DL	**<DL**
Ca	<DL	<DL	<DL	**<DL**	0.665	0.609	0.641	**0.638**	0.390	0.410	0.403	**0.401**
K	0.108	0.112	0.078	**0.099**	0.132	0.081	0.099	**0.104**	0.299	0.289	0.279	**0.289**
Na	<DL	<DL	<DL	**<DL**	2.912	2.926	3.015	**2.951**	9.141	8.669	8.903	**8.904**
Si	0	<DL	<DL	**<DL**	18.850	18.690	18.930	**18.823**	30.660	29.310	29.870	**29.947**
Sr	0.006	<DL	<DL	**<DL**	<DL	<DL	<DL	**<DL**	<DL	<DL	<DL	**<DL**
NOTE* Averages for K for ARM-1 & 76-68 sample have been blank corrected												

Mass loss calculations of leachates from 7- and 28-day corrosion testing on PNNL reference glasses ARM-1 and 76-68 were performed hereby the following equation was applied:

$$m_{ij} = \left(C_{ij} \times V_{fi}\right) - \sum_{k=1}^{a} \quad V_{Bk} \times \frac{B_{ik}}{a}$$

The results of element specific mass loss calculations for ARM-1 and 76-68 vitreous borosilicates after 7 days and 28 C1220-10 corrosion testing are shown in Figure 35 and the overall surface specific mass losses are displayed in Figure 36.

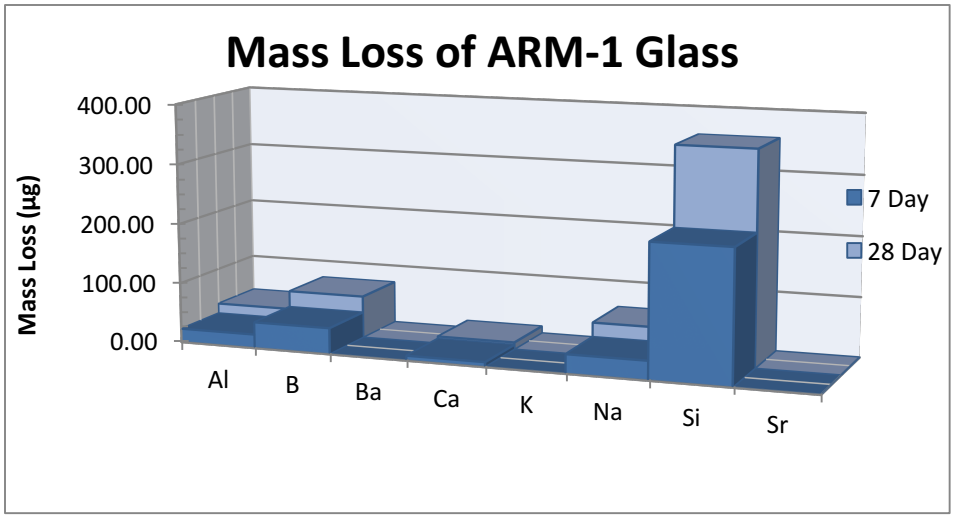

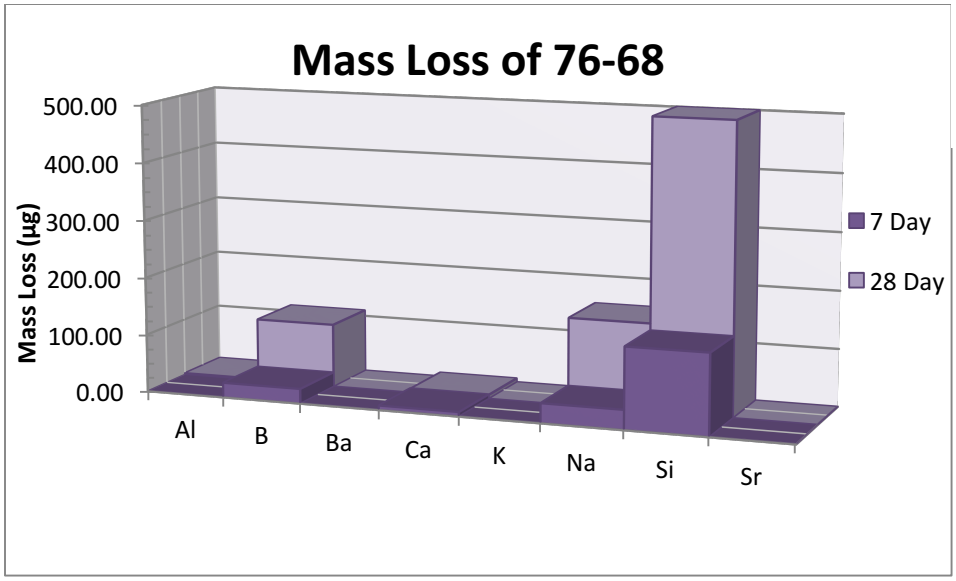

Figure 35: *Element specific mass-loss of ARM-1 and 76-68 borosilicate glasses after 7-days and 28 days corrosion tests*

The overall mass loss calculation for the ARM-1 and 76-68 glass samples indicates significant higher corrosion rates for the 76-68 glass than for the ARM-1 reference glass. The 28 days corrosion testing of 76-68 reference glass results in a nearly 4-fold higher mass loss compared with the mass loss of ARM-1 reference glass. The specific mass losses as $\Delta g/mm^2 \bullet day$ for the 7 days and the 28 days corrosion testing are shown in Figure 36.

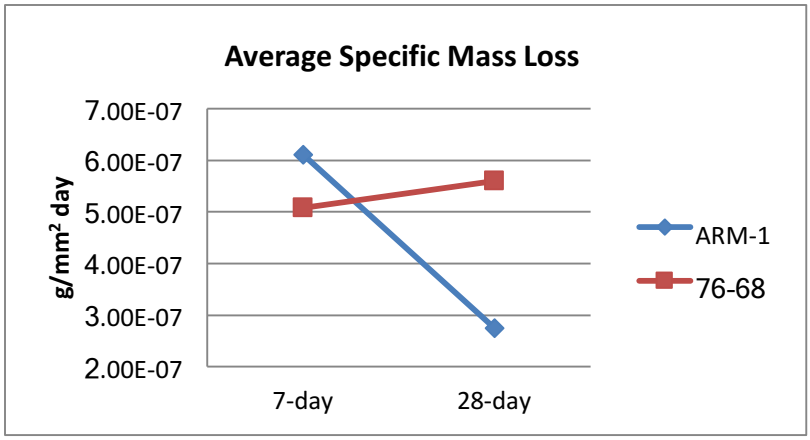

Figure 36: *Average specific mass losses ($\Delta g/mm^2 \bullet days$) for 7 days and 28 days C1220-10 corrosion testing of ARM-1 and 76-68 reference glasses.*

For the ARM-1 glass the corrosion rates were determined to average 6.11 10^{-7} g/mm^2•day for the 7 days test and 2.75 10^{-7} g/mm^2•day for the 28 days corrosion testing. For the 76-68 reference glass the average corrosion rate was 5.08 10^{-7} g/mm^2•day and 5.6 10^{-7} g/mm^2•day for the 7 days and the 28 days corrosion testing, respectively. It can be assumed, that the corrosion mechanism of ARM-1 within the first 7 days is mainly diffusion controlled, where network modifiers are leached out from the sample rim. The 28 days corrosion testing of ARM-1 is more likely to be controlled by the degradation of the glass network after the glass-network modifier content is depleted. Hereby the kinetic of the glass matrix corrosion rate and the break-down rate of the glass network of ARM-1 is significantly slower than the release rate of the diffusion-controlled process. As a result of compositional changes of the glass formulation and presumably lower concentration in network-formers (SiO_2, Al_2O_3, B_2O_3), the matrix corrosion rates of glass 76-68 are increased compared with the glass corrosion rates of ARM-1.

The corroded sample coupons of ARM-1 and 76-68 were imaged by optical polarization microscopy and are displayed in Figure 37.

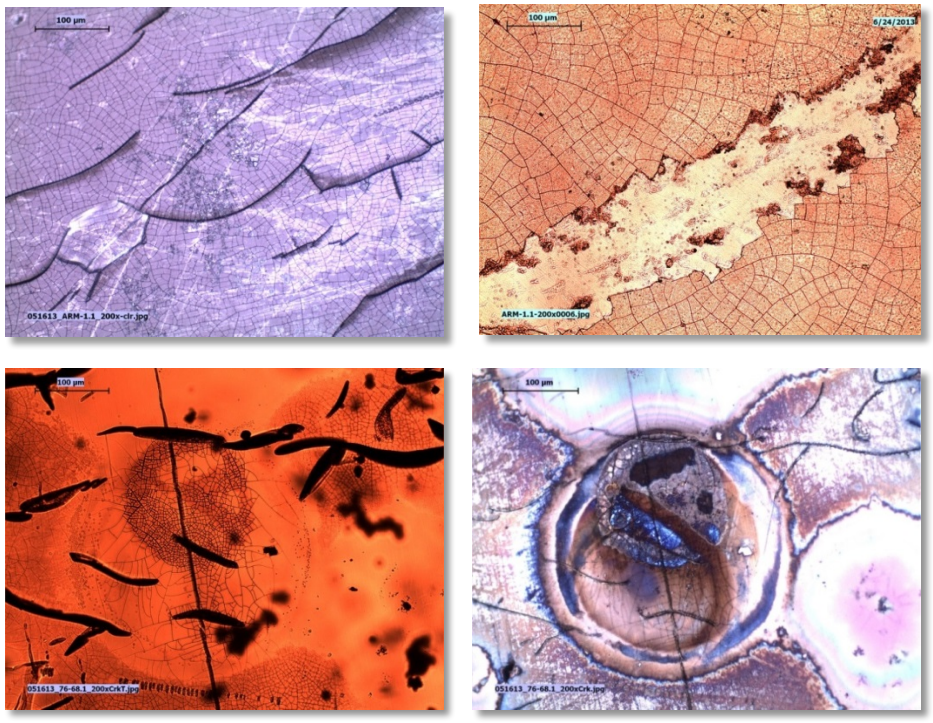

Figure 37: *Optical images of ARM-1 (top) and* 76-68 (bottom) borosilicate *glass and impact of corrosion and crack formation after 7 days (left) and 28 days (right) of corrosion testing*

The 7 days and the 28 days C1229-10 corrosion tests induced alterations in the microstructure of ARM-1 reference glass and the formation of micro-cracks on the surface are overlaid by larger fractures. After 28 days testing, part of the micro-cracked layer is removed from the surface, indicating a corrosion scenario of step-wise removal of µm thick fractured corrosion layers. On the other hand, the 76-68 reference glass showed a pitting type corrosion mechanism. This observation of different corrosion mechanism for reference glasses ARM-1 and 76-68 might also explain the differences in the corrosion rates especially after 28-days testing.

2.2.2 Corrosion of reference vitreous borosilicates: Tc-containing LAWE4

Technetium containing borosilicate LAWE4 glass was synthesized by fusing the salts at 1100 °C in a tube furnace under Air. The target Tc-content was 1-wt.-% and a 5 gram batch was synthesized. The LAWE4 Tc glass served as reference material on technetium-leaching and waste form matrix to compare the technetium-bearing ceramics with. The preparation of a triplicate samples set of ^{99}Tc containing borosilicate glass was performed with the upmost care. All samples were cut, ground and polished down to a mirror finish for 6 sides of each specimen (Figure 38).

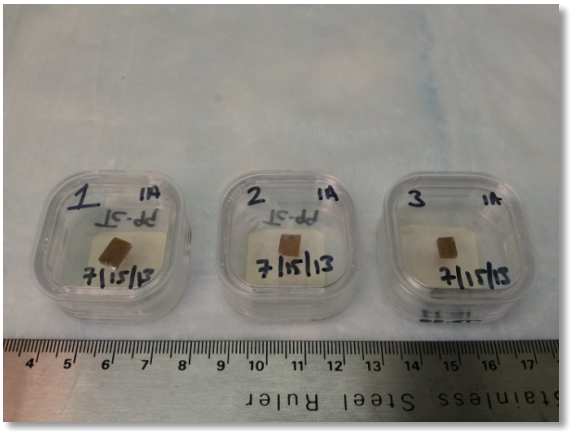

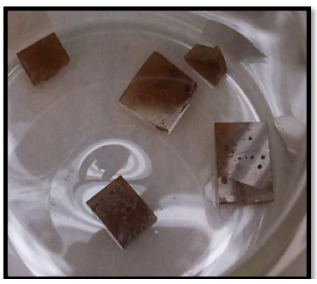

***Figure 38**: Tc-containing borosilicate glass coupons for C-1220 corrosion testing.*

Static corrosion tests on the ^{99}Tc containing glass samples were performed in triplicates for durations of 7 days and 28 days using ASTM C1220-10 (MCC-1) protocols. All experimental procedures were in close compliance with ASTM C1220. All solutions before and after cleaning of the PTFE vessels resulted in water-loss mass differences that were well below the maximum limit. All specimens were cleaned following close adherence to ASTM C1220-10 section 8.6 cleaning procedures. All specimens were initially treated to a 5-min ultrasonic wash in acetone to remove any residues from the polished surface area. Thereafter, the samples underwent three subsequent ultrasonic washes (each 5 minutes in duration) using absolute anhydrous ethanol. After proper and final cleaning of Tc-99 glass coupons, weights and measures were taken for each sample for the leaching experiment. Physical dimensions were recorded using digital calipers to the nearest 0.1 mm. Due to the irregularity of shape of the 28-day samples ASTM C1220-10 x3 "Method to determine surface area of the irregular face of a tablet test specimens" procedures were followed to get appropriate surface area calculations. SketchAndCalc™ program was used to obtain calculation for irregular shaped monoliths for the 28-day leach experiments (Tables 18 & 19).

***Table 18:** Experimental data for the 7-day C1220-10 corrosion test (Samples 1-2 & 6-7 are blanks)*

Vessel Number	Type For 7 days or 28 days	Weight of Empty Vessel + Lid + Glass (g)	Surface Area of Tc-99 Glass (mm^2)	Weight of Tc-99 Glass Sample (g)	Amount of H_2O Added (ml)	Weight of Vessel + Lid + Sample+ Solution (g)
1	Blank for 7	112.092	0.000	0.000	11.15	123.249
2	Blank for 7	111.788	0.000	0.000	11.15	122.933
3	7a	110.984	139.707	0.225	13.97	123.592
4	7b	111.535	107.004	0.140	10.70	122.157
5	7c	111.586	90.181	0.128	9.02	120.500
6	Blank for 28	112.512	0.000	0.000	16.95	128.909
7	Blank for 28	111.307	0.000	0.000	16.95	126.588
8	28a	112.076	171.220	0.325	17.12	129.476
9	28b	111.657	141.750	0.261	14.18	126.031
10	28c	111.736	195.620	0.318	19.56	131.398

Table 19: *Weights and measures for 28 day C1220-10 testing of ^{99}Tc-loaded LAWE4 glass*

Vessel Number	Type	Weight of vessel, lid, glass and support (g)	Total weight pre-leach with leachant added(g)	Amount of Solution added (mL)	Total Weight after 28 day Leaching (g)	Total Mass Loss (g)	Solution Mass Diff (%) After 28 days
6	Blank (28 day)	112.51	128.270	16.95	128.882	0.031	<<1%
7	Blank (28 day)	111.31	127.071	16.95	126.545	0.036	<<1%
8	28a	112.08	127.633	17.12	129.435	0.032	<<1%
9	28b	111.66	126.939	14.17	126.003	0.022	<<1%
10	28c	111.74	127.369	19.56	131.372	0.029	<<1%
NOTE * The loss of solution was <10% (maximum limit)							

ASTM C1220-10 (MCC-1) corrosion testing of Tc-LAWE4 glass was performed for 7 and 28 days and the total release of Tc-99 was measured to 0.64 %, and 1.01 %, respectively, which translated to a specific mass loss of 1.34 10^{-6} and 6.43 10^{-7} g/mm^2•day. The specific mass loss of the Tc-99 LAWE4 glass compares well to the PNNL reference glass ARM-1 which showed specific mass losses of 6.11 10^{-7}, and 2.75 10^{-7} g/mm^2•day for 7 days and 28 days C1220-10 testing, respectively (Table 20).

We engaged in optical microscopy (Leica DM 2500P) to determine macroscopic changes on microstructure and appearance of the glass coupons after leaching. The images of the glass coupons before and after leaching are provided in Figures 39. Static corrosion testing induced significant changes to the macro- and microscopic appearance of the glass coupons. Corrosion of the Tc-containing glass coupons was initiated at pores and inclusions of undissolved residuals (e.g. refractory metal oxides) within the glass matrix. Therefore, the expected homogeneous matrix corrosion is convoluted and overlaid by pitting-type corrosion associated with mass losses of up to 1 wt.%.

Table 20: *Mass-loss calculation of ^{99}Tc Glass coupons after 7 and 28 days C1220-10 corrosion testing*

Vessel No.	Type	Surface Area of Tc-99 Glass (mm^2)	Weight of Tc-99 Glass Sample (g)	Post Leach Glass (g)	Mass Loss (g)	Percent Mass Loss	Average % Mass Loss	Specific Mass Loss [g/mm^{2}x days]	Average Specific Mass Loss [g/mm^{2}x days]
3	**7-a**	139.707	0.225	0.2237	0.0013	**0.593**		1.33E-6	
4	**7-b**	107.004	0.140	0.1394	0.0006	**0.405**		8.01E-7	
5	**7-c**	90.181	0.128	0.1267	0.0012	**0.912**	**0.64**	1.90E-6	**1.34E-6**
8	**28-a**	171.220	0.325	0.3217	0.0029	**0.881**		6.04E-7	
9	**28-b**	141.750	0.261	0.2583	0.0023	**0.881**		5.79E-7	
10	**28-c**	195.620	0.318	0.3139	0.0041	**1.279**	**1.01**	7.48E-7	**6.43E-7**

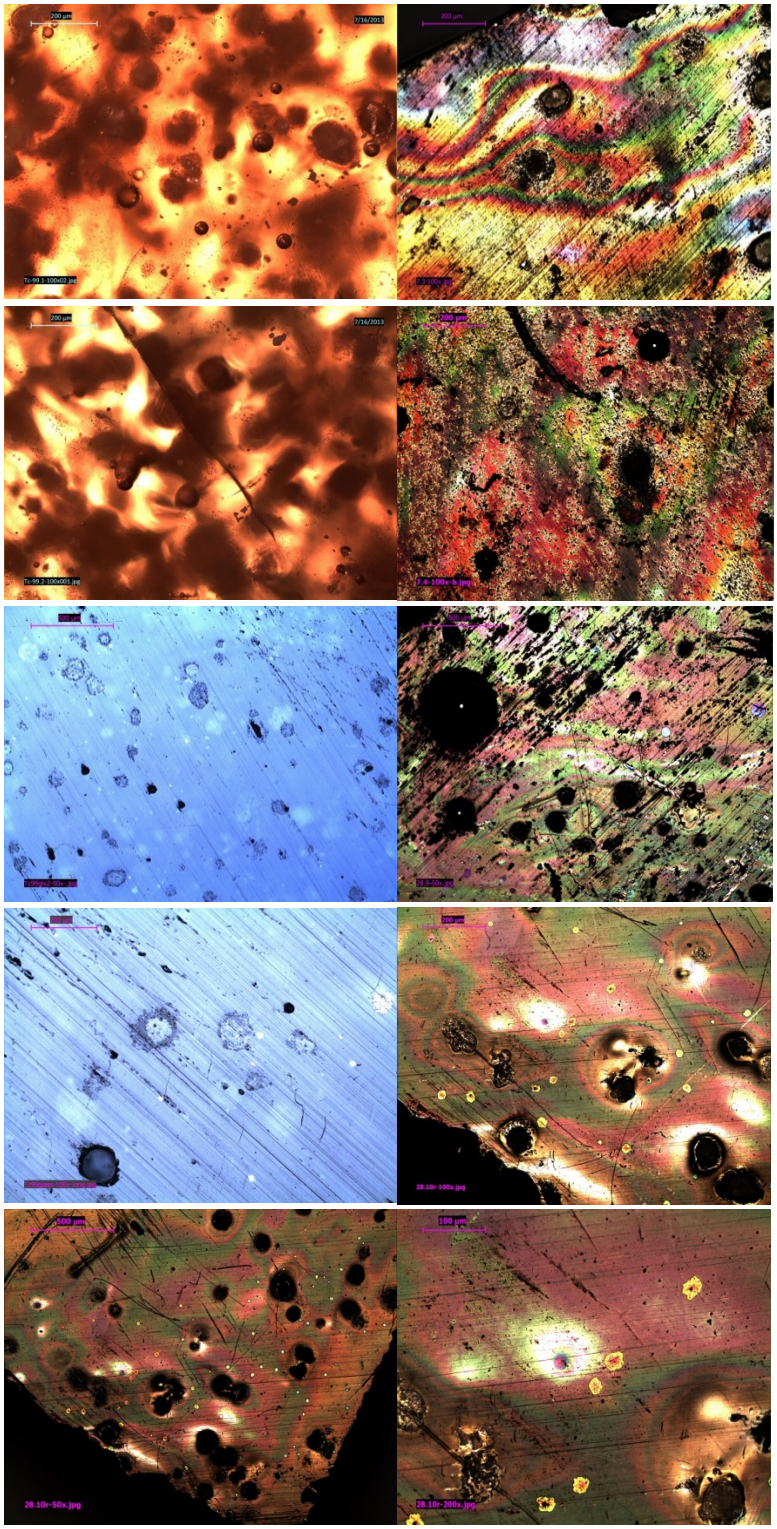

Pre Leaching ***Post Leaching***

Figure 39: *Optical transmission microscopic images of LAWE4 Technetium containing glass before (left) and after (right) 7 days and 28 days C1220-10 corrosion-testing in the following order (from top):*

a) *Sample 7a*
b) *Sample 7b*
c) *Sample 28a*
d) *Sample 28c(1)*
e) *Sample 28c(2)*

Liquid scintillation counting was performed to determine the absolute release of Tc-99 from the leached LAWE4 glass coupons. These Tc-99 glass coupons were leached for 7 days and 28 days in triplicates and

the absolute Tc-99 release was determined liquid scintillation counting (Table 21). After 7 days and 28 days ASTM testing the Tc-99 molarity (as NH_4TcO_4) in the leachates was 0.012 *mM* and 0.018 *mM* which corresponds to average Tc-99 release of 0.022 mg and 0.034 mg, respectively. Relative to the specimen mass, the relative Tc-99 release after 7 days testing was with 1.22 % in average higher than for the 28 days tests with a relative mass loss of 1.03% in average. This might be partly explained by the lower surface/mass ratios of the test specimens for 28 days testing of 562 mm^2/g compared with 697 mm^2/g for the glass coupons for the 7 days tests.

Table 21: *LSC Results for Tc-99 LAW4 Glass coupons tested for 7 and 28 days using ASTM C1220-10*

Sample	Specimen	Surface Area (mm^2)	Mass (mg)	CPM β̄	y = 2E+08x - 27.107	Observed Tc-99 Molarity (mM)	Total NH4TcO4 ~Mass (mg)	Tc-glass Mass Loss (mg)	% Tc Leached
Tc-7 day	**7a**	139.71	224.7	**3320**	6.64E+11	**0.017**	2.47	**0.030**	1.225
Tc-7 day	**7b**	107.00	140.0	**1911**	3.82E+11	**0.010**	1.54	**0.017**	1.123
Tc-7 day	**7c**	90.18	127.9	**2005**	4.01E+11	**0.010**	1.41	**0.018**	1.296
Tc-28 day	**28a**	171.22	324.6	**4019**	8.04E+11	**0.020**	3.57	**0.037**	1.026
Tc-28 day	**28b**	141.75	260.6	**3976**	7.95E+11	**0.020**	2.87	**0.036**	1.263
Tc-28 day	**28c**	195.62	318.0	**3035**	6.07E+11	**0.015**	3.50	**0.028**	0.790

2.2.3 ASTM C1220-10 static leaching of $Nd_2Tc_2O_7$ specimens for 28 days

$Nd_2Tc_2O_7$ pyrochlore pellets fabricated by dry chemical processing were cut to discs of 5mm in diameter and about 2-3 mm in thickness. Anhydrous ethanol was used as the wetting fluid to avoid interferes with aqueous Tc leaching prior to the actual experiment. All samples were initially ground with 240 grit silicon carbide papers on an Allied Multiprep system and polished to a 15-µm finish using diamond lapping paper (Figure 40). The sintered pellets are lacking density and mechanical strength but survived sample preparation. The microstructure of the pyrochlore pellets show few larger 50-µm grains but mainly gain sizes between 5 and 10 µm. The microstructure can be described as spongy, but also exhibits large 50-80-µm pores. Monolithic $Nd_2Tc_2O_7$ specimens which were corroded for 28 days in close compliance with ASTM C1220-10 and the results for static corrosion on these conventionally synthesized $Nd_2Tc_2O_7$ monoliths are summarized in Table 22. Despite the fact of sub-optimal properties of the fabricated ceramic in regards to density and mechanical strength, the specific mass loss was with 1.48 10^{-7} [g/mm^2•days] by about a factor 4 lower than the specific mass loss observed when corroding Tc-99 containing LAWE4-type borosilicate glass (6.43 10^{-7} g/mm^2•days). The total Tc-99 release was 0.67 % for

$Nd_2Tc_2O_7$, compared with 1.03 % for the Tc-99 containing borosilicate glass[5].

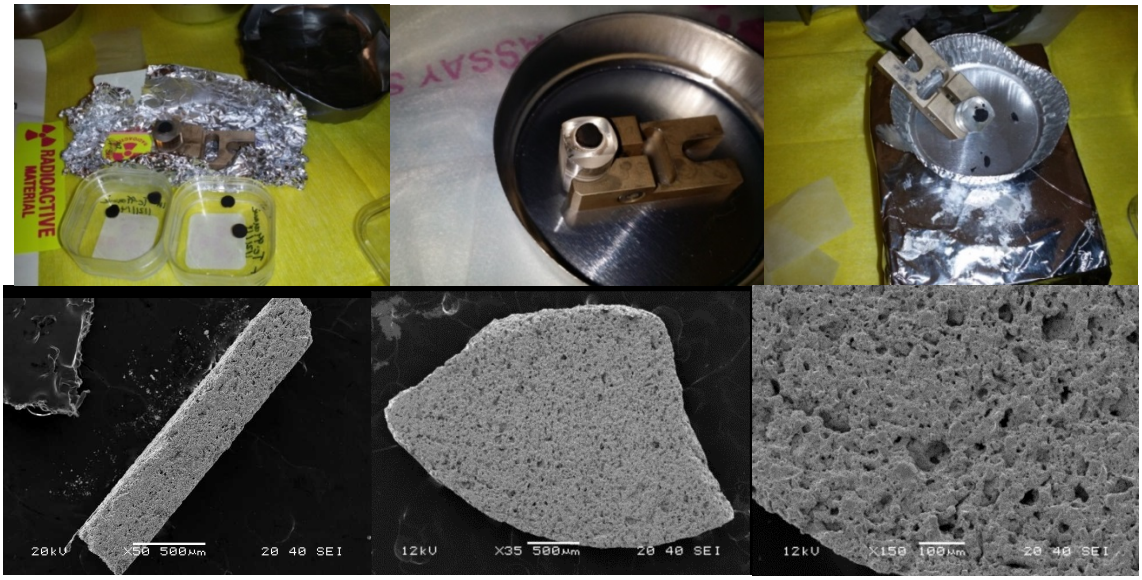

Figure 40: *Preparation of $Nd_2Tc_2O_7$ Pyrochlore Test Specimens for ASTM C1220-10 leaching experiments and SEM microstructure images of conventionally produced $Nd_2Tc_2O_7$ before C1220-10 corrosion testing*

Table 22*: Results on the corrosion of porous $Nd_2Tc_2O_7$ pyrochlore discs (ASTM C1220-10 for 28 days)*

Digestion Vessel	Duration [days]	Surface Area [mm^2]	Mass [g]	Relative Mass Loss [%]	Specific Mass Loss [g/mm^2 day]	Relative Tc-99 Release [%]
1	28	67.9	0.0203	0.44	4.6 E-8	0.74
2	28	72.4	0.1153	0.44	2.5 E-7	0.59
		Average for 28 days		**0.44**	**1.48 E-7**	**0.67**

In conclusion, the first corrosion experiments (ASTM C1220-10) on $Nd_2Tc_2O_7$ for 28 days showed significantly better leach and corrosion resistance of $Nd_2Tc_2O_7$ compared with Tc-99 containing LAWE4 type borosilicate glass, combined with optimal waste loading.

2.2.4 ASTM C1220-10 static leaching of $SrTcO_3$ perovskite specimens for 28 days

Three $SrTcO_3$ specimens produced by hot uniaxial pressing (7 days at 770 °C and 75 MPa) were prepared for 28 days ASTM C1220-10 corrosion testing. At this, the sintered $SrTcO_3$ perovskite specimens were initially ground with 240 grit silicon carbide papers on an Allied Multiprep system and polished to a 15-

[5] **T. Hartmann, I. J. Alaniz, A. J. Alaniz**: Fabrication and Chemical Durability of Ceramic Technetium-based Pyrochlores and Perovskites as Potential Waste Forms, CIMTEC 2014, 6th Forum on New Materials, Special Session FJ-10 "Materials Technology for Nuclear Waste Treatment and Disposal", 8-20 June 2014, Montecatini, Italy.

µm finish using diamond lapping paper (Figure 41).

***Figure 41**: Preparation of hot-pressed $SrTcO_3$ perovskite (SPE1) test specimens for ASTM C1220-10 leaching experiments for 28 days*

The monolithic $SrTcO_3$ perovskite samples were sintered to theoretical densities of 71 %, 33 % (SPE 2), 66 %. The density variation is a result of the addition on Zn-stearate as binder (0, 10, and 1 wt.-% binder) and the results of the corrosion testing are listed in Tables 23.

***Table 23:** Results on the corrosion of monolithic $SrTcO_3$ perovskite discs (ASTM C1220-10 for 28 days)*

Digestion Vessel	Mass of sample[g]	Surface Area [mm^2]	Volume of leachate [mL]	Strontium concentration in leachate (ppm)	Technetium concentration in leachate [mol/L]	Total amount of Sr in leachate [mg]	Total amount of Tc in Leachate [mg]
6	0.07588	53.97	5.4	2697	3.266E-04	14.564	17.462
7	0.04071	55.908	5.6	1950.2	2.150E-04	10.921	11.921
8	0.11287	58.008	5.8	1799.6	2.457E-04	10.438	14.106
Average				**2149 (±39)**	**2.624E-04**	**11.974**	**14.496**

Digestion Vessel	Relative Sr release [%]	Relative Tc-99 release [%]	Total mass dissolved [mg]	Relative Mass Loss [%]	Specific Mass Loss [g/mm^2 day]	Specific Mass Loss of LAWE4 Tc-glass [g/mm^2 day]
6	51.39	54.54	40.33	53.15	2.67E-05	6.43 E-7
7	71.83	69.40	28.69	70.47	1.83E-05	
8	24.76	29.62	31.01	27.47	1.91E-05	
Average	**49.33**	**51.18**	**33.34**	**50.37**	**2.14E-05**	

In conclusion, the first corrosion experiments (ASTM C1220-10) on $SrTcO_3$ for 28 days demonstrate very low corrosion resistance and low leach-resistance in the applied static corrosion tests. The specific mass loss of monolithic $ScTcO_3$ is with 2.14 10^{-05} (g/mm^2•days) about a factor of 33 larger than the specific mass loss of our reference Tc-loaded borosilicate glass LAWE4. The corrosion scenario can be described as congruent (homogeneous) overlaid with pitting corrosion. The average release of strontium and technetium were measured to 49 % and 51 % of the total inventory. The technetium release rates are

slightly higher than those of strontium. Also sample density significantly impacts the hydrodynamic properties. The sample with the lowest theoretical density (33 %) and was nearly completely corroded, and about 69 % of the Tc-99 inventory was dissolved in the leachate.

The $SrTcO_3$ specimens were embedded in epoxy resign and polished to a 1 μm finish for subsequent optical microscopy and SEM-EDS analysis (Figures 42, 43 & 44).

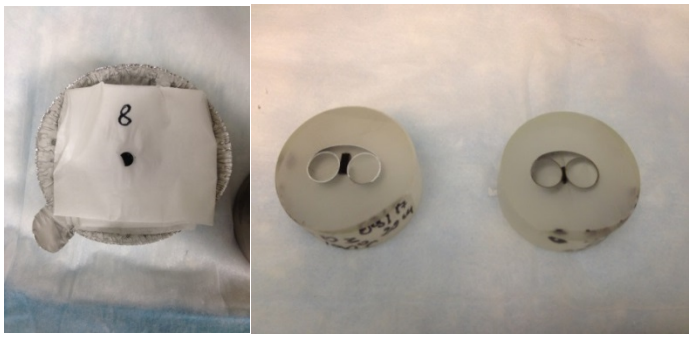

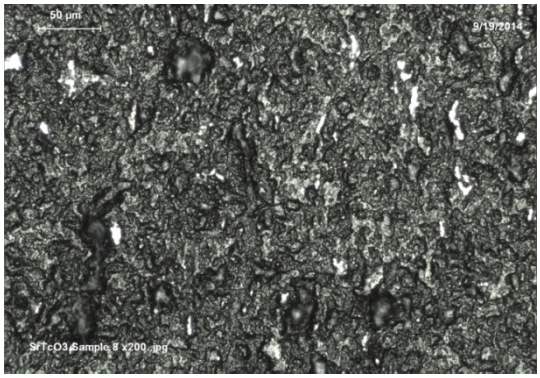

Figure 42: *$SrTcO_3$ pellet after 28 days C-1220-10 testing (left) and embedded for subsequent imaging and EDS analysis (right).*

Optical image of $SrTcO_3$ pellet after 28 days C-1220-10 testing x 200. The microstructure indicates that homogeneous corrosion is overlaid with pitting corrosion (bottom)

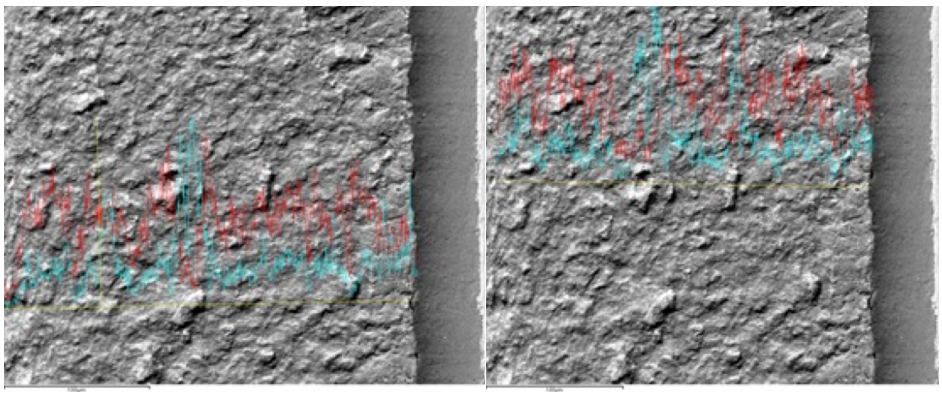

Figure 43: *Backscattered electron image of $SrTcO_3$ pellet. EDS elemental line-scans at the corroded surface (right of each image) for Sr (red) and Tc (cyan) are shown. Congruent (homogeneous) leaching and corrosion can be assumed and no chemical gradient is observed. The microstructure is showing some larger 20-30 μm Tc-enriched grains.*

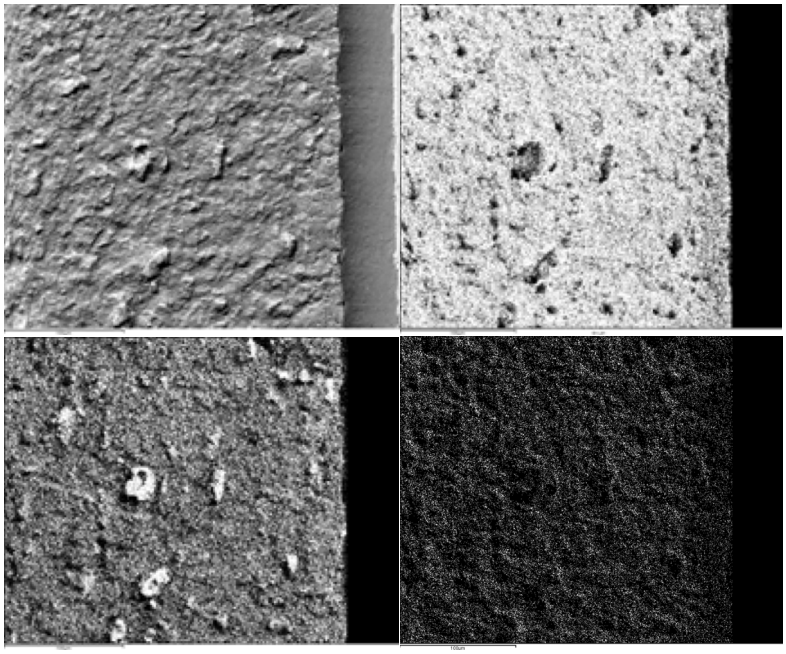

Figure 44: *Backscattered electron image of $SrTcO_3$ (top left) together with X-ray maps for strontium (top right), technetium (bottom left), and oxygen (bottom right). The microstructure is showing some larger 20-30 µm Tc-enriched grains, eventually indicating the presence of metallic Tc inclusions.*

2.2.5 Tc-99 release and specific mass loss of monolithic $Nd_2Tc_2O_7$ pyrochlore produced by hot-uniaxial pressing

In this chapter, the results of 7 days ASTM C1220-10 corrosion test of monolithic $Nd_2Tc_2O_7$ pyrochlore, fabricated by hot uniaxial pressing at 80 MPa and 1100 °C or 80 MPa and 900 °C are shown. These samples were prepared for corrosion testing by grinding and polishing down to 15 µm. The monolithic pyrochlore samples were sintered to theoretical densities of 74 %, 57 %, and 54 %. Applying hot pressing with graphite die material induces the reduction of Tc[IV] oxide to metallic technetium and the formation of Tc[IV] pyrochlore was not fully successful. The results of the corrosion testing are listed in Table 24.

Table* 24: Results on the corrosion of monolithic $Nd_2Tc_2O_7$ pyrochlore discs (ASTM C1220-10 for 7 days)*

Digestion Vessel	Mass of sample[g]	Surface Area [mm^2]	Volume of leachate [mL]	Neodymium concentration in leachate [mol/L]	Technetium concentration in leachate [mol/L]	Total Nd in leachate [µg]	Total Tc in Leachate [mg]
6	0.05474	49.996	4.99	2.578E-07	1.060E-05	37.18	1.049
7	0.09480	58.189	5.82	3.723E-07	2.425E-05	53.70	2.425
8	0.17020	65.851	6.59	1.712E-07	4.727E-05	24.69	4.679
Average				2.671E-07	2.745E-05	38.52	2.718

Digestion Vessel	Relative Nd release [%]	Relative Tc-99 release [%]	Total mass dissolved [mg]	Relative Mass Loss [%]	Specific Mass Loss [g/mm^2 day]	Specific Mass Loss of LAWE4 Tc-glass [g/mm^2 day]
6	0.141	5.80	1.087	1.98	3.106E-06	**6.43 E-7**
7	0.118	7.73	2.478	2.61	6.084E-06	
8	0.030	8.31	4.704	2.76	1.021E-05	
Average	0.096	7.280	2.757	2.45	**6.465E-06**	

The leachates of this corrosion tests were analyzed also in regard to dissolved oxygen and pH. The dissolved oxygen concentration increased from 4.63 mg/L to 6.64 mg/L for the blanks and to 6.71 mg/L for the samples in average. The pH decreased during the course of these leaching tests from 6.92 to 4.485 for the blanks and to 5.81 for the pyrochlore leachates.

Additional $Nd_2Tc_2O_7$ pyrochlore samples fabricated by hot-uniaxial pressing were prepared for 28-days corrosion testing. The synthesis of these samples was not fully successful and technetium oxide was nearly completely reduced to Tc metal due to the reducing conditions during hot-pressing and high-temperature sintering. We have completed the 28 days C1220-10 corrosion testing on pyrochlore samples (Table 25). The ceramic pyrochlore fabricated by hot pressing can be described as cermet materials and the corrosion experiments will reveal the impact of metallic technetium inclusion on technetium leaching.

Table 25: *Results of corrosion testing of monolithic $Nd_2Tc_2O_7$ pyrochlore discs (ASTM C1220-10 for 28 days)*

Digestion Vessel / Sample	Mass of sample[g]	Surface Area [mm^2]	Volume of leachate [mL]	Neodymium in leachate [mol/L]	Tc-99 in leachate [mol/L]	Total Nd in leachate [mg]	Total Tc in Leachate [mg]
6 - PY 4 7 - PY 5 8 - PY 6	0.2091 0.3019 0.1777	85.996 98.408 74.311	8.6 9.84 7.43	2.31 E-07 1.50 E-07 2.83 E-07	1.72 E-03 1.10 E-03 2.00 E-03	0.911 0.675 0.966	14.7 10.7 14.7
Average				**3.70 E-07**	**1.61 E-03**	**0.851**	**13.4**

Digestion Vessel / Sample	Relative Nd release [%]	Relative Tc release [%]	Metals dissolved [mg]	Relative Mass Loss [%]	Specific Mass Loss [g/mm^2 days]	Specific Mass Loss of LAWE4 Tc glass
6 - PY 4 7 - PY 5 8 -PY 6	0.904 0.464 1.127	21.20 10.75 25.00	15.611 11.375 15.666	9.79 4.97 11.58	8.50E-06 5.44E-06 9.89E-06	6.43E-7 (reference)
Average	**0.832**	**18.98**	**14.22**	**8.78**	**7.94E-06**	

The results for the 7-days and the 28-days corrosion tests show that metallic Tc-inclusions in a ceramic matrix are leading to increased Tc-leaching since the retention of Tc-99 as metallic inclusion is apparently far lower than bonded as $Tc^{[IV]}$ in the ceramic pyrochlore structure. Applying C1220-10 corrosion experiments the metallic inclusions undergo intense corrosion and about 19 % of the initial Tc inventory was dissolved, compared with less than 1 % for Nd. Overall, the samples show a specific mass loss of 6.47 10^{-6} $g/mm^2 \bullet$days after 7-days, and 7.94 10^{-6} $g/mm^2 \bullet$days after 28-days corrosion testing, which is by a factor 10 to 12 higher than the specific mass loss of the LAWE4 Tc-glass reference glass.

2.2.6 C1220-10 testing of monolithic $Pr_2Tc_2O_7$ and $Nd_2Tc_2O_7$ pyrochlore fabricated by hot –pressing of pyrochlore precursors followed by high-temperature sintering

We have fabricated ceramic monolithic $Pr_2Tc_2O_7$ and $Nd_2Tc_2O_7$ pyrochlore pellets after hot-pressing and high temperature sintering of pyrochlore precursors. The results of 7days C1220-10 corrosion testing are summarized in Table 26.

Table 26: *Results of corrosion testing of monolithic $Pr_2Tc_2O_7$ & $Nd_2Tc_2O_7$ pyrochlore pellets (ASTM C1220-10 for 7 days)*

Digestion Vessel / Sample	**Mass of sample[g]**	**Surface Area [mm^2]**	**Volume of leachate [mL]**	**Pr/Nd in leachate [mol/L]**	**Tc-99 in leachate [mol/L]**	**Total Pr/Nd in leachate [mg]**	**Total Tc in Leachate [mg]**
6 - PY 7 **7 - PY 8**	0.2783 0.2551	93.677 92.605	9.368 9.261	7.129 E-5 3.948 E-5	1.886 E-04 1.280 E-03	0.1807 0.1014	0.1749 1.1732
Average				**5.539 E-5**	**0.734 E-03**	**0.1410**	**0.6741**
Digestion Vessel / Sample	**Relative Pr/Nd release [%]**	**Relative Tc release [%]**	**Relative Mass Loss (weight) [%]**	**Relative Mass Loss (solution) [%]**	**Specific Mass Loss (solution) [g/mm^2 days]**	**Specific Mass Loss (weight) [g/mm^2 days]**	**Specific Mass Loss of LAWE4 Tc glass**
6 - PY 7 **7 - PY 8**	0.1364 0.0824	0.1879 1.3901	1.012 1.292	0.159 0.655	6.755 E-07 2.577 E-06	4.29 E-06 5.08 E-06	**6.43 E-7 reference**
Average	**0.1094**	**0.789**	**1.152**	**0.407**	**1.626 E-06**	**4.68 E-06**	

After applying 7 days C1220-10 corrosion testing , the ceramic pyrochlore samples $Pr_2Tc_2O_7$ (PY 7) and $Nd_2Tc_2O_7$ (PY 8) show a specific mass loss of 6.76 10^{-7} g/mm^2•days and 2.58 10^{-6} g/mm^2•days based on solubility data and elemental analysis, and 4.29 10^{-6} g/mm^2•days and 5.08 10^{-6} g/mm^2•days based on the physical mass loss. Hereby the corrosion is not congruent and the release of Tc is about a factor 7 higher than the release of the lanthanides. We further noticed significantly larger Tc release from $Nd_2Tc_2O_7$ compared with the Tc release from $Pr_2Tc_2O_7$ (1.17 mg vs 0.17 mg). The higher specific mass loss of $Nd_2Tc_2O_7$ and its increased susceptibility for Tc leaching can be partly explained by its lower achieved theoretical density (55.3 % vs. 68.2 %) and its higher porosity and enhanced inner surface area.

2.2.6.1 Matrix corrosion and microstructure of $Pr_2Tc_2O_7$ and $Nd_2Tc_2O_7$

After 7-days C1220-10 corrosion testing pellets of $Pr_2Tc_2O_7$ and $Nd_2Tc_2O_7$ were mounted in epoxy resin and polished to a 1 μm finish. The microstructure of $Pr_2Tc_2O_7$ after hot-pressing and high-temperature sintering and 7-days C1220-10 corrosion testing shows an open porosity of about 50 % and rather loosely arranged crystallites in the size range of 2 to 50 μm. Most crystallites are about 5 μm in size and appear as short prisms. The low density of the ceramic waste form and its microstructure of weakly embedded crystallites might explain its limitation in regard to mechanical properties. However, we could not identify any microstructural changes due to corrosion testing, and secondary phase formation and potential alteration along the grain boundaries were not observed (Figure 45).

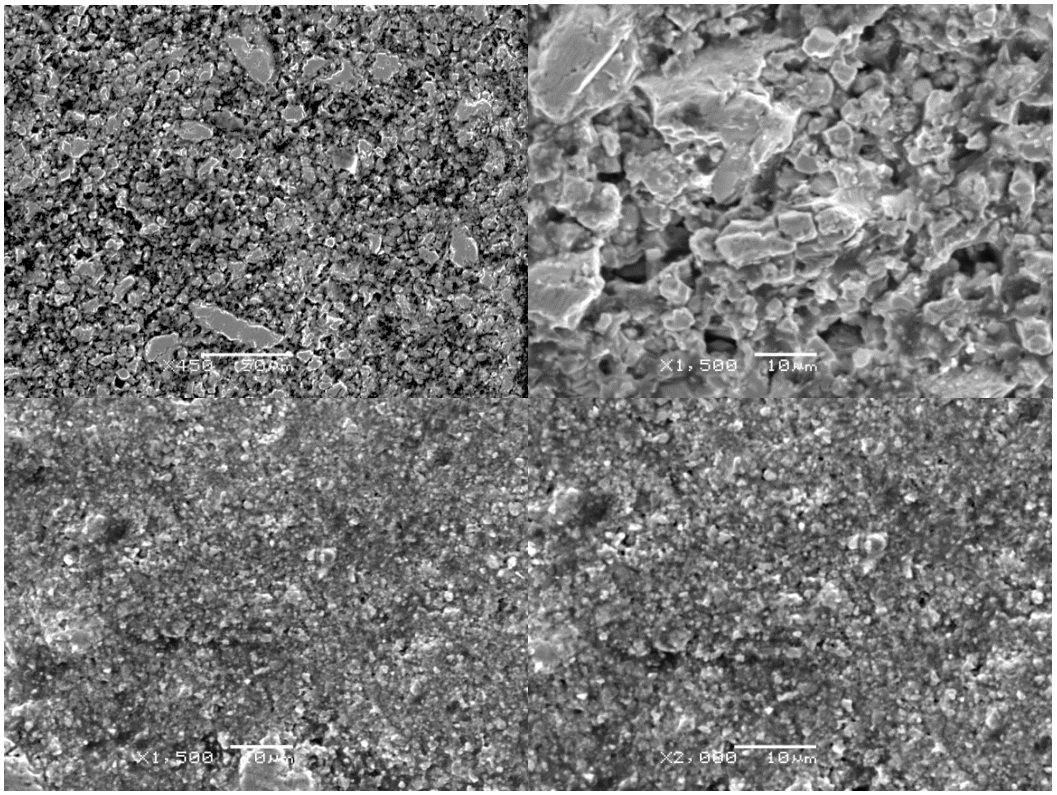

***Figure 45**: SEM (SEI) images of $Pr_2Tc_2O_7$ (top) x450 (left), and x1500 (right) of $Nd_2Tc_2O_7$ (bottom) x1500 (left), and x2000 (right) after 7 days C1220-10 testing*

We have noticed also by the results of X-ray diffraction that the microstructure of $Nd_2Tc_2O_7$ shows lower crystallinity compared with the microstructure of $Pr_2Tc_2O_7$ and the majority of the crystallites are with a size range of 1-2 μm too small for EPMA-based quantitative elemental analysis. Only in few locations, grains in the size range of 5-15 μm can be observed. Elemental analysis on $Pr_2Tc_2O_7$ using SEM-based EDS did not provide conclusive results so far as well. This might be partly related to the high porosity and small grain sizes within the microstructure of the pyrochlore (Figure 46). Within larger grains (> 5μm) the elemental ratio Pr/Tc is about 1 as expected. However, better quantitative data are needed for more profound statements and to gain knowledge if the elemental Ln/Tc ratio shows changes relative to spot location ant its distance to the surface exposed to the leachate.

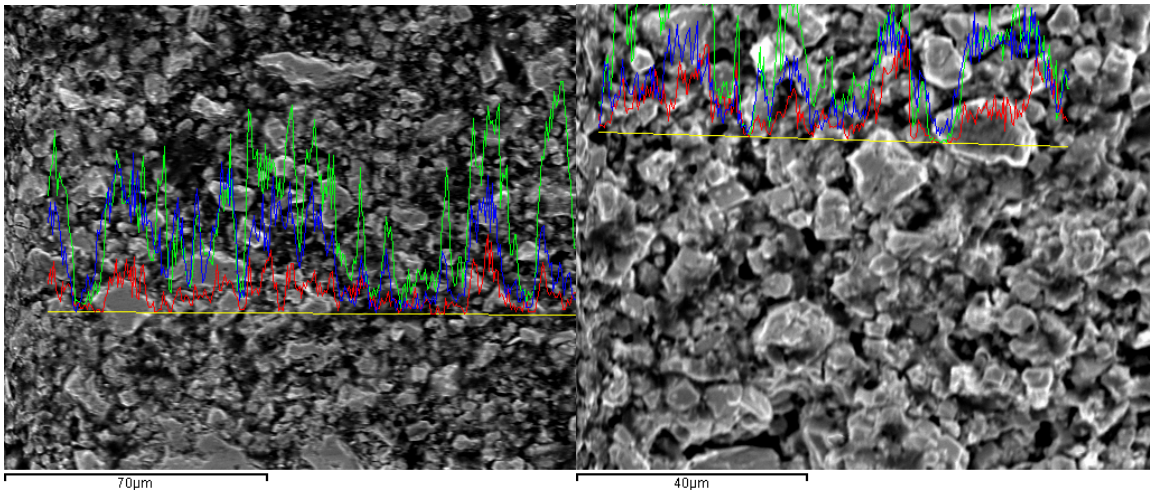

Figure 46: *SEM (BSE) image of $Pr_2Tc_2O_7$ (PY 7) x650 (left), and x1000 (right). The EDS signal for Tc (green), Pr (blue), and O (red) is displayed*

2.2.7 C1220-10 testing of monolithic $Sm_2Ru_2O_7$ pyrochlore fabricated by hot–pressing using AL23 corundum die followed by high-temperature sintering

Monolithic $Sm_2Ru_2O_7$ pyrochlore samples were prepared for corrosion testing by grinding and polishing and 7-days C1220-10 corrosion tests were completed. Results on the specific mass loss can be reported based on physical data (Table 27) and elemental chemical analysis of the leachates (Table 28). Based on physical data we can conclude a relative mass loss of 0.92 wt.-% in average and an average specific mass loss of 2.998 10^{-6} g/mm^2•days. Chemical analysis of the leachates are consistent with the physical data and through elemental analysis a specific mass loss of 3.70 10^{-6} g/mm^2•days was determined. These results compare well with the mass losses for $Pr_2Tc_2O_7$ and $Nd_2Tc_2O_7$ as reported in Chapter 2.2.6. Post-leaching phase analysis by X-ray diffraction did not reveal any changes in the crystalline phase content and a hydration phase for samarium or ruthenium was not observed.

Table 27: *Results of corrosion testing of monolithic $Sm_2Ru_2O_7$ pyrochlore specimens (ASTM C1220-10 for 7 days) based on physical data*

Digestion Vessel / Sample	Pre-Leaching Mass of Sample(g)	Pre Leaching Surface Area (cm^2)	Post-Leaching Mass of Sample(g)	Post Leaching Surface Area (cm^2)	Material Dissolved (g)	Relative Mass Loss (%)	Specific Mass Loss (g/mm^2 days)
6 - PY 9 7 - PY 10 8 – PY 11	0.20065 0.18708 0.21585	0.87607 0.88467 0.87825	0.19753 0.18601 0.21451	0.85678 0.86986 0.85030	0.00312 0.00107 0.00134	1.55 0.57 0.62	5.088 E-6 1.728 E-6 2.180 E-6
Average					**0.00184**	**0.916**	**2.998 E-6**

Table 28: *Results of corrosion testing of monolithic $Sm_2Ru_2O_7$ pyrochlore specimens PY 9, PY 10, & PY 11 (ASTM C1220-10 for 7 days)*

Digestion Vessel / Sample	Initial Mass of Sample [g]	Final Mass of Sample [g]	Mass Loss [mg]	Initial SA [mm^2]	Initial Volume [cm^3]	Initial Leachate Volume [mL]	Density of Pellet [g/cm^3]
6 – PY 9	0.2007	0.1976	3.0750	87.609	0.058	8.761	3.480
7 – PY 10	0.1871	0.1860	1.0700	88.467	0.060	8.847	3.134
8 – PY 11	0.2172	0.2145	2.6767	87.965	0.059	8.798	3.707
Average	0.2016	0.1994	2.2739	88.014	0.059	8.802	3.440

Digestion Vessel / Sample	Relative Mass Loss [%]	Specific Mass Loss (by mass) [g/mm^2/day]	Max. Sm in Sol. [mg]	Max. Ru in Sol. [mg]	Relative Sm release [%]	Relative Ru release [%]
6 – PY 9	1.53	5.01E-06	1.5040	1.0109	1.48	0.67
7 – PY 10	0.57	1.73E-06	0.5233	0.3518	0.48	0.22
8 – PY 11	1.23	4.35E-06	1.3091	0.8800	1.39	0.63
Average	1.11	**3.70E-06**	1.1121	0.7476	**1.10**	**0.50**

The corrosion behavior of $Sm_2Ru_2O_7$ pyrochlore monoliths shows a deviation of the expected congruent characteristics, and the retention of Ru in the pyrochlore structure is higher than the Sm retention under the given corrosion scenario. As a result, Sm is by a factor 2 more susceptible to leaching than Ru and the relative Sm concentrations within the leachates are elevated relative to the concentrations of Ru. These findings are also confirmed by SEM-based EDS studies on the leached surface of $Sm_2Ru_2O_7$ where higher remaining Ru concentration of the pyrochlore were measured, especially at the pellet rim area exposed to the leachate (Chapter 2.2.7.1)

2.2.7.1 Matrix corrosion and microstructure of $Sm_2Ru_2O_7$

We further performed a quantitative study on the surrogate wasteform $Sm_2Ru_2O_7$ and on the elemental distribution of Sm and Ru within the pyrochlore matrix after a 7-days C1220-10 corrosion test. Hereby pellets of $Sm_2Ru_2O_7$ were mounted in epoxy resin and polished to a 1 μm finish and SEM-based EDS analysis (JEOL 5600, Oxford Instruments) was performed. We quantified samarium and ruthenium contents within suitable grains using point analysis associated with a spatial resolution of ~3-5 μm. The elemental ratios Ru/Sm were plotted over r/r_0, the relative distance from the rim to the center of the pellet (Figure 47)

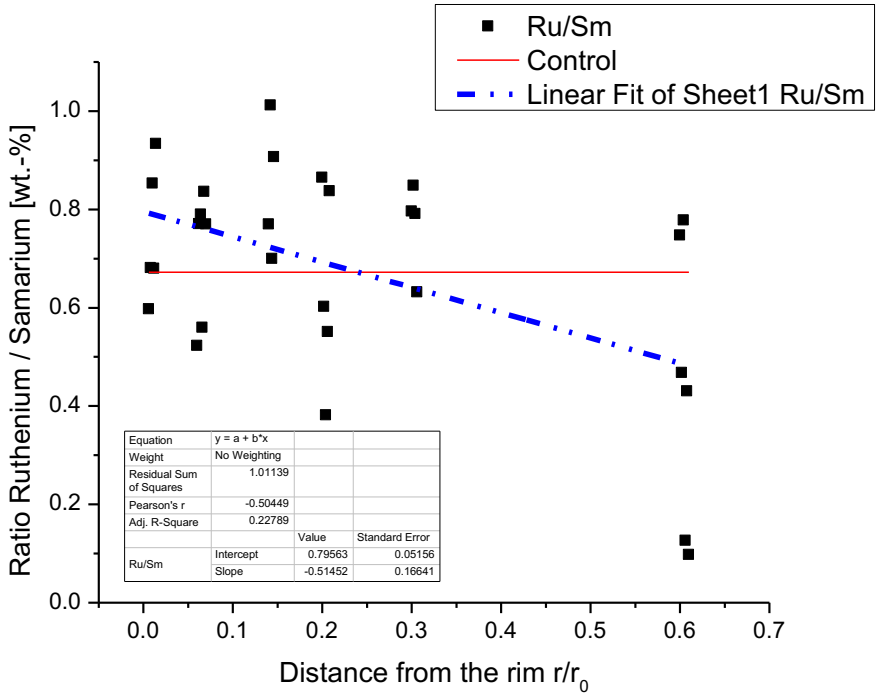

Figure 47: *Quantitative SEM-based EDS Analysis of $Sm_2Ru_2O_7$ (PY 9). The ratios Ru/Sm are plotted against the relative distance from the rim as r/r_0, for r = 5.0 mm. The data show significant scattering but the overall trend shows higher Ru concentrations (lower Sm concentrations) at the rim-area of the pellet.*

Even though the data show significant scattering, the overall trend shows higher relative Ru concentrations and lower Sm concentrations at the rim-area of the pellet. Therefore we can propose a slight deviation of the expected congruent corrosion scenario due to relatively increased leaching of samarium in contact to the leachate under the condition conditions of C1220-10. This observation is also confirmed by the results of chemical analysis of the leachates, where the retention of Ru in the pyrochlore structure is found higher than the Sm retention under the given corrosion scenario. This provides a good argument for pyrochlore based ceramics as technetium host phase.

2.2.8 C1220-10 testing of monolithic $Nd_2Tc_2O_7$ pyrochlore fabricated by hot–pressing using AL23 corundum die followed by high-temperature sintering

$Nd_2Tc_2O_7$ pyrochlore samples were fabricated by hot pressing and/or high temperature sintering (1 day at 1000 °C @ 80 MPa, or 24 hrs @ 700 °C/80 MPa followed by sintering at 1150 °C for 6 days) and the monolithic specimens were prepared for 7-days C-1220-10 corrosion testing. The samples contain besides $Nd_2Tc_2O_7$ pyrochlore also Nd_2O_3, Nd_3TcO_7 and Tc-metal. In table 29 corrosion data on $Nd_2Tc_2O_7$ pyrochlore are shown which was fabricated entirely through hot pressing at 1000 °C and contained residual Nd_2O_3.

***Table 29: Results** of corrosion testing of monolithic $Nd_2Tc_2O_7$ pyrochlore specimen PY 12 produced by hot uniaxial pressing (ASTM C1220-10 for 7 days)*

Digestion Vessel / Sample	Initial Mass of Sample [g]	Final Mass of Sample [g]	Sample Mass Loss [mg]	Initial Pellet SA [mm^2]	Initial Pellet Volume [cm^3]	Density of Pellet [g/cm^3]	Relative Mass Loss [%]	Specific Mass Loss (by mass) [g/mm^2/day]
6 – PY 12	0.1446	0.1412	3.3767	65.413	0.032	4.466	2.34	**7.37E-06**

Digestion Vessel / Sample	Relative Nd release [%]	Relative Tc release [%]	Nd in leachate (g/ml)	Tc in leachate (mol/L)	Total Nd in leachate (mg)	Total Tc in leachate (mg)
6 –PY 12	1.63	0.47	1.77E-06	0.0003	1.1330	0.224

Digestion Vessel / Sample	Specific Mass Loss by chem. analysis [g/mm^2/day]	Max. Nd in Sol. [mg]	Max. Tc in Sol. [mg]
6 –PY 12	**3.53E-06**	1.6276	1.1171

$Nd_2Tc_2O_7$ fabricated by hot-unaxial pressing using AL23 dies showed a specific mass loss of 3.53 10^{-6} g/mm^2•days based on elemental analysis of the leachate and a specific mass loss of 7.37 10^{-6} g/mm^2•days derived from physical data. The leaching data for $Nd_2Tc_2O_7$ showed, similar to the data of $Sm_2Ru_2O_7$, a noticeable deviation from congruent waste-form corrosion. As it appears, the tetravalent Tc or Ru cations which occupy the *16 c* positions within the crystal structure of pyrochlore show larger bonding energies than the trivalent Sm or Nd cations occupying the *16 d* and their contribution to the overall lattice energy of pyrochlore is higher. This also demonstrates that the pyrochlore structure is an excellent host for technetium in the tetravalent state and Tc shows by a factor 2 to 3 lower susceptibility to corrosion than the trivalent lanthanide cations.

2.2.9 C1220-10 testing of monolithic surrogate $Sm_2(Ru_{0.5}Ti_{0.5})_2O_7$ pyrochlore fabricated by wet-chemical co-precipitation

ASTM C1220-10 corrosion testing was employed to measure the chemical retention in the co-precipitated pellets in ASTM Type II water at 90 °C. PTFE Teflon vessels and the respective stainless steel autoclaves were utilized to contain the leachant and the pellets. Prior to testing, these vessels were rinsed three times with deionized water and subsequently with 0.1M HNO_3. The pellets were dried overnight after specimen cleaning at which, time the dimensions, diameter and height were recorded (Figure 30).

***Table 30**: Pre-Corrosion Data for $Sm_2(Ru_{0.5}Ti_{0.5})_2O_7$ Pellets*

Pre-Corrosion Surface Area of Pellets, Pellet Mass and Corresponding Leachant Volume and Leachant Mass							
Pellet Number	Mass (g)	Surface Area (cm^2), S	Surface Area (mm^2)	Volume ASTM H_2O (mL), V	Corrosion Vessel Number	Volume of Leachate (mL)	Mass (g) of Lid, Vessel, Frame w/ Wire, Leachate, and Pellet
3	0.13655	0.627	62.7	6.270	8	6.270	118.0453
4	0.2744	0.792	79.2	7.920	4	7.920	119.2084
5	0.271	0.785	78.5	7.850	9	7.850	119.3556
6	0.3332	0.902	90.2	9.020	10	9.020	121.0492
Blank Vessel Number	Corresponding to Corrosion Vessel	Volume of Leachate (mL)	Mass (g) of Lid, Vessel, Leachate				
7	8	6.27	115.5102				
1	4	7.92	117.5161				
2	9	7.85	117.5859				
3	10	9.02	117.4933				

Note: Surface Area, **S**, to Volume ASTM H_2O, **V** Ratio, **S/V**, is **$10m^{-1}$**

All of the PTFE vessels were placed in the stainless steel enclosures which were tightened to ensure minimal leachant loss. The enclosures containing the PTFE vessels were placed in a ThermoScientific® HeraTherm® furnace which was set to 90°C. The vessels remained in the furnace for a period of 7 days at which time they were removed and allowed to cool overnight. The PTFE vessels were carefully removed from the stainless steel enclosures and weighed. The leachate contained no visible residual solids so it was decanted from the corrosion vessels and saved for ICP-MS analysis. Next, the pellets were carefully removed from the frame and wires of corrosion vessels (Figure 48) rinsed with high purity water, and allowed to dry overnight. The post corrosion mass and surface area of each pellet were determined and recorded in Table 31.

***Table 31:** Post Corrosion Data for $Sm_2(Ru_{0.5}Ti_{0.5})_2O_7$ Pellets*

Post Corrosion Surface Area of Pellets, Pellet Mass and Corresponding Leachate Volume and Leachate Mass							
Pellet Number	Mass (g)	Height (mm)	Diameter (mm)	Surface Area (mm^2)	Surface Area (cm^2)	Corrosion Vessel Number	Mass (g) of Lid, Vessel, Frame w/ Wire, Leachant, and Pellet
3	0.13649	1.54	4.98	63.0	0.630	8	118.0387
4	0.27076	2.98	4.73	79.4	0.794	4	119.1924
5	0.26828	2.91	4.74	78.6	0.786	9	119.3501
6	0.32815	3.64	4.76	90.0	0.900	10	121.0387
Blank Vessel Number	Corresponding to Corrosion Vessel	Mass (g) of Lid, Vessel, Leachant					
7	8	115.4965					
1	4	117.5105					
2	9	117.5802					
3	10	117.4886					

The final mass fell within 0.015 % of the initial mass for all the vessels (Table 31). The mass loss was completely attributed to water loss (with density of 1 g/mL) which did not exceed 0.002 mL/day. These findings rendered the corrosion test valid according to the designation and were attributed to the use of the stainless steel enclosures in preventing water loss.

Figure 48: *Pellets in Leachate in PTFE Vessels after corrosion test. No visible solids were seen the leachate.*

The measured concentrations (in ppb) of samarium, ruthenium, and titanium in the leachates are recorded in Table 32 and were used in conjunction with the volume of the leachates for each corresponding pellet to compute the masses of dissolved elements (Sm, Ru, and Ti). The formula used was

$$\boldsymbol{m_{element} = C * V_f}$$

where $\boldsymbol{m}$ is the mass of the dissolved element, $\boldsymbol{C}$ is the concentration of said element, and $\boldsymbol{V_f}$ is the final volume of the leachate in the respective vessel. Normalized elemental mass loss values were then calculated using the formula

$$\boldsymbol{NL_E = \frac{m}{f * S}}$$

Where $\boldsymbol{NL_E}$ is the normalized elemental mass loss where $\boldsymbol{E}$ denotes the element, $\boldsymbol{m}$ is the elemental mass in the leachate, $\boldsymbol{f}$ is the mass fraction of the element and $\boldsymbol{S}$ is the surface area in m^2 of the pellet. The mass fraction, $\boldsymbol{f}$, was found using the stoichiometry of the intended pyrochlore $Sm_2(Ru_{0.5}Ti_{0.5})_2O_7$. The specimens were not homogeneous as they contained two to three phases and even within phases, such as the pyrochlore phase, a range of stoichiometry was possible. The normalized elemental mass loss was divided by the number of days of the experiment, to obtain the characteristic elemental mass loss. The release of ruthenium was about a factor of 10 greater in pellets 4, 5, and 6 while the release of samarium was about a factor of 10 greater in pellet 3 compared to the other specimens. This may be attributed to the presence of ruthenium metal in pellets 4, 5, and 6. The normalized mass loss of ruthenium was calculated to be the lowest of the three elements for all test specimens suggesting that it is most resistant to corrosion. The release of titanium from pellets 4 and 6 was relatively equal.

Because the normalized mass loss result for samarium was computed to be the highest, an indication of non-stoichiometric release of this element is plausible. Or, it may be that the samarium leached out of the orthorhombic, Sm_2TiO_5, phase. A separate corrosion test involving only the orthorhombic phase would shed some light on this matter.

Next, the normalized mass loss was determined by

$$NL_{\#} = \frac{m_{\#}}{S}$$

where $NL_{\#}$ is the normalized mass loss with a subscript denoting the pellet number, $m_{\#}$ is the mass loss of the numbered pellet and S is the respective surface area in m^2. This computation was divided by the number of days to obtain characteristic normalized mass loss. The results of the calculations are summarized in Table 33.

Table 32: *Mass of Elements Released from Pellets into Leachate*

Mass of Elements (Sm, Ru, Ti) Released From Pellets				
Pellet Number	3	4	5	6
Concentration of Samarium measured in Leachate (ppb)	2708	37.361	225.91	281.74
Concentration of Samarium measured in Leachate (g/L), ***C***	0.002708	0.000037361	0.00022591	0.00028174
Final Volume if Leachate in Vessel Containing Pellet(L), V_f	0.006263	0.007904	0.007845	0.009007
Mass of Samarium released from from Pellet (g), m_{Sm}	1.6961E-05	2.9530E-07	1.7722E-06	2.5376E-06
Ruthenium measured in Leachate (ppb)	0.028	0.354	0.297	0.395
Concentration of Ruthenium measured in Leachate (g/L), ***C***	0.000000028	0.000000354	0.000000297	3.95E-07
Final Volume if Leachate in Vessel Containing Pellet(L), V_f	0.006263	0.007904	0.007845	0.009007
Mass of Ruthenium released from from Pellet (g), m_{Ru}	1.7538E-10	2.7980E-09	2.3298E-09	3.5577E-09
Concentration of Titanium measured in Leachate (ppb)	negative value	0.59	negative value	0.476
Concentration of Titanium measured in Leachate (g/L), ***C***	N/A	0.00000059	N/A	4.76E-07
Final Volume if Leachate in Vessel Containing Pellet(L), V_f	0.006263	0.007904	0.007845	0.009007
Mass of Titanium released from from Pellet (g), m_{Ti}	N/A	4.66336E-09	N/A	4.2872E-09

Table 33: *Normalized and Characteristic Elemental Mass Loss*

Normalized Elemental Mass Loss Based on Release of Elements (Sm, Ru, Ti)				
Element	Samarium	Ruthenium	Titanium	
Mass of Element in Leachate in Pellet (g), ***m***	m_{Sm} **(g)**	m_{Ru} **(g)**	m_{Ti} **(g)**	***Surface Area of Pellet (m^2)***
Pellet 3	1.6961E-05	1.7538E-10		6.30E-05
Pellet 4	2.9530E-07	2.7980E-09	4.66336E-09	7.94E-05
Pellet 5	1.7722E-06	2.3298E-09		7.86E-05
Pellet 6	2.5376E-06	3.5577E-09	4.28724E-09	9.00E-05
Mass Fraction of Element in $Sm_2(Ru_{0.5}Ti_{0.5})_2O_7$, ***f***	0.5354	0.18	0.0852	
	Pellet 3	**Pellet 4**	**Pellet 5**	**Pellet 6**
Normalized Elemental Mass Loss from Pellet Based on Samarium (g/m^2), NL_{Sm}	0.502	0.00694	0.0421	0.0526
Characteristic Elemental Mass loss ($g/(m^2 \bullet day)$)	0.0718	0.00099	0.00601	0.00752
Normalized Elemental Mass Loss from Pellet Based on Ruthenium (g/m^2), NL_{Ru}	0.0000155	0.000196	0.000165	0.000220
Characteristic Elemental Mass Loss ($g/(m^2 \bullet day)$)	0.00000221	0.0000280	0.0000235	0.0000314
Normalized Elemental Mass Loss from Pellet Based on Titanium (g/m^2), NL_{Ti}		0.000689		0.000559
Characteristic Elemental Mass Loss ($g/(m^2 \bullet day)$)		0.0000984		0.0000799

Normalized Mass Loss from Pellet						
Mass Loss of Pellet, **m**		Pellet	Surface Area of Pellet (m^2)	Normalized Mass Loss from Pellet (g/m^2), **NL**	Characteristic Mass Loss from Pellet ($g/(m^2 \bullet day)$)	
Mass Loss of Pellet 3 (g), m_3	6E-05	*Pellet 3*	6.30E-05	0.95	0.14	NL_3
Mass Loss of Pellet 4 (g), m_4	0.00364	*Pellet 4*	7.94E-05	45.83	6.55	NL_4
Mass Loss of Pellet 5 (g), m_5	0.00272	*Pellet 5*	7.86E-05	34.59	4.94	NL_5
Mass Loss of Pellet 6 (g), m_6	0.00505	*Pellet 6*	9.00E-05	56.10	8.01	NL_6

Pellet 3 was fabricated under different conditions (e.g. calcination at 600°C and sintering under continuous argon flow) and the relatively low normalized mass loss can be attributed to the lack of ruthenium metal. The normalized mass loss of pellets 4, 5, and 6 is linked to the presence of ruthenium metal and other impurities in the specimens.

2.2.9.1 Matrix corrosion and microstructure of $Sm_2(Ru,Ti)_2O_7$

To harvest information on the thermodynamics and kinetics of waste form matrix corrosion SEM-based investigation using energy-dispersive X-ray spectroscopy (EDS) were performed. After fabrication and

corroding, we prepared 5 sample pellets for EDS based analysis by grinding and polishing to 1-µm finish. The surfaces of the corroded pellets were examined using SEM/EDS (Figures 49 to 53) and the microstructures shows large 50-100 grains embedded in a porous matrix. Elemental semi-quantitative EDS analyzed was used to determine the relative ratios of the metal cations at different locations relative to the rim area of the pellet. All pellets are composed of two phases: a) Sm_2TiO_5 and b) the solid solution phase $Sm_2(Ti,Ru)_2O_7$. The dense grain in Figure 50, Region 1 represents Sm_2TiO_5 and shows no measurable solubility for Ru (Table 34, spectra 1-5). The dense grain (Figure 51, Region 2) represents the pyrochlore solid solution phase $Sm_2(Ru_xTi_{1-x})O_7$ with ruthenium contents in the range of 4 to 9 at.-%.

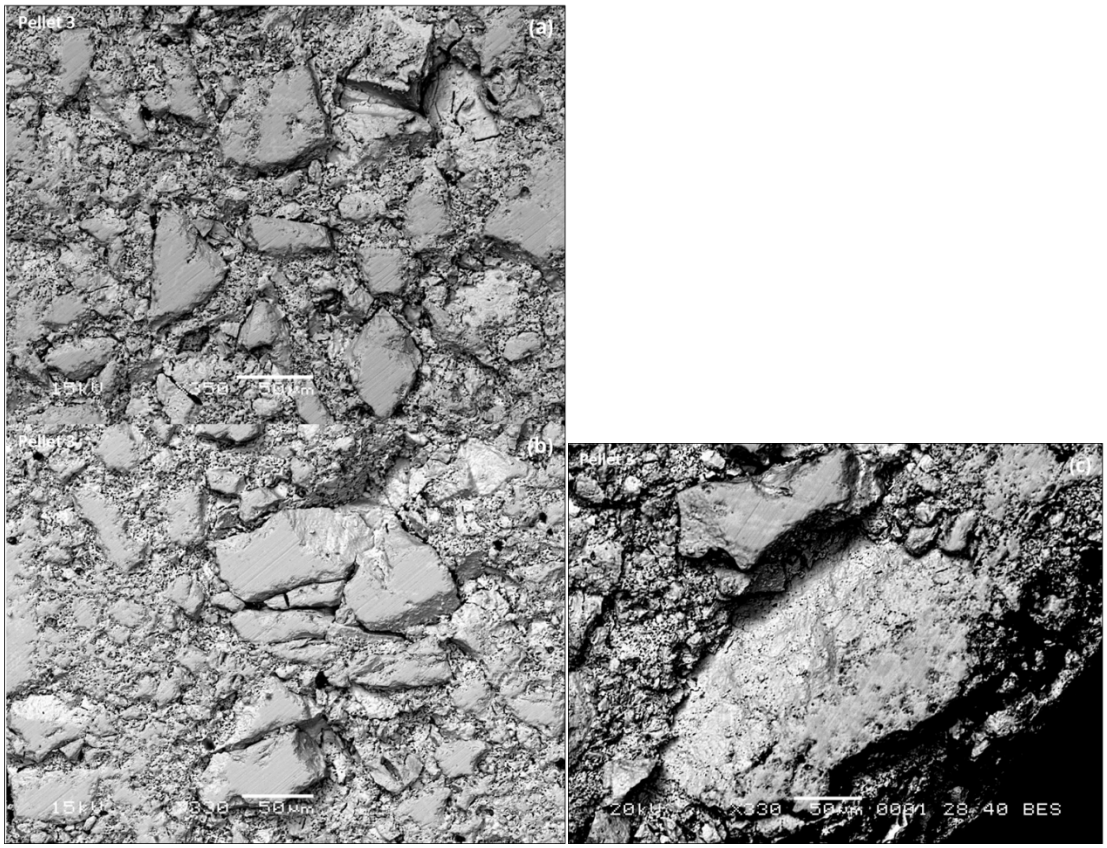

Figure 49: *SEM Images of Pellet 3 after corrosion testing. Backscattering at (a) Magnification X350 (b) Magnification X330 (c) Magnification X330, Pellet Edge*

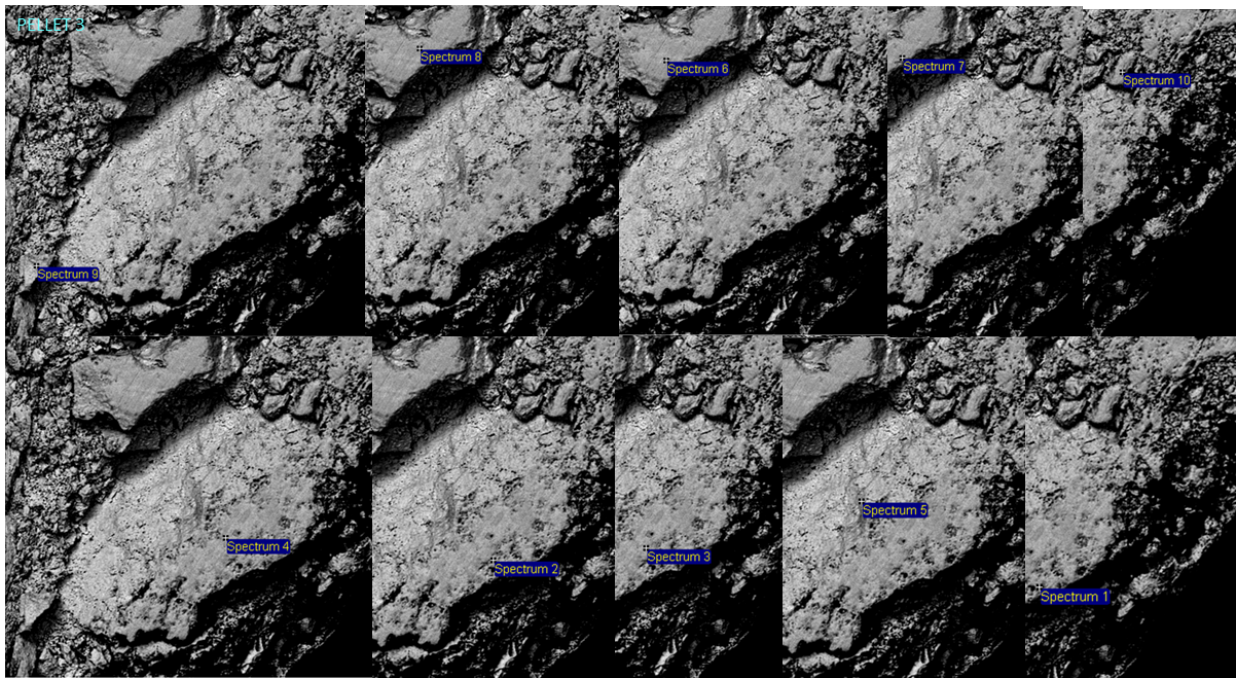

Figure 50: *(Overlapping) SEM images of edge of Pellet 3 indicating Point Spectra Locations used in EDS analysis*

Figure 51: *Two Distinct Regions of Edge of Pellet 3. Region 1 shows no trace of Ruthenium and represents* Sm_2TiO_5 *and Region 2 shows a significant amount of Ruthenium and represents the solid solution pyrochlore phase* $Sm_2(Ru_xTi_{1-x})O_7$. [6]

[6] **T. Hartmann**, Advanced ceramic waste forms to immobilize technetium, 2016 Summer School, Nuclear and Radiochemistry (NCSS), June 13-22, 2016.

Table 34: *Atomic Ratio of Titanium to Ruthenium obtained from EDS from the Edge of Pellet 3 (region 1).*

Point Spectra Analysis Data for Edge Region of Pellet 3				
Spectrum Number	*Atomic Percent Titanium, %*	*Atomic Percent Ruthenium,%*	*Atomic Ratio of Titanium to Ruthenium, Ti%:Ru%*	*Appearance of Location of Spectra*
1	12.34	0	100.00 : 0.00	dense
2	12.3	0	100.00 : 0.00	dense
3	11.64	0	100.00 : 0.00	dense
4	11.63	0	100.00 : 0.00	dense
5	29.91	0	100.00 : 0.00	dense
6	10.87	6.72	61.80 : 38.20	dense
7	11.82	0	100.00 : 0.00	dense
8	9.49	9.38	50.29 : 49.71	dense
9	7.47	0	100.00 : 0.00	dense
10	10.81	4.18	72.11 : 27.89	dense

Based on the EDS analysis the stoichiometry for the pyrochlore phase was determined to $Sm_2(Ru_XTi_{1-X})_2O_7$, for $0.30<x<0.49$ and the composition of the solid solution phase varied between $Sm_2(Ru_{0.3}Ti_{0.7})_2O_7$ and $Sm_2(Ru_{0.49}Ti_{0.51})_2O_7$.

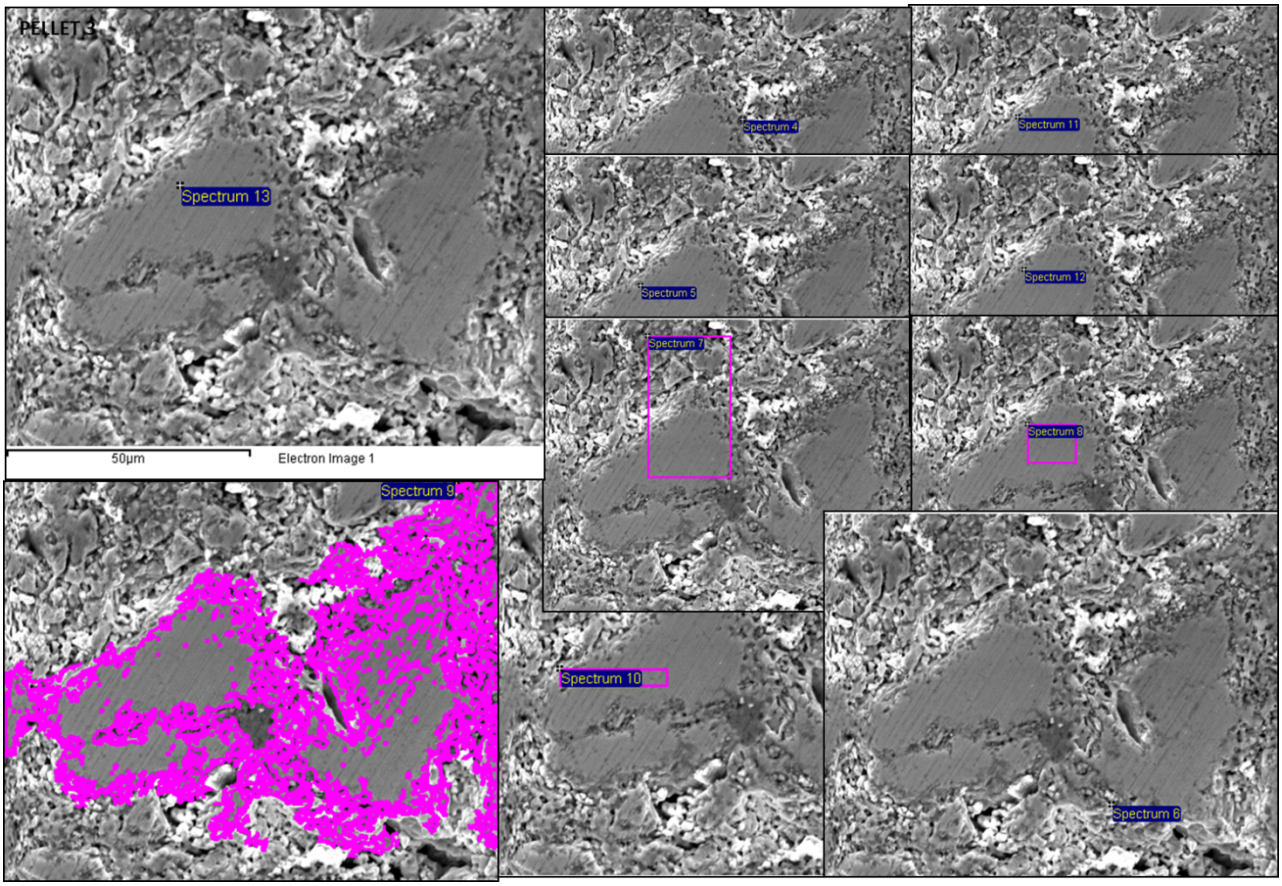

Figure 52*: EDS Point Spectra/Area Scans of Center Region of Cross Section of Pellet 3. Secondary Electron Images.*

Table 35: *Atomic Ratios of Titanium to Ruthenium in Center of Pellet 3 obtained by EDS Point/Area Scans*

Point Spectra Analysis Data for Center Region of Pellet 3				
Spectrum Number	*Atomic Percent Titanium, %*	*Atomic Percent Ruthenium,%*	*Atomic Ratio of Titanium to Ruthenium, Ti%:Ru%*	*Appearance of Location of Spectra*
3	8.05	0	100.00 : 0.00	porous
4	8.81	7.92	52.66 : 47.3	slightly porous
5	11.65	0	100.00 : 0.00	dense
6	9.9	4.27	69.87 : 30.1	dense
7	14.92	7.46	66.67 : 33.3	dense
8	16.16	7.97	66.97 : 33.0	dense
9	9.8	6.67	59.50 : 40.5	porous
10	39.29	0	100.00 : 0.00	dense
11	10.5	6.46	61.91 : 38.1	dense
12	10.42	6.99	59.85 : 40.1	dense
13	9.61	9.08	51.42 : 48.6	dense

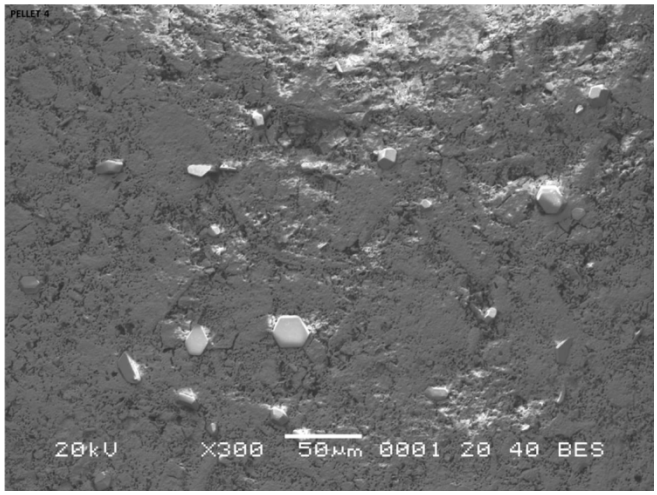

Figure 53: *SEM Backscattering Image of Pellet 4 at x300 Magnification with visible crystallized ruthenium as hexagonal prisms*

In pellet 4 (Figure 53) the presence of crystalline ruthenium inclusions are very well indicated by hexagonal prismatic crystallites of up to 20 µm in diameter. For pellet 5 successive point spectra were recorded starting from the edge and therefore from the surface in direct contact with the leachate, and then moving inwards in steps of 30 µm. The analytical results are listed in Table 36 and the spectra with highest ruthenium percentages are highlighted. As shown in Figure 54, the samarium and titanium concentrations are relatively consistent from the edge inwards, while the ruthenium concentration is generally low and varies considerably. EDS analysis in which ruthenium concentrations of several wt.-% is measured indicate the presence of the pyrochlore solid solution phase, and on the other hand, the absence of ruthenium combined with a near 2:1 Sm/Ti ratio indicated the presence of orthorhombic Sm_2TiO_5.[78]

[7] **T. Hartmann**, Fabrication and properties of technetium waste forms, Miami, July 27, 2016, Florida International University, Technical Exchange meeting

[8] **T. Hartmann**, Synthesis and properties of advanced technetium waste forms, Las Vegas, July 14, 2016, Technical exchange meeting with NA-20

Table 36: *Atomic Ratios of Titanium to Ruthenium from EDS using Point analysis*

Point Spectra Analysis for Pellet 5 Edge						
Spectrum	Atomic Percent Titanium, %	Atomic Percent Ruthenium, %	Atomic Percent Samarium, %	Percent Ratio of Titanium to Ruthenium		
Spectrum 1	40.54	7.27	52.20	84.80	:	15.20
Spectrum 2	33.87	0.00	68.52	100.00	:	0.00
Spectrum 3	14.35	58.09	27.56	19.81	:	80.19
Spectrum 4	28.96	14.52	56.52	66.60	:	33.40
Spectrum 5	38.14	3.05	58.81	92.61	:	7.39
Spectrum 6	50.91	1.64	47.45	96.88	:	3.12
Spectrum 7	28.49	1.14	70.37	96.15	:	3.85
Spectrum 8	45.53	0.99	53.48	97.87	:	2.13
Spectrum 9	34.32	20.68	45.00	62.40	:	37.60
Spectrum 10	39.64	2.51	57.85	94.05	:	5.95
Spectrum 11	29.22	2.59	68.19	91.86	:	8.14
Spectrum 12	31.52	0.00	68.77	100.00	:	0.00
Spectrum 13	37.11	0.01	62.88	99.97	:	0.03
Spectrum 14	37.52	12.90	49.58	74.42	:	25.58
Spectrum 15	31.14	4.67	64.19	86.96	:	13.04
Spectrum 16	38.23	0.82	60.95	97.90	:	2.10
Spectrum 17	30.68	9.80	59.52	75.80	:	24.20
Spectrum 18	36.29	5.25	58.45	87.36	:	12.64

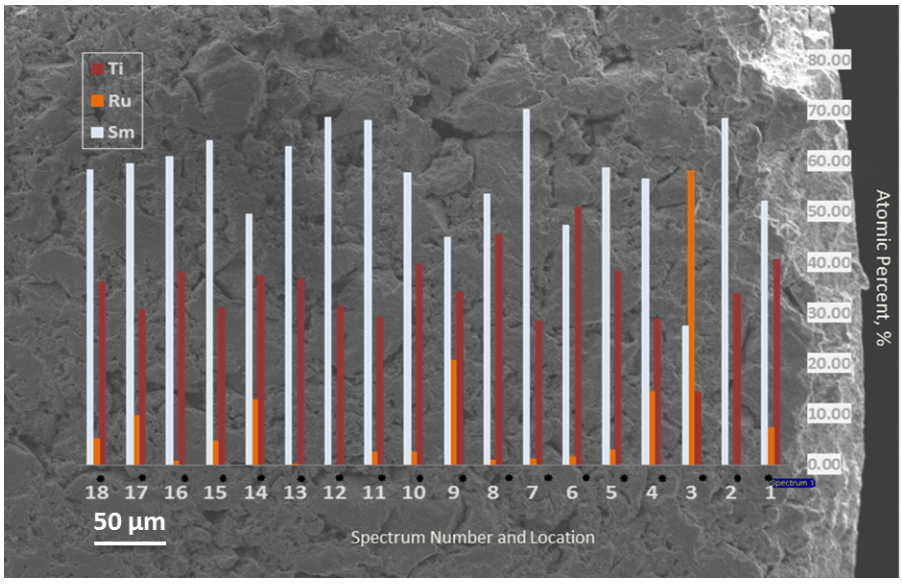

Figure 54: *Plot of Relative Atomic Percentages of Ru, Ti, and Sm in Pellet 5*

3. Conclusions

This NEUP project 12-3445 under the work package NU-12-NV-UNLV-0202-06: "Thermodynamic and Microstructural Mechanisms in the Corrosion of Advanced Ceramic Technetium-bearing Waste Forms and Thermophysical Properties" is a major contribution to the knowledge on ceramic technetium waste forms. Our work especially on technetium pyrochlores was groundbreaking and we gained vast knowledge on their synthesis, microstructure, crystal structure and their susceptibility for technetium leaching and waste form matrix corrosion in ASTM corrosion tests such as C1220-10 on monolithic waste forms. Strontium technetium perovskite can be synthesized at rather low temperature but showed poor performance in corrosion testing, and strontium technetium layered perovskites could not be synthesized as large monoliths. Our main focus was to develop synthesis routes for fabrication of gram-size monolithic lanthanide technetium pyrochlores and to advance their density and mechanical properties. We further developed a process flowsheet which could be implemented to the current flowsheet for vitrifying low-and highly radioactive effluents at the Waste Treatment Plant and the Hanford site.

Lanthanide technetium pyrochlores have shown their ability as superior waste form in corrosion testing experiments compared with the (layered) perovskites and the LAWE4 based technetium containing borosilicate glass, but their fabrication requires high-temperature annealing at typically 1150 °C and the sintered densities are with about 50 % theoretical, low. The lanthanide technetium pyrochlores as well as the ruthenium surrogates do not undergo densification during sintering and the final sintered densities are very much identical with the green pellet densities. The strontium technetium perovskites, on the other hand, sinter to theoretical densities of 70 % or higher at rather low temperatures of 570 °C for the tetragonal Sr_2TcO_4 layered perovskite and 770 °C for the orthorhombic perovskite $SrTcO_3$. Even though the perovskites might not serve well as final technetium host phases due to their susceptibility for corrosion, they can act as excellent intermediates for introducing technetium in the tetravalent state in processes for vitrification or the fabrication of glass-ceramics. We have developed a radiological hot uniaxial press to allow for sintering at 1100 °C under 50 to 400 MPa load with the reason to improve pellet densities and the mechanical properties of the monoliths such as compressive strength and fracture toughness. The use of hot-uniaxial pressing to fabricate technetium or ruthenium pyrochlores was only partly successful and in contact with the graphite-die materials, the oxides of technetium and ruthenium undergo reduction to the metals at temperatures starting as low as 700 °C. Mitigation of technetium or ruthenium reduction was achieved by the use of custom-made AL23 corundum dies. AL23, however, is not completely inert at temperatures of 1000 °C or higher and reactions of the powders in contact with the alumina surface were observed. As a result, the pistons got jammed in the dies and the use of an appropriate lubricant might be researched further. The fabrication of technetium pyrochlores using hot-pressing at 700 °C (AL23 die) followed by high temperature sintering at 1150 °C was successful and at 1160 °C the formation of a new phase: orthorhombic $Nd_3Tc^{[V]}O_7$, was observed. For producing technetium pyrochlore of higher theoretical densities we introduced titanium oxide as sintering agent. Titanium also forms lanthanide pyrochlores such as technetium and ruthenium do, but its introduction to the dry chemical process only slightly increases sintered theoretical densities.

To further increase densities and to also enhance mechanical strength of the ceramic pyrochlore waste forms, we have developed a wet-chemical synthesis route which could be deployed as a technical solution for continuously depleting the Tc-content of the glass melter feed by precipitating Tc from the effluents of the off-gas capture and recycling systems and subsequently for effectively immobilizing Tc as durable ceramic waste form. This process involves a wet-chemical coprecipitation-based synthesis route to fabricate gram-size, phase-pure Tc-based pyrochlores with the model composition $Sm_2(Tc_{0.5-x}Ru_xTi_{0.5})_2O_7$ and is up-scalable to technical scale. Pertechnetate ($Tc^{(VII)}O_4^-$), the dominant Tc-species in the off-gas washer solution, was successfully reduced to technetate ($Tc^{[IV]}O_2$) within hours using tin(II) chloride in excess at pH 4.5 to 7 to subsequently allow for its immobilization and the fabrication of Tc-pyrochlore. Microstructure and mechanical properties of surrogate waste form $Sm_2(Ru_{0.5}Ti_{0.5})_2O_7$ could be significantly improved compared with earlier studies and theoretical densities of 72 % were measured. On the other hand the technetium-pyrochlore $Sm_2(Tc_{0.25}Ru_{0.25}Ti_{0.5})_2O_7$ is still lacking these properties and a more intense sintering regime has shown to induce volatilization and/or Tc-reduction to the metallic state. The pyrochlores of the surrogate quaternary system contain two phases: $Sm_2(Ru_{0.5}Ti_{0.5})_2O_7$ and $Sm_2(Ti_{1-x}Ru_x)O_5$ with a ratio of about 50:50 in wt.%.

$Nd_2Tc_2O_7$ fabricated by standard dry processing showed with 1.48 10^{-7} g/mm^2•days a lower specific mass loss than LAWE4 Tc-containing borosilicate glass (6.43 10^{-7} g/mm^2•day) and far better technetium retention combined with optimal waste loading. Fabrication by hot-unaxial pressing using graphite (and also AL23 dies to some degree) induces the formation of metallic technetium inclusions, with the consequence of significant increased specific mass losses of about 4 10^{-6} to 7 10^{-6} g/mm^2•day. The pyrochlore microstructure is not affected by corrosion (using ASTM C1220-10 protocols) and noticeable changes were not observed with the tools on hand. On the other hand, leaching data for the technetium ($Nd_2Tc_2O_7$) and the ruthenium pyrochlores ($Sm_2Ru_2O_7$) indicated noticeable deviations from congruent leaching. The tetravalent Tc or Ru cations occupy the *16 c* positions within the crystal structure of pyrochlore, showing larger bond strength than the trivalent Sm or Nd cations, which are occupying the *16 d* positions, and their contribution to the overall lattice energy of pyrochlore is higher. This further demonstrates that the pyrochlore structure is an excellent host for tetravalent technetium and Tc shows by a factor 2 to 3 higher retention to remain in the crystal structure than the trivalent lanthanide cations do.

4. Acknowledgements

The research under this NEUP project was performed with financial support from the DOE Office of Nuclear Energy's Nuclear Energy University Programs, DOE-NEUP 12-3445, to allow research work in the frame of the work package NU-12-NV-UNLV-0202-06: “Thermodynamic and Microstructural Mechanisms in the Corrosion of Advanced Ceramic Technetium-bearing Waste Forms and Thermophysical Properties”.

Between 2006 and 2011 and prior to the NEUP project 12-3445 research on technetium pyrochlores was partly funded through to DOE-NE Fuel Cycle R&D Program - Waste Forms Campaign, Alternative Waste Forms for Fission Products. Cooperate agreement No. DE-AC52-06NA25396.

The experimental work scope of this project would not have been possible without the support or the UNLV Radiochemistry Program and its radiological & administrative support.

We wish to also acknowledge the involvement of Dr. Kurt Sickafus from the University of Tennessee, Dr. Gordon Jarvinen and Dr. Ming Tang from Los Alamos National Laboratory, Dr. John Vienna and Dr. Michael Schweiger from Pacific Northwest National Laboratory.